System Identification of a Nonlinear Flight Dynamics Model for a Small, Fixed-Wing UAV

Benjamin M. Simmons

Thesis submitted to the Faculty of the
Virginia Polytechnic Institute and State University
in partial fulfillment of the requirements for the degree of

Master of Science
in
Aerospace Engineering

Craig A. Woolsey, Chair
Harry Pat Artis
Mayuresh J. Patil
Pradeep Raj

April 18, 2018
Blacksburg, Virginia

Keywords: Output Error Method, Unmanned Aerial Vehicle, Vortex Lattice Method, Flight Testing, Aerodynamic Modeling, Parameter Estimation

System Identification of a Nonlinear Flight Dynamics Model for a Small, Fixed-Wing UAV

Benjamin M. Simmons

(ABSTRACT)

This thesis describes the development of a nonlinear flight dynamics model for a small, fixed-wing unmanned aerial vehicle (UAV). Models developed for UAVs can be used for many applications including risk analysis, controls system design and flight simulators. Several challenges exist for system identification of small, low-cost aircraft including an increased sensitivity to atmospheric disturbances and decreased data quality from a cost-appropriate instrumentation system. These challenges result in difficulties in development of the model structure and parameter estimation. The small size may also limit the scope of flight test experiments and the consequent information content of the data from which the model is developed. Methods are presented to improve the accuracy of system identification which include data selection, data conditioning, incorporation of information from computational aerodynamics and synthesis of information from different flight test maneuvers. The final parameter estimation and uncertainty analysis was developed from the time domain formulation of the output-error method using the fully nonlinear aircraft equations of motion and a nonlinear aerodynamic model structure. The methods discussed increased the accuracy of parameter estimates and lowered the uncertainty in estimates compared to standard procedures for parameter estimation from flight test data. The significant contributions of this thesis are a detailed explanation of the entire system identification process tailored to the needs of a small UAV and incorporation of unique procedures to enhance identification results. This work may be used as a guide and list of recommendations for future system identification efforts of small, low-cost, minimally instrumented, fixed-wing UAVs.

System Identification of a Nonlinear Flight Dynamics Model for a Small, Fixed-Wing UAV

Benjamin M. Simmons

(GENERAL AUDIENCE ABSTRACT)

This thesis describes identification of a series of equations to model the flight motion of a small unmanned airplane. Model development for small unmanned aerial vehicles (UAVs) is a challenging process because they are significantly affected by small amounts of wind and they usually contain inexpensive, lower quality sensors. This results in lower quality data measured from flying a small UAV, which is subsequently used in the process to develop a model for the aircraft. In this work, techniques are discussed to improve estimation of model parameters and increase confidence in the validity of the final model. The significant contributions of this thesis are a comprehensive explanation of the model development process specific to a small UAV and implementation of unique procedures to enhance the resulting model. This work as a whole may be used as a guide and list of recommendations for future model development efforts of small, low-cost, unmanned aircraft.

Dedication

To those who will always strive to Invent the Future

Acknowledgments

Firstly, I would like to thank Craig Woolsey for being an outstanding advisor. From the beginning of my journey into graduate school, Dr. Woolsey believed in me and gave me confidence that I could finish a thesis in one school year as well as make a seamless transition from a different undergraduate background. Dr. Woolsey was very supportive of my rigid graduation timeline and his optimism fueled my efforts in producing a successful final result. I am very thankful that Dr. Woolsey assigned me to this research project because it proved to be a phenomenal learning experience which will be valuable in my future career. I am incredibly grateful for his commitment and time invested in my professional development, as well as his advice, mentorship and encouragement throughout my studies and this thesis.

I would like to thank my committee members, Pat Artis, Mayuresh Patil and Pradeep Raj, for their time and commitment in providing feedback on this thesis and attending my thesis defense. I would also like to thank Hunter McClelland for his advice and assistance throughout the project, including preparing and flying the aircraft as well as his wealth of knowledge of the Pixhawk instrumentation system. Thank you to both Hunter and Javier González-Rocha for the great discussions we have had about system identification over the past year. Thank you also to all those in the Nonlinear Systems Laboratory who have given advice and suggestions that have contributed to this project. Additionally, thank you to my coworkers who taught me knowledge of flight testing and flight dynamics that greatly contributed to the success of this project.

On a more general level, I would like to thank all the friends I have made in both Aerospace Engineering and Engineering Science and Mechanics for their companionship throughout my five years of undergraduate and graduate education at Virginia Tech throughout the "fun" engineering curricula. Also, thank you to Roger Chang and Pat Artis for being great teachers, friends and mentors since I met both in my early undergraduate years. Thank you to Lauren for being my best friend and for all her support and encouragement through my studies and this thesis. Lastly, but certainly not least, thank you to my parents and family for their love and support through college, this thesis and throughout my life; I would not have gotten to this point without them.

Contents

List of Figures

List of Tables

List of Abbreviations

α	Angle of Attack
$\bar{c}$	Mean Aerodynamic Chord
$\bar{q}$	Dynamic Pressure
β	Angle of Sideslip
$\boldsymbol{P}$	Parameter Covariance Matrix
$\boldsymbol{u}(t)$	Input (Control) Vector
$\boldsymbol{v}(t)$	Noise Vector
$\boldsymbol{x}(t)$	State Vector
$\boldsymbol{y}(t)$	Model Output Vector
$\boldsymbol{z}(t)$	Measured Output Vector
δa	Aileron Deflection
δe	Elevator Deflection
δr	Rudder Deflection
$\hat{p}$	Non-Dimensional Body-Axis Roll Rate
$\hat{q}$	Non-Dimensional Body-Axis Pitch Rate
$\hat{r}$	Non-Dimensional Body-Axis Yaw Rate
$\hat{u}$	Non-Dimensional x Body-Axis Velocity Component
$\hat{v}$	Non-Dimensional y Body-Axis Velocity Component
$\hat{w}$	Non-Dimensional z Body-Axis Velocity Component
ϕ	Euler Roll Angle
ψ	Euler Yaw (Heading) Angle
ρ	Atmospheric Density
ρ_{ij}	Correlation Coefficient

σ	Cramér-Rao Lower Bound (Standard Error)
Θ	Unknown model parameters
θ	Euler Pitch Angle
ζ	Damping Ratio
a_x	x Body-Axis Translational Acceleration
a_y	y Body-Axis Translational Acceleration
a_z	z Body-Axis Translational Acceleration
b	Projected Wing Span
C_l	Body-Axis Rolling Moment Coefficient
C_m	Body-Axis Pitching Moment Coefficient
C_n	Body-Axis Yawing Moment Coefficient
C_X	x Body-Axis Force Coefficient
C_Y	y Body-Axis Force Coefficient
C_Z	z Body-Axis Force Coefficient
f	Natural Frequency
I_x	Roll Moment of Inertia
I_y	Pitch Moment of Inertia
I_z	Yaw Moment of Inertia
I_{xz}	Product of Inertia
L	Dimensional Body-Axis Aerodynamic Rolling Moment
M	Dimensional Body-Axis Aerodynamic Pitching Moment
m	Aircraft Mass
N	Dimensional Body-Axis Aerodynamic Yawing Moment
p	Body-Axis Roll Rate
q	Body-Axis Pitch Rate

r Body-Axis Yaw Rate

S Projected Wing Area

T Oscillation Period

T Thrust

t_2 Time to Double Amplitude

$t_{1/2}$ Time to Half Amplitude

u x Body-Axis Velocity Component

v y Body-Axis Velocity Component

V_a Airspeed

V_D +Down Earth-Fixed Velocity Component

V_E +East Earth-Fixed Velocity Component

V_N +North Earth-Fixed Velocity Component

V_o Reference Airspeed

w z Body-Axis Velocity Component

X Dimensional x Body-Axis Aerodynamic Forces

x +North Earth-Fixed Position

Y Dimensional y Body-Axis Aerodynamic Forces

y +East Earth-Fixed Position

Z Dimensional z Body-Axis Aerodynamic Forces

z +Down Earth-Fixed Position

AHRS Altitude and Heading Reference System

ANMAE Average Normalized Mean Absolute Error

ANRMSE Average Normalized Root-Mean-Square Error

BBR Bank-to-Bank Roll

CFD Computational Fluid Dynamics

CG Center of Gravity

CI Confidence Interval

DR Dutch Roll

EEM Equation-Error Method

EKF Extended Kalman Filter

FPR Flight Path Reconstruction

FTD Flight Test Data

GOF Goodness of Fit

GPS Global Positioning System

IMU Inertial Measurement Unit

MAD Median Absolute Deviation

MAE Mean Absolute Error

OEM Output-Error Method

RMSE Root-Mean-Square Error

SP Short Period

TIC Theil's Inequality Coefficient

UAV Unmanned Aerial Vehicle

VLM Vortex Lattice Method

Chapter 1

Introduction

System identification for fixed-wing aircraft can be used for many applications including risk assessment, control system design, flying qualities analysis, flight simulators, and validation of results obtained from other computational or experimental methods. System identification for full-sized aircraft has been well characterized and many methods exist for characterizing their flight dynamics [1, 2]. With the increasing presence of small, low-cost unmanned aerial vehicles (UAVs), there is an increasing need to identify models to characterize these aircraft which is accompanied by several challenges not encountered with full-scale aircraft.

Full-scale commercial and military fixed-wing aircraft have the luxury of significant time, resources and experience to develop high quality models over the entire operational envelope. The ability to afford high quality instrumentation and the scale of aircraft to be resistant to atmospheric disturbances results in high quality experimental flight test data; the high quality data can then be used to identify high quality models to characterize their flight dynamics. Additionally, full-scale aircraft generally have strict flight envelopes and maneuvering restrictions limiting the required range of model validity. Small fixed-wing UAVs on the other hand are more susceptible to atmospheric disturbances, which make deterministic modeling a challenge for modeling a UAV in a stochastic atmosphere. Consequently, any experimental data collected will contain an increased presence of process noise due to atmospheric disturbances. Small, inexpensive UAVs also face the challenge that the

instrumentation system used for model development must equivalently be low-cost typically making the sensors less accurate and contain higher levels of measurement noise, as well as possibly lack certain key measurements. Both of these major challenges cause degradation of experimental data quality which would ultimately be used for system identification. Data quality is critical for system identification because the quality of the model will only be as good as the experimental data it is derived from [2]. An additional challenge for model development is that UAVs have few, if any, envelope or maneuvering restrictions which may result in needing a more intricate model to quantify their dynamics in the desired flight regime.

The goal of this work was to investigate and characterize system identification phenomena specific to small, low-cost, fixed-wing UAVs with the intention of recommending a methodology to overcome the discussed challenges and identify useful models of their flight dynamics. The experimental aircraft in this work, the HobbyKing^{TM} Bix3 [3], is a 1.2 kg (2.6 lbs) fixed-wing UAV containing a limited, inexpensive instrumentation system. The size of this platform is notably smaller than the size of aircraft studied in other works on the topic of fixed-wing UAV system identification [4, 5, 6, 7, 8]. The specific goal for the system identification effort was to develop the best possible nonlinear flight dynamics model to characterize a large portion of the Bix3's flight envelope for simulation purposes. The model developed was specifically intended to be used for future research in model-based wind estimation.

System identification from flight test data is a preferred method for model development of an aircraft in flight [1]. For a small UAV, however, the data collected in flight may be of lower quality compared to large-scale aircraft. This makes identifying all model parameters from individual flight maneuvers a challenge resulting in low quality parameter estimates with a high level of uncertainty. Since all the information required for system

identification may not be explicitly present in the available data, techniques to enhance the information content from flight test data or knowledge from other sources, such as analytical or computational methods, may be needed to create a useful model. Methods of this sort will be investigated in this work in an attempt to improve the final model. The results of this study will provide insight into the process of system identification for a small, low-cost, fixed-wing UAV and allow for future applications to use this insight to improve and streamline the system identification process.

The general process of aircraft system identification involves analyzing experimental flight test data to create a model structure, estimate the parameters in the model and estimation of the model's accuracy. The process starts by design of flight experiments to excite the dynamics of the aircraft such that a model can be formed from all possible explanatory variables. The data must then be analyzed and corrected for bias, kinematic inconsistencies, and/or excessive noise. Procedures may then be taken to develop a model structure and to estimate the unknown model parameters. Validation and uncertainty analysis of the developed model is the final step before using the model for other application.

The significant contributions of this thesis are summarized as follows:

- Presentation of a detailed procedural guide for system identification specific to small, fixed-wing UAVs with limited instrumentation systems
- Development and validation of a nonlinear longitudinal and lateral-directional flight dynamics model for the HobbyKing^{TM} Bix3 fixed-wing UAV
- Investigation of using the vortex lattice method to supplement parameter estimation from flight test data
- Development of a method to combine favorable characteristics of two different lateral-directional maneuvers to identify an accurate and unique set of lateral-directional parameter estimates
- Overall investigation of system identification methods applied to small fixed-wing UAVs and an analysis of their relative accuracy and applicability

Chapter 2

Background

This chapter presents the theory and methods used for aircraft system identification. Previous works in system identification of small, fixed-wing unmanned aerial vehicles (UAVs) are summarized. The software packages and their built-in methods of analysis used for this research effort are also discussed.

2.1 General Overview of System Identification

Identification of an appropriate mathematical model to describe a generic system is necessary for a variety of applications. A system in this context is a deterministic dynamic entity that may be experimented on while allowing collection of measured data. A mathematical model of a system can be developed using theoretical and/or experimental approaches. A theoretical approach to modeling is developed from a basis of the fundamental laws of nature, such as Newton's laws of motion. An experimental approach to modeling is formed from a basis of observation of the behavior of a system over time subject to variable inputs. This empirical method to modeling is useful for systems that are complex and difficult to adequately describe on a level of theoretical first principles. Limitations of empirical models, however, are that they can inhibit physical intuition and that they are only reliable over the range of variables where past data is available [9].

System identification is a procedure for developing a meaningful mathematical model

that relates system inputs to outputs using empirical data measured from the system [9]. For the general process of system identification, the inputs and outputs of the system are known and are used to create a model of the process dynamics. The process of system identification begins by experimenting on the system while recording measurements of the system inputs and outputs. Once data has been collected the focus shifts to developing a model framework, or general equations that describe the system. Then, unknown parameters that may appear in the model framework are determined from the experimental data [2].

There are several types of models that can occur in system identification. The model type is determined by the amount of preliminary knowledge of the dynamics of the system. A model that does not contain any fundamental laws of nature or constitutive relations is termed a black-box model. This type of model is established without any knowledge of the relationship between system inputs and outputs. If some knowledge of the dynamics of the process is known but some parameters remain ambiguous, modeling of this form is termed gray-box modeling. White-box models are defined by well known process dynamics and can be described predominantly by physical governing equations and relationships [10]. Parameter identification is a type of system identification where the general form of the mathematical model to describe the system is known and the primary task is to find the values of model terms which result in the most accurate modeling of the system [11].

2.2 Aircraft Equations of Motion

The aircraft equations of motion contain kinematic and dynamic relationships which describe translational and rotational motion for a wide variety of fixed-wing aircraft. The dynamic equations are related to external aerodynamic forces and moments on the aircraft, which are generally the primary interest of aircraft model identification. While the aircraft

equations of motion are well defined, the model for the aerodynamic forces and moments on the aircraft will change between individual aircraft and flight conditions. The main task of system identification for an aircraft involves modeling these aerodynamic forces and moments [2]. Without simplification the resulting equations are coupled, nonlinear ordinary differential equations as will be shown below.

The important aircraft frames of reference used throughout this work include the earth-fixed and body-fixed reference frames. Both are right-handed coordinate systems with axes that are mutually orthogonal. The inertial earth-fixed reference frame is defined as the x, y and z axes oriented north, east and downward, respectively, with an arbitrary origin. The standard aircraft body-fixed reference frame has its origin at the aircraft's center of gravity; the x-axis points through the aircraft nose, the y-axis points through the right side of the aircraft and the z-axis points through the bottom of the aircraft [1].

The derivation of the 12 general nonlinear aircraft equations of motion is developed from first principles in Etkin and Reid [12], and only the important results critical for system identification are presented here. The aircraft is treated as a six degree of freedom rigid body that is acted upon by gravitational and aerodynamic forces. It is assumed that the earth is a flat, inertial reference frame. Mass and moments of inertia are assumed to be unchanging with symmetry along the xz plane such that $I_{xy} = I_{yz} = 0$. Gravitational acceleration and atmospheric density are assumed to be constant. The gyroscopic effects from a propeller are assumed to be negligible and are thus neglected. For the form of the equations presented, it is assumed that there is no wind present. The 12 states of the system are the inertial position of the center of gravity of the aircraft (x, y, z), inertial orientation or Euler angles (ϕ, θ, ψ), body-fixed translational velocities (u, v, w) and body-fixed angular velocities (p,

q, r). The kinematic equations are as follows:

$$\dot{x} = u\cos\theta\cos\psi + v(\sin\theta\cos\psi\sin\phi - \sin\psi\cos\phi) + w(\sin\theta\cos\psi\cos\phi + \sin\psi\sin\phi) \quad (2.1)$$

$$\dot{y} = u\cos\theta\sin\psi + v(\sin\theta\sin\psi\sin\phi + \cos\psi\cos\phi) + w(\sin\theta\sin\psi\cos\phi - \cos\psi\sin\phi) \quad (2.2)$$

$$\dot{z} = -u\sin\theta + v\cos\theta\sin\phi + w\cos\theta\cos\phi \quad (2.3)$$

$$\dot{\phi} = p + (q\sin\phi + r\cos\phi)\tan\theta \quad (2.4)$$

$$\dot{\theta} = q\cos\phi - r\sin\phi \quad (2.5)$$

$$\dot{\psi} = (q\sin\phi + r\cos\phi)\sec\theta \quad (2.6)$$

Equations (2.1)-(2.3) describe the aircraft's translational kinematics and are used to calculate the inertial position of the aircraft's center of gravity, x, y and z. Equations (2.4)-(2.6) describe the aircraft's rotational kinematics and are used to calculate the aircraft's orientation angles, roll attitude ϕ, pitch attitude θ and yaw attitude ψ. The quantities p, q and r are the aircraft's roll rate, pitch rate and yaw rate in the body frame, respectively. The translational velocity at the center of gravity of the aircraft in the body frame are given as u, v and w [12]. The aircraft dynamic equations, which include the aerodynamic forces and moments exerted on the aircraft, are as follows:

$$m\left(\dot{u} + qw - rv\right) = X + T - mg\sin\theta \quad (2.7)$$

$$m\left(\dot{v} + ru - pw\right) = Y + mg\cos\theta\sin\phi \quad (2.8)$$

$$m\left(\dot{w} + pv - qu\right) = Z + mg\cos\theta\cos\phi \quad (2.9)$$

$$I_x\dot{p} - I_{xz}\dot{r} + qr\left(I_z - I_y\right) - I_{xz}pq = L \quad (2.10)$$

$$I_y\dot{q} + rp\left(I_x - I_z\right) + I_{xz}\left(p^2 - r^2\right) = M \tag{2.11}$$

$$I_z\dot{r} - I_{xz}\dot{p} + pq\left(I_y - I_x\right) + I_{xz}qr = N \tag{2.12}$$

$$X = \bar{q}SC_X, \quad Y = \bar{q}SC_Y, \quad Z = \bar{q}SC_Z, \quad L = \bar{q}bSC_l, \quad M = \bar{q}\bar{c}SC_m, \quad N = \bar{q}bSC_n \tag{2.13}$$

Equations (2.7)-(2.9) describe the aircraft's translational dynamics which are dependent on the external aerodynamic forces exerted on the aircraft, X, Y and Z. The thrust force T is assumed to be acting along the x body-axis through the aircraft's center of gravity. Other quantities appearing in the equations are the aircraft mass m, gravitational acceleration g, the time derivative of the body-axis velocity components ($\dot{u}$, $\dot{v}$, $\dot{w}$), and previously defined state variables ϕ, θ, ψ, p, q, r, u, v, w. Equations (2.10)-(2.12) describe the aircraft's rotational dynamics which are dependent on the external aerodynamic moments exerted on the aircraft, L, M and N. The nonzero moments and product of inertia (I_x, I_y, I_z, I_{xz}) as well as the body-axis angular rates (p, q, r) and their time derivatives ($\dot{p}$, $\dot{q}$, $\dot{r}$) also appear in these equations [12]. Equation (2.13) shows the conversion between dimensional forces and moments, and the non-dimensional force and moment coefficients C_X, C_Y, C_Z, C_l, C_m, C_n [1]. In these conversions, ρ is the air density, S is the wing reference area, $\bar{c}$ is the mean aerodynamic chord, b is the wing span and $\bar{q} = \rho V_a^2/2$ is the dynamic pressure where V_a is the airspeed. Equations (2.1)-(2.12) can be written in the following general form:

$$\dot{\boldsymbol{x}}(t) = f(\boldsymbol{x}(t), \boldsymbol{u}(t), \Theta), \quad \boldsymbol{x}(t_0) = \boldsymbol{x}_0 \tag{2.14}$$

$$\boldsymbol{y}(t) = g(\boldsymbol{x}(t), \boldsymbol{u}(t), \Theta) \tag{2.15}$$

$$\boldsymbol{z}(t) = \boldsymbol{y}(t) + \boldsymbol{v}(t) \tag{2.16}$$

The generalized from of the aircraft equations of motion, Equations (2.14)-(2.16),

will be useful for the discussion of system identification methods which will be described in Section 2.3.5 [1]. The state vector, $\boldsymbol{x}$, includes the inertial position, orientation angles, body-axis angular rates and body-axis translational velocities. The control vector, $\boldsymbol{u}$, typically contains the throttle command and control surface deflections. Measured aircraft responses are included in the output vector, $\boldsymbol{z}$, which are disturbed by the noise vector $\boldsymbol{v}$. The output predicted by a model is the output vector $\boldsymbol{y}$. The external aerodynamics are included in Θ, which is typically unknown and needs to be identified.

The aerodynamic forces and moments cannot be measured directly on-board an aircraft. These quantities must be calculated from measured aircraft states, aircraft geometry and aircraft inertial properties using the aircraft equations of motion. Aerodynamic forces are computed directly from the measured translational acceleration, dynamic pressure, mass and reference area, as shown in Equations (2.17)-(2.19) [1]. The thrust T appears in the equation for C_X (Equation (2.17)). In some situations, the thrust T may be omitted to develop a model for the joint effects of aerodynamics and thrust. Identification for the purpose of simulation may use this approach [1]. In order for thrust and aerodynamics to be separated, a measurement of thrust is necessary. Thrust is typically measured separately from ground testing rather than in flight and is a function of airspeed. Propeller aircraft are generally assumed to be constant power systems meaning that the product of thrust and airspeed is approximately constant for a constant throttle setting.

$$C_X = \frac{ma_x - T}{\bar{q}S} \tag{2.17}$$

$$C_Y = \frac{ma_y}{\bar{q}S} \tag{2.18}$$

$$C_Z = \frac{ma_z}{\bar{q}S} \tag{2.19}$$

The aerodynamic moments are calculated using the aircraft dynamic equations in the

form of Equations (2.20)-(2.22) [1]. The contribution from the angular momentum of the propulsion system is assumed to be insignificant which results in this form of the equations. The moment coefficients are dependent on the the body-axis angular rates and accelerations, inertial/geometric aircraft properties and dynamic pressure.

$$C_l = \frac{1}{\bar{q}bS}\left(I_x\dot{p} - I_{xz}\left(\dot{r} + pq\right) + qr\left(I_z - I_y\right)\right) \tag{2.20}$$

$$C_m = \frac{1}{\bar{q}\bar{c}S}\left(I_y\dot{q} + rp\left(I_x - I_z\right) + I_{xz}\left(p^2 - r^2\right)\right) \tag{2.21}$$

$$C_n = \frac{1}{\bar{q}bS}\left(I_z\dot{r} - I_{xz}\left(\dot{p} - qr\right) + pq\left(I_y - I_x\right)\right) \tag{2.22}$$

A major topic in flight dynamics is model development for aerodynamic forces and moments exerted on an aircraft in flight [12]. Relations can be developed using a Taylor series expansion about an operational point. Derivatives of an external force or moment are termed stability derivatives or aerodynamic derivatives. It is acceptable for many applications to keep only linear terms of low order derivatives to create a sufficient aerodynamic model. Other modeling scenarios, such as rapid or large amplitude maneuvers, may require nonlinear terms to achieve sufficient accuracy [1]. A significant amount of past research has involved experimental and theoretical methods for developing aerodynamic derivatives.

A general framework for a nonlinear aerodynamic model for aircraft was developed in Grauer and Morelli [13]. This model was developed using multivariate orthogonal functions to determine the model structures. The aerodynamic databases of eight different aircraft were used for simulation from their respective wind tunnel databases. The identification process separated longitudinal and lateral-directional dynamics because they are marginally coupled in normal flight conditions. The aerodynamic model developed in Grauer and Morelli [13] (shown in Equations (2.23)-(2.28)) incorporated data ranging from fighter aircraft to transport aircraft to small-scale commuter aircraft. The benefit to this approach is that a

large range of aircraft can be modeled using a model consisting of 45 parameters rather than a large aerodynamic database. The model developed was stated to work well for a large variety of aircraft.

$$C_D = \Theta_1 + \Theta_2\alpha + \Theta_3\alpha\hat{q} + \Theta_4\alpha\delta_e + \Theta_5\alpha^2 + \Theta_6\alpha^2\hat{q} + \Theta_7\alpha^2\delta_e + \Theta_8\alpha^3 + \Theta_9\alpha^3\hat{q} + \Theta_{10}\alpha^4 \quad (2.23)$$

$$C_Y = \Theta_{11}\beta + \Theta_{12}\hat{p} + \Theta_{13}\hat{r} + \Theta_{14}\delta_a + \Theta_{15}\delta_r \quad (2.24)$$

$$C_L = \Theta_{16} + \Theta_{17}\alpha + \Theta_{18}\hat{q} + \Theta_{19}\delta_e + \Theta_{20}\alpha\hat{q} + \Theta_{21}\alpha^2 + \Theta_{22}\alpha^3 + \Theta_{23}\alpha^4 \quad (2.25)$$

$$C_l = \Theta_{24}\beta + \Theta_{25}\hat{p} + \Theta_{26}\hat{r} + \Theta_{27}\delta_a + \Theta_{28}\delta_r \quad (2.26)$$

$$C_m = \Theta_{29}+\Theta_{30}\alpha+\Theta_{31}\hat{q}+\Theta_{32}\delta_e+\Theta_{33}\alpha\hat{q}+\Theta_{34}\alpha^2\hat{q}+\Theta_{35}\alpha^2\delta_e+\Theta_{36}\alpha^3\hat{q}+\Theta_{37}\alpha^3\delta_e+\Theta_{38}\alpha^4 \quad (2.27)$$

$$C_n = \Theta_{39}\beta + \Theta_{40}\hat{p} + \Theta_{41}\hat{r} + \Theta_{42}\delta_a + \Theta_{43}\delta_r + \Theta_{44}\beta^2 + \Theta_{45}\beta^3 \quad (2.28)$$

The force and moment coefficients in these equations, C_D, C_Y, C_L, C_l, C_m and C_n, are functions of the 45 unknown aerodynamic coefficients Θ_i multiplied by non-dimensional states and control surface deflections. The states are angle of attack α, angle of sideslip β, non-dimensional body-axis angular rates ($\hat{p}$, $\hat{q}$, $\hat{r}$), and control surface deflection angles (δe, δa, δr); all angles are measured in radians. Equations (2.23)-(2.28) include the lift and drag coefficients, C_L and C_D, rather than the body-axis force coefficients, C_X and C_Z, because the model structure was developed from wind tunnel testing where these forces and moments can be measured directly contrary to flight testing [13]. The conversion from C_X and C_Z to C_L and C_D is shown in Equations (2.29) and (2.30). When performing model identification from flight test data, it is generally better to formulate the structure of the aerodynamic model in terms of the force coefficients C_X and C_Z rather than C_L and C_D. The reasoning for this is because the measured angle of attack α is required to calculate C_L and C_D, in addition to translational acceleration and thrust, which can result in more measurement errors and

noise [1].

$$C_L = C_X \sin\alpha - C_Z \cos\alpha \tag{2.29}$$

$$C_D = -C_X \cos\alpha - C_Z \sin\alpha \tag{2.30}$$

2.3 Aircraft System Identification

There are three general classes of problems in aircraft flight dynamics: simulation, control and system identification. The task of simulation involves prediction of outputs when the control inputs and system dynamics are known. In controls problems, the goal is to find control inputs when the system dynamics and outputs are prescribed. System identification involves determining the system dynamics when given the control inputs and measured aircraft outputs. Specifically, system identification involves determining the effect of aerodynamic forces and moments on aircraft dynamics [1]. This usually entails developing a model structure for aerodynamic forces and moments and identifying approximate values of aerodynamic coefficients. The usefulness of the model is greatly dependent on the degree of accuracy with which the forces and moments on a vehicle can be modeled [2].

Flight testing, wind tunnel testing, computational fluid dynamics (CFD) and analytical method can be used to determine aerodynamic models. While analytical or computational methods may be useful, the best models are typically developed through empirical methods which include flight testing and wind tunnel testing. Reasons to perform system identification from flight test data include validation of results obtained from other methods, obtaining high fidelity models to describe aircraft dynamics and developing models from actual flight conditions rather than simulated environments. Complex aircraft dynamics cannot be adequately recreated using wind tunnel testing, analytical techniques or computational methods which is why flight test data is preferred for modeling in these scenarios [1].

2.3.1 Aircraft System Identification from Flight Test Data

There are several steps in the process for system identification of an aircraft from flight test data. Prior knowledge of aircraft dynamics and external aerodynamics can be used to create a preliminary model before examining any data. This typically includes the standard equations of motion for fixed-wing aircraft, and perhaps other preliminary knowledge of the aircraft dynamics, such as estimates of its dynamic modes. Then, an experiment can be designed by prescribing flight maneuvers for system identification and ensuring the instrumentation system will be able to accurately capture the aircraft's dynamics. After data has been collected, it must be examined by comparing sensor measurements to identical states calculated using the aircraft kinematic equations to ensure validity of measurements and discover any measurement error which occurs systematically. The preliminary model must be refined by selecting a model structure using the measured data to model aerodynamic forces and moments. The structure of aerodynamic forces and moments is generally a function of aircraft states and inputs. A parameter estimation method is then used to estimate the unknown parameters in the mathematical model. The final step is to validate the model developed through system identification to prove its usefulness [1]. Each of these steps will be discussed in further detail in the proceeding sections.

2.3.2 Experimental Setup and Implementation

The experimental setup defines the instrumentation, flight conditions, control inputs and specific flight maneuvers used to collect flight test data for system identification [1]. This is a critical step in aircraft system identification because the model development relies primarily on the behavior shown in the data. Flight testing for system identification involves perturbing the aircraft with predefined control inputs along different axes to excite the

dynamic response of the aircraft so that all aerodynamic parameters can be estimated [2].

Instrumentation System

The instrumentation system on-board the aircraft records all information required for system identification. Accurate in-flight measurements are critical to the subsequent system identification to be accurate. An important characteristic of the instrumentation system is the sampling frequency. System identification routines typically require all quantities have the same time vector, and thus, it is preferable to record all measurements at the same discrete points in time at the same sampling frequency. If this is not the case, interpolation may be used to convert all quantities to the same sampling rate. Measurements useful for system identification include the airspeed, aerodynamic angles, translational accelerations, angular rates, orientation angles and engine parameters. The sampling frequency must be at least twice the Nyquist frequency to capture the full dynamics, however the sampling frequency for system identification should be about twenty-five times the minimal frequency of interest [1]. Typically aircraft are sampled at a rate of 20-25 Hz for system identification [2]. Ideally, the measurements should not be excessively noisy or contain time delays. Filters can be applied to measurements to better capture the true aircraft motion.

Input Design for System Identification

Choice of proper inputs is important in order to properly excite the dynamic modes of interest. Input design can be chosen to excite all potential dynamic frequencies if no prior knowledge is known about the system. Common methods for this are frequency sweeps or multi-sine inputs. Conversely, inputs can be designed to stimulate the dynamic frequencies of the system directly if estimates of natural frequencies of the dynamic modes are known

from prior knowledge. Variation in the designed inputs can help to improve the model by exciting different dynamics of the aircraft. Variation of input can take the form of reversing the maneuver deflections, changing the magnitude of the input, or changing the input frequency. A benefit of a test pilot over computer generated inputs is that unintentional human imperfections in the inputs can help the identification process by stimulating a larger frequency range. Good inputs are typically square waves near the estimated dynamic frequencies of the system. Typical inputs designed using prior knowledge include impulses, doublets and multi-steps [1].

Doublets are two sided pulses which follow the shape of a square wave. This is performed by starting from a neutral position, quickly moving the control surface in one direction for a set time, then quickly moving the control surface in the opposite direction for the same amount of time, and finally returning to neutral [2]. The design of a doublet should be such that its frequency is near the expected frequency of the aircraft dynamic mode of interest. A square wave input is preferred over a sine wave because a square wave can excite a larger range of frequencies which allows for variability in the estimate of the natural frequencies. The magnitude of the doublet input should be large enough such that there is a large signal-to-noise ratio but still small enough to not violate the assumptions of the model [1].

Another common input is the 3-2-1-1 multi-step input which is useful because it can excite a larger range of frequencies than the doublet input. This involves alternating the direction of the control surface rapidly and holding at 3, 2, 1, and 1 time steps, respectively [2]. The second pulse should be chosen to be close to half of the period of the corresponding expected dynamic mode of the system. The downside of the 3-2-1-1 input is that it is an asymmetric input that can perturb the aircraft out of the designed flight condition. Another option is the 2-1-1 input which may be more successful at keeping the aircraft near the

trim condition. An alternate approach is to design a sequence of doublet inputs at different frequencies around the expected frequency to provide a larger frequency range while also utilizing the simplicity of the doublet [1].

Flight Maneuvers for System Identification

A group of typical system identification maneuvers given in Jategaonkar [2] are the Short Period, Phugoid, Pushover Pull-Up, Level Turn, Thrust Variation, Bank-to-Bank Roll, Dutch Roll, and Steady Heading Sideslip. This list of maneuvers is designed primarily for aircraft significantly larger than the platform examined in this paper. As an additional challenge, the research presented here involves flight testing with the pilot located on the ground. This makes any maneuver involving a long time-period or coordination impractical for this scenario. This eliminates the Phugoid, Pushover Pull-Ups, Level Turn, Dynamic Thrust, and Steady Heading Sideslip maneuvers. A previous work in UAV system identification [4], used only the Dutch Roll, Bank-to-Bank Roll and Short Period maneuvers. These dynamic maneuvers have the ability to show characteristics of both the static and dynamic aerodynamic coefficients of the aircraft [2].

The Short Period maneuver is a measure of dynamic longitudinal stability of an aircraft characterized by a fast dynamic response along the longitudinal axis. The Short Period mode is excited by applying an elevator doublet or multi-step input, at an appropriate time interval to excite the Short Period motion. Short Period is used to identify the longitudinal stability derivatives associated with pitch and vertical aircraft motion [2].

Bank-to-Bank Roll and Dutch Roll are used to identify the aircrafts lateral-directional stability derivatives [2]. Bank-to-Bank Roll is a maneuver targeted at measuring rolling performance of an aircraft. This maneuver is typically performed by a 1-2-1 aileron input,

where the aircraft rolls to a bank angle of at least 30 degrees to one side then the aileron input is quickly reversed to roll to the opposite side before returning to trimmed flight. This maneuver is typically performed by rolling to different target bank angles, such as 30°, 45° and 60° [2]. The Dutch Roll maneuver is used to measure the frequency and damping of the Dutch Roll oscillatory mode of aircraft which is characterized by a combination of rolling, yawing and sideslipping [14]. Dutch Roll maneuver is typically initiated with a rudder doublet. Combination of the Dutch Roll and Bank-to-Bank Roll maneuvers by performing them sequentially may be beneficial for system identification purposes [2].

Flight testing for system identification should be performed at times where there are limited aerodynamic disturbances due to wind or turbulence [2]. In an ideal scenario, there should be at least four or five of each individual maneuver at each different flight condition so that corrupted maneuvers can be removed [1]. The accuracy and quality of the model improves by averaging the value of each parameter over a number of equivalent maneuvers. The different flight conditions may be defined by the airspeed, altitude, weight, center of gravity, throttle setting, angle of attack and aircraft configuration. A maneuver should be started at a predefined trim condition and data for a few seconds prior to the maneuver control inputs should be included in each data set. After the control inputs the aircraft should be allowed to move freely without pilot input for several seconds. While it is generally preferred to start and end a maneuver in trimmed steady level flight, modeling can still be performed when the beginning and end of the maneuver are not at these conditions [1].

It is preferable to perform system identification maneuvering for an aircraft as open-loop, or bare airframe, when the aircraft is open-loop stable [1]. If an aircraft is open-loop unstable and requires a feedback control system at all times, system identification should ideally be performed with the feedback gains lowered to the minimum values possible while

still maintaining safe flying conditions. While closed-loop feedback control does not change the bare airframe dynamics of the aircraft, it results in several adverse consequences for system identification. Feedback control functions to eliminate the natural motions of the aircraft which the system identification maneuvers are designed to expose; control surfaces are deflected such that the natural motion is quickly silenced which acts against the objective of system identification. The control system can also alter designed control inputs rendering them less effective in exciting the aircraft dynamics. Additionally, the control system may be designed to move control surfaces proportionally to other control surfaces and/or aircraft states which results in data collinearity. This causes problems in parameter estimation because the effects of two or more explanatory variables cannot be separated [1].

2.3.3 Data Processing and Analysis of Kinematic Consistency

After flight experiments have been performed, the critical step of data conditioning must be performed prior to using system identification routines. This process involves smoothing data signals to remove stochastic noise, syncing time vectors from different sensors, and calculating unmeasured signals using the aircraft equations of motion and/or numerical differentiation. This process also includes the step of analyzing the kinematic consistency of the data.

Before proceeding with system identification, the data set should be shown to satisfy the kinematic relations between measured parameters, termed data compatibility analysis [1]. This approach can be used to determine the magnitude of instrumentation errors and fix systematic errors. The kinematic equations described in Equations (2.1)-(2.6) are used in this analysis in addition to a modified form of the aircraft translational dynamic equations (Equations (2.7)-(2.9)). The translational dynamic equations are modified to include the

measured translational acceleration (a_x, a_y, a_z) instead of the aerodynamic forces. The modified translational dynamics equations are shown in Equations (2.31)-(2.33) [1]; this form of the translational dynamic equations is purely a function of kinematic variables.

$$\dot{u} = rv - qw + a_x - g\sin\theta \tag{2.31}$$

$$\dot{v} = pw - ru + a_y + g\cos\theta\sin\phi \tag{2.32}$$

$$\dot{w} = qu - pv + a_z + g\cos\theta\cos\phi \tag{2.33}$$

The compatibility analysis is performed by simulating the kinematic equations with the measured translational accelerations (a_x, a_y, a_z) and measured body-fixed angular rates (p, q, r) as the inputs into these equations [1]. The calculated, or reconstructed, outputs which may include u, v, w, ϕ, θ, ψ, x, y and z are then compared to their respective measured values. The process of calculating aircraft states based on kinematic relations and measurements is called flight path reconstruction (FPR). An associated challenge with FPR is that error in any of the measured inputs will cause the reconstructed parameters to diverge from the measured value of the respective parameter over time. If the calculated and measured states are nearly identical, then the measured quantities are kinematically consistent. If the measured states do not emulate the computed states, the kinematics are corrupted by some form of instrumentation errors [1]. In the situation where some or all of the outputs are not kinematically consistent, corrective mechanisms must be applied. Corrections can be made through bias correction, calculation of poor signals from more reliable signals, or using the estimation methods which will be discussed in Section 2.3.5.

2.3.4 Model Structure Identification

The form of an appropriate aerodynamic model may not be known confidently or at all for certain modeling scenarios. The structure of the aerodynamic model of an aircraft is dependent on the aircraft and range of flight conditions where the model is valid, and thus, generally must be developed from experimental data. This is not to be confused with the aircraft dynamic equations (Equations (2.7)-(2.12)), which are well defined and are generally the same for a majority of fixed-wing aircraft under a standard set of assumptions discussed in Section 2.2. The purpose of aerodynamic model development is to develop a model structure for the aerodynamic forces and moments X, Y, Z, L, M, N which appear in the aircraft dynamic equations. The model is typically expressed in terms of non-dimensional aerodynamic force and moment coefficients C_X, C_Y, C_Z, C_l, C_m, C_n (Equation (2.13)) to eliminate the dependence on atmospheric density and airspeed. A model structure consists of the number of unknown parameters to be estimated as well as the form of the explanatory variables multiplying the unknown parameters. For system identification from flight test data, the aerodynamic model is generally expressed in terms of the x and z body-axis force coefficients, C_X and C_Z, instead of the lift and drag coefficients, C_L and C_D, as discussed in Section 2.2 [1].

The aerodynamic model is generally dependent on the series of states u, v, w, p, q, r, or V_a, α, β, p, q, r, and the control surface deflections; these are termed the independent or explanatory variables. The aerodynamic force and moments are termed the response or dependent variables. The model is generally written in the form of a Taylor series expansion of the explanatory variables. Longitudinal forces and moments (X, Z, M) are typically only a function of the longitudinal states u, w, q, or V_a, α, q and longitudinal control variables such as elevator deflection δe. Lateral-directional forces and moments (Y, L, N) are typically only a function of the lateral-directional states v, p, r, or β, p, r and lateral-directional control

variables such as aileron deflection δa and rudder defection δr [1]. The longitudinal and lateral-directional dynamics are typically treated independently because they exhibit little coupling in normal flight [13].

For small perturbation flight test maneuvers, a model structure linear in explanatory variables is typically sufficient. Generic values for perturbation limits for full-scale aircraft are $\pm 3^\circ$ in angle of attack or sideslip angle, $\pm 20^\circ$/sec in angular rates, and $\pm 0.1g$-$0.3g$ in translational acceleration [1]. A linear model offers the benefit of simplicity, however is only valid near conditions where the identifying maneuver was performed. Nonetheless, a linear aerodynamic model structure about reference flight condition can adequately model the primary aerodynamic effects on the aircraft in a majority of scenarios. Nonlinear terms in the model structure are typically required to model more aggressive, high amplitude flight maneuvers with large angular rates, significant deviations from reference flight conditions, or near stall. Nonlinearity in the aerodynamic model, however, should only be used to model aerodynamics not captured by the dependence on linear terms [1].

A completed set of flight test data only contains a certain amount of information from which a model can be created. There is a fine line between including enough terms to capture the range of maneuvering desired, and including too many model parameters. The accuracy of each parameter estimate decreases as the number of terms in the model increases for a given amount of data. As a result, if more model parameters are desired, more information must be added in order to accurately estimate all parameters. The model structure should include as few terms as possible to adequately model the variations in the aerodynamic force and moment coefficients in the flight regime of interest [1].

Methods for Model Structure Identification

Two methods of model structure determination are the stepwise regression method and use of multivariate orthogonal functions. The stepwise regression method evaluates individual model structures by varying the regression terms one at a time. This method uses both addition of new terms and elimination of ineffective terms until an adequate model is formulated. Multivariate orthogonal function modeling is implemented by orthogonalization potential regression terms. This decoupling of regressors dependence allows for a more straightforward approach of identifying the structure of the model and allows the process to be automated [1].

When using the more common stepwise regression method, there are several metrics to assess the merit of different model structure in addition to qualitative fit. A common metric of the overall fit is the coefficient of determination, R^2, which is shown in Equation (2.34) where $\boldsymbol{z}$ is the measured response variable, $\bar{\boldsymbol{z}}$ is the mean of the measured response variable, $\boldsymbol{y}$ is the model prediction of the response variable and N is the number of data points [1].

$$R^2 = \frac{\boldsymbol{y}^T\boldsymbol{z} - N\bar{\boldsymbol{z}}^2}{\boldsymbol{z}^T\boldsymbol{z} - N\bar{\boldsymbol{z}}^2} \tag{2.34}$$

A higher R^2 value suggests a better model fit, but addition of a new regressor to the model structure will increase the R^2 value by default. When a new term is added, the R^2 value will only increase significantly if the term is beneficial to the overall model structure rather than adding unnecessary complexity. Thus, if a new term does not significantly increase R^2, it should be omitted from the model. A rule of thumb given in Morelli and Klein [1] is to exclude terms which increase R^2 by less than 0.5%. A point of convergence of a model structure based on the R^2 is when addition of any term not in the model is unable to significantly increase R^2. The adjusted-R^2 metric may be used to add a penalty

for including a larger number of terms in the model.

Useful metrics pertaining to analysis of individual model terms in the stepwise regression method include the partial F statistic, F_0, for terms included in the model and the partial correlation to the response variable, r, for terms currently omitted from the model structure [1]. The F_0 metric indicates the importance of the respective model term included in the model, where a large value of F_0 indicates a greater importance. The equation for F_{0_i} for the i^{th} model term is shown in Equation (2.35) where $\hat{\Theta}_i$ is the individual parameter estimate and σ_i is the corresponding standard error, which will be formally discussed in Section 2.3.5 [1]. The partial correlation to the response variable indicates the relative importance of including model terms currently outside of the model structure and ranges from $-1 < r < 1$. A model term has a magnitude of r closer to 1 if there is a significant relationship between the response variable and the potential regressors. The equation for r_i is shown in Equation (2.36) where $\boldsymbol{x}_i$ is the vector of values of the i^{th} excluded model term and $\boldsymbol{z}$ is the vector of value of the response variable; $\bar{\boldsymbol{x}}_i$ and $\bar{\boldsymbol{z}}$ are the mean values of the corresponding vectors [1]. As terms are added to the model, the response variable used in the calculation for r changes by subtracting variation already captured by the terms included in the model structure, such to quantify the unmodeled variation at each iteration. At each iteration of the stepwise regression, either a term is moved into the model because of a high correlation coefficient, or a term is removed from the model due to a low value of F_0 [1].

$$F_{0_i} = \frac{\hat{\Theta}_i^2}{\sigma_i^2} \tag{2.35}$$

$$r_i = \frac{(\boldsymbol{x}_i - \bar{\boldsymbol{x}}_i)^T(\boldsymbol{z} - \bar{\boldsymbol{z}})}{\sqrt{\left[(\boldsymbol{x}_i - \bar{\boldsymbol{x}}_i)^T(\boldsymbol{x}_i - \bar{\boldsymbol{x}}_i)\right]\left[(\boldsymbol{z} - \bar{\boldsymbol{z}})^T(\boldsymbol{z} - \bar{\boldsymbol{z}})\right]}} \tag{2.36}$$

2.3.5 Methods of Parameter Estimation

After the model structure has been identified the next step is to estimate the unknown parameters in the model. The most common methods used for aircraft parameter estimation include the output-error method and the equation-error method [1]. Another less common method is the filter-error method. In an experiment to identify a model for the Cessna Citation II aircraft, the output-error method and equation-error method both yielded similar results [15]; the output-error method was shown to have somewhat better prediction abilities than the equation-error method, however, the output-error method was slower computationally. The equation-error method is typically based on the method of least-squares regression and minimizes the difference between aerodynamic forces and moments calculated from flight test data and aerodynamics forces and moments predicted by a mathematical model. A solution using this approach constitutes a linear optimization problem. The output-error method minimizes the weighted summation of square differences between measured aircraft outputs and outputs computed by the mathematical model through integration of the aircraft equations of motion. This method results in a more computationally intensive nonlinear optimization problem [1]. For linear systems, the task of parameter estimation may be formulated in the frequency domain; this section, however, will be primarily focused on time domain parameter estimation.

Equation-Error Method

Equation-error methods refer to a series of methods which minimize a cost function directly in terms of an analytical relationship between model terms and the dependent variable. One form of the equation-error family of methods is the least-squares regression which minimizes the sum of squared errors between the actual response and computed response [2].

For an aircraft, the independent variables, or explanatory variables, are typically the velocity, angular rates, the aerodynamic angles and the deflections of the different control surfaces. The dependent variables, or response variables, are typically the aerodynamic forces and moments. Another form of an equation-error method is a maximum likelihood formulation which requires a linear state space form of the equations of motion with the response variables being the state derivatives [1]. For the remainder of this work, the equation-error method will refer to the least-squares formulation where the response variables are the aerodynamic forces and moments.

The least-squares parameter estimation formulation is shown in Equation (2.37) [2]. Here $z(k)$ is the measured dependent variable containing N total data points collected at discrete points k. A series of n independent variables $x_1(k)$, $x_2(k)$, ..., $x_n(k)$ are sampled at the same time as the corresponding dependent variable. The dependent variables are linearly dependent on each independent variable multiplied by a corresponding unknown coefficient Θ_1, Θ_2, ..., Θ_n and an error term $\epsilon(k)$ which contains the error between the model prediction of the dependent variable and the actual measured dependent variable. A bias term can be added as an independent variable to Equation (2.37). The equation error $\epsilon(k)$ at a discrete point of time is given in Equation (2.38). The method of least-squares requires that the errors, or residuals, are unrelated to the values of the independent variables, the distribution of residual variation is constant with time and the residuals are a zero mean, white noise process. It is also assumed that the independent variables are exact and have zero noise [2].

$$z(k) = \Theta_1 x_1(k) + \Theta_2 x_2(k) + ... + \Theta_n x_n(k) + \epsilon(k), \quad k = 1, 2, ..., N \tag{2.37}$$

$$\epsilon(k) = z(k) - [\Theta_1 x_1(k) + \Theta_2 x_2(k) + ... + \Theta_n x_n(k)] \tag{2.38}$$

The vector of unknown parameters Θ is calculated by finding the minimum of the

sum of squared residuals. The least-squares cost function $J(\Theta)$ is shown in Equation (2.39) where $\boldsymbol{z}$ is a $N \times 1$ vector containing all discrete $z(k)$ and $\boldsymbol{X}$ is a $N \times n$ matrix containing all $x_1(k)$, $x_2(k)$, ..., $x_n(k)$. The gradient of the cost function is shown in Equation (2.40). Since the equation-error is a linear function of all unknown parameters, the cost function is minimized by equating its gradient to zero which leads to Equation (2.41). Finally, the least-squares estimate of the unknown parameters $\hat{\Theta}$ is obtained using Equation (2.42) which requires the assumption that the information matrix, $\boldsymbol{X}^T\boldsymbol{X}$, is non-singular [2].

$$J(\Theta) = \frac{1}{2}\sum_{k=1}^{N}\epsilon(k)^2 = \frac{1}{2}[\boldsymbol{z} - \boldsymbol{X}\Theta]^T[\boldsymbol{z} - \boldsymbol{X}\Theta] \tag{2.39}$$

$$\frac{\partial J(\Theta)}{\partial \Theta} = -\boldsymbol{z}^T\boldsymbol{X} + \Theta^T\left(\boldsymbol{X}^T\boldsymbol{X}\right) \tag{2.40}$$

$$\boldsymbol{X}^T\boldsymbol{z} = \left(\boldsymbol{X}^T\boldsymbol{X}\right)^T\Theta \tag{2.41}$$

$$\hat{\Theta} = \left(\boldsymbol{X}^T\boldsymbol{X}\right)^{-1}\boldsymbol{X}^T\boldsymbol{z} \tag{2.42}$$

Under the assumption that residuals are independent, the parameter covariance matrix $\boldsymbol{P}$ is given in Equation (2.43) which requires an estimate of the measurement error variance $\hat{\eta}^2$ shown in Equation (2.44) [1, 2]. The standard error σ_i of each parameter Θ_i estimate is the square root of the respective diagonal elements of $\boldsymbol{P}$ (Equation (2.45)). The correlation coefficient ρ_{ij} between individual parameter estimates Θ_i and Θ_j is given in Equation (2.46). When using measured flight test data, the local residuals are often not independent of surrounding residuals because they are ordered by the respective time they occurred, which effects the covariance matrix for the estimated parameters. A correction to account for the fact that residuals are correlated for regression methods is discussed in Morelli and Klein [1].

$$\boldsymbol{P} = \hat{\eta}^2\left(\boldsymbol{X}^T\boldsymbol{X}\right)^{-1} \tag{2.43}$$

$$\hat{\eta}^2 = \frac{1}{N-n}\sum_{k=1}^{N}\left(z(k) - \boldsymbol{x}(k)\hat{\Theta}\right)^2 \tag{2.44}$$

$$\sigma_i = \sqrt{p_{ii}} \tag{2.45}$$

$$\rho_{ij} = \frac{p_{ij}}{\sqrt{p_{ii}p_{jj}}} \tag{2.46}$$

The equation-error method can be nonlinear in explanatory variables, but the parameters to be estimated must be linearly related to the outputs. The solution to this method is algebraic and does not involve integration of the aircraft equations of motion. It also does not require iterative methods which makes this method very computationally efficient. The equation-error approach is also valid even if an aircraft is unstable. The equation-error method can also be used to estimate parameters from multiple maneuvers in parallel by appending different maneuvers together in the same data set. This requires the assumption that the relative noise of the maneuvers is similar and that the model parameters are supposed to be the same. The equation-error method does not require the data points be in the order of occurrence [1]. The solution accuracy of this method is governed by the quality of the measurements. The assumption is made that there is no noise or error present in the explanatory variables and the response variable contains only random noise. For this method to be effective, the errors must be minimized by using good instrumentation and data processing [2].

Output-Error Method

The output-error approach minimizes the error between predicted and measured output values using an iterative optimization approach. The mathematical model that the parameters are fit to can be nonlinear, and thus, the parameter estimation using this method is valid for the nonlinear aircraft equations of motion [1]. Due to the complexities in op-

timization, the computational cost of this method can be high. Weighted least-squares is the simplest method in this class, but the principle of maximum likelihood is a more robust scheme that is used more in practice [2]. The output-error method assumes a model structure and identifies parameters such that the model is able to predict the dynamic response of an aircraft. The problem setup for an aircraft using the output error method uses the form of the aircraft equations of motion in Equations (2.14)-(2.16). This model does not include methods to account for process noise, which includes atmospheric turbulence and wind [16].

Maximum likelihood estimates are asymptotically unbiased and consistent [1, 2]. For a fixed model structure assumed to be representative of the system, the vector of maximum likelihood parameter estimates $\hat{\Theta}$ will approach their true values Θ as the amount of data increases. The estimate of the minimum variance in individual parameter estimates are given by the Cramér-Rao lower bound (discussed in further detail below) which also theoretically approaches its true value as the amount of data increases [17]. The distribution of parameter estimates obtained from different data sets approaches a normal distribution as the amount of data increases [2].

Several assumptions must be made to use the maximum likelihood formulation of output-error method. The system inputs must be independent of system outputs and the control inputs must be able to excite the dynamic modes of the system. The measurement errors at individual points in time must be independent events and the system can only have error due to measurement noise. After making these assumptions, the cost function used in optimization is given in Equation (2.47), where N is the number of data points at discrete points in time t_k, $\boldsymbol{y}(t_k)$ is the model output vector at each point in time, $\boldsymbol{z}(t_k)$ is the vector of system output measurements at each point in time and $\boldsymbol{R}$ is the measurement covariance matrix [2]. In most cases, the matrix $\boldsymbol{R}$ is unknown so the estimate shown in Equation (2.48) may be used [2]. Typically only the diagonal elements of $\boldsymbol{R}$ are used to

reduce computation time by incorporating the assumption that measurement noise of the outputs are unrelated [1]. The objective is then to find values in the vector of unknown parameters Θ that minimize the cost function $J(\Theta)$ using a nonlinear optimization method.

$$J(\Theta) = \frac{1}{2}\sum_{k=1}^{N}[\boldsymbol{z}(t_k) - \boldsymbol{y}(t_k)]^T \boldsymbol{R}^{-1}[\boldsymbol{z}(t_k) - \boldsymbol{y}(t_k)] \tag{2.47}$$

$$\boldsymbol{R} = \frac{1}{N}\sum_{k=1}^{N}[\boldsymbol{z}(t_k) - \boldsymbol{y}(t_k)][\boldsymbol{z}(t_k) - \boldsymbol{y}(t_k)]^T \tag{2.48}$$

The cost function is commonly minimized using the Gauss-Newton algorithm for the purpose of time domain aircraft system identification. This method is a second-order nonlinear optimization algorithm that is a derivative of the Newton-Raphson method. The estimates Θ are systematically updated at each iteration i using Equation (2.49), where each update is improved by solving Equation (2.50) at each iteration [2]. The gradient of the cost function is given in Equation (2.51) and, under the assumption of zero mean noise and independence between data points, the Hessian of the cost function can be estimated using Equation (2.52) [2].

$$\Theta_{i+1} = \Theta_i + \Delta\Theta \tag{2.49}$$

$$\Delta\Theta = -\left[\left(\frac{\partial^2 J}{\partial\Theta^2}\right)_i\right]^{-1}\left(\frac{\partial J}{\partial\Theta}\right)_i \tag{2.50}$$

$$\frac{\partial J}{\partial\Theta} = -\sum_{k=1}^{N}\left[\frac{\partial \boldsymbol{y}(t_k)}{\partial\Theta}\right]^T \boldsymbol{R}^{-1}\left[\boldsymbol{z}(t_k) - \boldsymbol{y}(t_k)\right] \tag{2.51}$$

$$\frac{\partial^2 J}{\partial\Theta^2} \approx \sum_{k=1}^{N}\left[\frac{\partial \boldsymbol{y}(t_k)}{\partial\Theta}\right]^T \boldsymbol{R}^{-1}\left[\frac{\partial \boldsymbol{y}(t_k)}{\partial\Theta}\right] \tag{2.52}$$

There are several problems that could arise from the nonlinear optimization problem. The cost function may have multiple points of local minima, or the cost function may not be continuous. This requires that the starting value of Θ be close to the global minimum.

Initial estimates of Θ may be obtained using the regression methods discussed above, which can help to alleviate this potential problem [1].

The theoretical best accuracy of the estimates is given by the Cramér-Rao lower bound. An approximation of the parameter error covariance matrix, $\boldsymbol{P}$, for a maximum likelihood estimate is shown in Equation (2.53); this is simply the inverse of the Hessian used for optimization (Equation (2.52)) which is already available information at each optimization iteration [2]. The elements on the diagonal of $\boldsymbol{P}$ are the variances of each of the respective parameter estimates Θ. The Cramér-Rao bounds are synonymous with the standard errors σ_i of each individual parameter estimate Θ_i which is the square root of the variance of each parameter, as shown in Equation (2.54) [2]. The Cramér-Rao bounds are calculated under the assumption that the output residuals are white, Gaussian and have constant distribution properties with time. Real flight test data typically contains colored noise which is inconsistent with the assumptions in the output-error method [17].

$$\boldsymbol{P} \approx \left(\sum_{k=1}^{N} \left[\frac{\partial \boldsymbol{y}(t_k)}{\partial \Theta} \right]^T \boldsymbol{R}^{-1} \left[\frac{\partial \boldsymbol{y}(t_k)}{\partial \Theta} \right] \right)^{-1} \tag{2.53}$$

$$\sigma_i = \sqrt{p_{ii}} \tag{2.54}$$

Standard Cramér-Rao bounds are typically too optimistic because the residuals of the outputs are typically colored and correlated with surrounding values [17]. Residuals become colored because of model structure errors, unmodeled dynamics and the necessary overall simplifications for implementation. Measurement noise in the output-error method is assumed to be white, Gaussian, and band-limited by the Nyquist frequency. These assumptions are made for simplified implementation of the methods, but are often violated which is why the standard Cramer-Rao lower bounds severely under-predicted the actual variance in parameter estimates [17].

The meaning of a colored residual is that power spectral densities of the output residuals have uneven distribution of power across the frequency spectrum [1]. The assumption of white residuals put more simply assumes that the model structure used for parameter estimation perfectly represents the flight data, which is not the case in estimation from experimental data. The assumption of white output residuals will, however, hold for simulation data.

Morelli and Klein [1, 17, 18], proposed a post-processing method to account for the presence of colored residuals in aircraft parameter estimation. The corrected parameter covariance matrix, $\boldsymbol{P_c}$, accounting for residual coloring and time correlation is shown in Equation (2.55), where the form presented in Morelli and Klein [1, 17, 18] has been modified slightly to be consistent with the notation used in this work. In this equation, $\boldsymbol{P}$ is the ordinary parameter covariance matrix calculated in Equation (2.53), $\boldsymbol{R}$ is the measurement covariance matrix calculated using Equation (2.48) and $\hat{\mathfrak{R}}_{vv}$ is the autocorrelation matrix for the residuals of the outputs estimated using Equation (2.56). The parameter m in Equation (2.56) sets the maximum time step used to calculate the autocorrelation matrix. The standard error accounting for colored residuals σ_{c_i} of each parameter estimate Θ_i is given in Equation (2.57). A different approach to accounting for residual coloring suggested by Jategaonkar [2], is to simply multiply the standard error bounds assuming white residuals by a "fudge factor" of 5 to 10.

$$\boldsymbol{P_c} = \boldsymbol{P}^{-1}\left[\sum_{k=1}^{N}\left[\frac{\partial \boldsymbol{y}(t_k)}{\partial \Theta}\right]^T \boldsymbol{R}^{-1}\sum_{j=1}^{N}\hat{\mathfrak{R}}_{vv}(k-j)\boldsymbol{R}^{-1}\left[\frac{\partial \boldsymbol{y}(t_j)}{\partial \Theta}\right]\right]\boldsymbol{P}^{-1} \tag{2.55}$$

$$\hat{\mathfrak{R}}_{vv}(i) = \hat{\mathfrak{R}}_{vv}(-i) = \frac{1}{N}\sum_{k=1}^{N-i}\left[\boldsymbol{z}\left(t_k\right) - \boldsymbol{y}\left(t_k\right)\right]\left[\boldsymbol{z}\left(t_{k+i}\right) - \boldsymbol{y}\left(t_{k+i}\right)\right]^T,\ i = 0, 1, 2, ..., m \tag{2.56}$$

$$\sigma_{c_i} = \sqrt{p_{c_{ii}}} \tag{2.57}$$

The correlation coefficient, ρ_{ij}, is a measure of the dependence of the different parameters Θ_i and Θ_j on one another and is calculated using elements of $\boldsymbol{P}$ as shown in Equation (2.58). If the correlation coefficient is greater than 0.9, the estimation may require reformulation, and if the correlation coefficient is greater than 0.95, the estimated parameters are considered nearly linearly dependent. Linear dependence is an undesirable property of a model that means nearly the same model can be obtained by changing parameters proportionally which are nearly linearly dependent [2]. This phenomena, also termed data collinearity, causes problems in parameter estimation because the effects of different signals on the aircraft dynamics cannot be adequately separated [1]. Small values of the standard errors σ_i and correlation coefficients ρ_{ij} indicate high accuracy of the parameter estimates [2].

$$\rho_{ij} = \frac{p_{ij}}{\sqrt{p_{ii}p_{jj}}} \tag{2.58}$$

Filter-Error Method

The filter-error method is built off of the output-error method and includes methods for removing both process noise and measurement noise. This method allows parameter estimation from data corrupted by atmospheric turbulence and may improve results from data that is seemingly low noise. The method incorporates a Kalman filter or extended Kalman filter for state estimation into the parameter estimation optimization procedures which usually leads to superior results. The downside to the filter-error method is significantly increased complexity compared to the output-error and equation-error methods [2]. It is for this reason that the filter-error method is not developed further or used in this system identification effort but is included for completeness.

2.3.6 Model Validation and Uncertainty Analysis

Due to the fact that models are estimates of reality, validation of a particular model is important to determine if it is adequate for describing the true aerodynamic interactions of the aircraft. Investigation of model validity requires statistical analysis of estimated parameters and the ability of the model to predict aircraft motion. The overall objective of this step is to determine if the identified model will be satisfactory for its intended use [2].

In order to improve confidence and increase the merit of parameter estimates from individual flight maneuvers, their respective uncertainties must be investigated. As discussed previously in Section 2.3.5, a metric of uncertainty of parameter estimate for a fixed model structure is the predicted standard error of the parameters. For the output-error method, this is quantified by the Cramér Rao lower bound, which is the predicted minimum variation in the parameter estimate [17]. The uncertainty of the parameter estimates can be decreased by including more or higher-quality data [16].

Another metric of uncertainty is the distribution of parameter estimates from several different maneuvers designed to estimate the same parameters. For any maximum likelihood method, such as the output-error method, as the amount of data increases, the probability distribution of the estimated parameters emulates a Gaussian distribution with its center approaching the actual value of the parameter [17]. Analysis of the probability distribution provides increased confidence in the uncertainty estimate because it includes a larger amount of information about the variability of estimates compared to the results from a single maneuverer. This is why confidence in parameter estimates can be increased by performing the same maneuver multiple times and averaging the values of the parameters computed [1].

The ability of a model to predict motion of an aircraft is analyzed by comparing the simulated model response to the measured outputs of a flight maneuver subject to the same

inputs. Flight maneuvers that are not used to identify the model should be used to check the model accuracy, thus, it is important to collect data both for model development and model validation. Important considerations in collecting validation maneuvers are choosing the right comparison data, initial conditions and validation criteria. In a perfect situation, it is best to use the exact initial conditions and control inputs in the validation flight data. However, it may be necessary to average the first few data points to use as an initial condition to reduce noise or adjust the initial conditions slightly to test the model accuracy. It may also be necessary to allow slight biases in the control inputs [2]. Additionally, it may be necessary to tweak the bias terms in the model to correct for slight measurement bias errors [1]. The model is considered adequate if the measured response matches the response obtained through simulation of the model within a certain allowable variation. The set tolerances are checked more rigorously for the relevant outputs of the dominant axis of the maneuver whereas for the less significant axes, a general visual match is acceptable [2].

2.3.7 System Identification Programs for Aircraft (SIDPAC)

System IDentification Programs for AirCraft (SIDPAC) is a MATLAB based collection of programs developed for the process of aircraft system identification [19]. These programs were developed over an extended period of time by Eugene A. Morelli at NASA Langley Research Center. The programs have been validated extensively through various flight test programs and wind tunnel tests. SIDPAC contains a series of different methods for system identification of aircraft, however, choice of methods and data processing is left as a task to the user. The programs are written such that they are largely non-automated requiring user knowledge and decision making throughout the system identification process. The user must be fully knowledgeable about system identification methods and their implementation in order to obtain quality results. The routines are written in this manner

because system identification problems for aircraft are typically different based on the individual application and each require modified methods of analysis. Several routines included in SIDPAC were used for this system identification effort, each of which are described in Morelli and Klein [1].

2.4 System Identification of Small, Fixed-Wing UAVs

System identification is a useful tool for model development, simulation and control system design for small unmanned aerial vehicles (UAVs). UAVs can be used for a variety of applications requiring models of their dynamics including scientific data collection and aerial imaging. One critical design goal of autonomous systems is a dependable control system that can ensure public safety while completing the desired mission and returning unharmed. Control systems must be robust enough to recover from challenges such as turbulence or unmapped obstacles and reliable so that the mishap rate is very low. Quality flight dynamics models are needed to develop a control system meeting these requirements [11].

UAVs face several differences compared to full-scale aircraft including high maneuverability due to proportionally lower moments of inertia, larger effects due to propulsive forces and moments, and slow speeds with a corresponding lower Reynolds number. These effects may render parameter estimation from wind tunnel testing less effective. Additionally, the significant time and money associated with conducting wind tunnel testing makes them unpractical for low-cost UAVs. Models of fixed-wing UAVs may also be developed from analytical techniques and computational fluid dynamics (CFD), but it may be difficult to develop accurate estimates for all parameters needed for the model to be useful. UAV flight testing for system identification can provide remedies to many of these difficulties by

providing the ability to identify a useful flight dynamics model from the flight data [11].

Similar to full-scale aircraft, system identification for UAVs is defined by developing a mathematical relationship between control inputs and the dynamic response of the aircraft. The process is similar to the procedures described in Section 2.3 but include other additional considerations specific to small, low-cost UAVs. System identification flight tests are typically performed by a ground-based pilot due to challenges associated with programming an autopilot system to perform maneuvering, although, system identification efforts which utilized autopilot capabilities have been performed [11]. Small UAVs have payload limits and small cargo space which limits the ability to have quality sensors and computing ability on-board. The sensors are also limited by the low-cost nature of the aircraft and, therefore, cannot be prohibitively expensive. Certain important parameters, such as aerodynamic angles (α, β), may not be accurately computed or be available at all. Additionally, the data accumulated from flight testing of a small UAV may be noisy rendering it a challenge to perform accurate system identification. The challenges associated with accuracy of data collection can make certain methods acceptable for use with full-scale aircraft inaccurate for small, low-cost UAVs [6].

The remainder of this section will describe past work in the field of system identification of small, fixed-wing UAVs. Previous research efforts have implemented different system identification methods in both the time domain and frequency domain. The intent of this section is not to describe all past work in this heavily populated field, but rather highlight noteworthy procedures specific to small fixed-wing UAVs which have been successfully implemented in other UAV identification efforts. Hoffer et al. [11] provides an extensive list of references of many past UAV system identification research efforts. The bold titles which will follow are the corresponding title of the respective work which will be described.

Development and Modeling of a Low-Cost Unmanned Aerial Vehicle Research Platform [4]

Arifianto and Farhood [4], described the development of a fixed-wing UAV intended to be used for control system research requiring identification of a model of the aircraft's flight dynamics. The platform was developed using a commercially available fixed-wing UAV and commercially available sensors with the exception of airdata probes developed by the researchers. The instrumentation system included an altitude and heading reference system (AHRS), global positioning system (GPS), and the aforementioned airdata probes used to measure angle of attack, angle of sideslip and airspeed. The moments of inertia of the aircraft were measured experimentally using the compound pendulum method for all axes since a small UAV can be easily tilted sideways for measurement, contrary to full-scale aircraft. A thrust model was developed for the propeller using the Javaprop applet which incorporates blade element theory [20]. The thrust model was a function of throttle setting and airspeed assuming that the motor ran at constant RPM for a given throttle setting.

The time domain formulation of the output-error method was used to estimate the unknown parameters in a longitudinal and lateral-directional aerodynamic model of the aircraft. This method was chosen due to its ability to account for measurement noise while still using an algorithm which had a practical computational expense. Flight test data was collected using the Short Period, Dutch Roll and Bank-to-Bank Roll maneuvers because they could be adequately performed by a ground-based pilot. The Short Period maneuver was performed using a 3-2-1-1 elevator input, the Dutch Roll maneuver was performed with a doublet (1-1) rudder input and the Bank-to-Bank Roll maneuver was performed using a 1-2-1 aileron input. The pilot experienced difficulty in achieving trim prior to system identification maneuvers so multiple tests were performed and only the maneuvers where trimmed steady level flight was achieved were used in the system identification process. The specified control

inputs for the maneuvers themselves were implemented by the flight computer at a fixed time step. The structure of the model used was mostly linear, with nonlinearity in C_X, C_Z and C_m in the form of α^2. The structure was chosen such that a single model could describe all dynamics in the flight regimes of interest. The end result of the effort was a "reasonably accurate" model of the aircraft dynamics [4].

Two-Step System Identification and Trajectory Tracking Control of a Small Fixed-Wing UAV [5]

Grymin and Farhood [5] developed a model for the same small UAV used in [4], but incorporated some notable different methods of analysis which is why it is described here. The equation-error method was used for parameter estimation with a technique called estimation-before-modeling (EBM) [21]. EBM is a method which includes uses of an extended Kalman filter (EKF) for obtaining time histories of aircraft states and aerodynamic forces and moments when the measured values contain flaws from measurement noise or sampling rate. EBM is presumably used in this work because the equation-error method requires nearly noise-free estimates of aircraft states. The flight test data was collected by performing the Short Period, Dutch Roll, Bank-to-Bank Roll and Throttle Doublet maneuvers. The model structure was developed using the stepwise regression method and resulted in a nonlinear model structure which included polynomial spline models with knot points depending on the values of certain aircraft states. The model created was analyzed using forward simulation and its performance was characterized quantitatively using the goodness of fit (GOF) and Theil's inequality coefficient (TIC) [22] metrics. The model validation showed that the model was able to successfully characterize the aircraft dynamics for its intended application.

System Identification for Small, Low-Cost, Fixed-Wing, Unmanned Aircraft [6]

Dorobantu et al. [6] performed system identification from flight test data of a small, fixed-wing UAV using a method similar to the output-error method formulated in the frequency domain. A linear aerodynamic model was identified for the longitudinal and lateral-directional dynamics using only accelerometers and rate gyroscope measurements from an inertial measurement unit (IMU) and controls data. A preliminary model of the UAV's flight dynamics was obtained from wind tunnel tests of UAVs with similar aerodynamics but of different scales; this information was used to design the flight test experiments for system identification. For the flight experiments, the aircraft was manually brought to steady level flight, and then the flight computer performed a designed frequency sweep input which consisted of logarithmically varying sine waves. During the frequency sweeps the pilot needed to manually assist the aircraft to keep it on course. Pilot flown doublet inputs were also collected for validation of the model in the time domain. Certain parameters in the longitudinal model were difficult to estimate from flight test data and were fixed to those in the baseline model obtained from wind tunnel testing. Validation in the time domain indicated good modeling results and showed that the preliminary model created from wind tunnel testing had poor accuracy of the actual dynamics in flight.

Modeling with Vortex Lattice Method and Frequency Sweep Flight Tests for a Fixed-Wing UAV [7]

A work by Park [7] used the vortex lattice method (VLM) and flight testing to develop a linear model of flight dynamics of a small, fixed-wing UAV in the frequency domain. The preliminary stability and control derivatives for the UAV were obtained from VLM using the Athena Vortex Lattice (AVL) software. The experimental UAV's instrumentation system for flight testing included an altitude and heading reference system (AHRS), global positioning

system (GPS), and a pitot-static tube for airspeed measurements. Flight test experiments were performed using frequency sweeps of exponential chirp signals. The frequency response of the model created from VLM was then compared to the flight data containing frequency sweeps. This comparison was used to correct for deficits in the model created strictly from VLM to better represent the flight test data—specifically the normal acceleration, lateral acceleration, pitch rate, roll rate and yaw rate measurements were used for this process. The results indicated that all the control derivatives were over-predicted by VLM and were reduced by trial and error such that the model better represented the frequency response of the flight data. This can be attributed to the fact that VLM tends to over-predict control authority because unmodeled viscous effects become important in deflection of control surfaces [23]. The coefficient C_{n_β} also needed to be modified due to unmodeled propeller effects which were amplified by the flat plate fuselage configuration of the aircraft. After the aforementioned modifications were made to the longitudinal and lateral-directional model created from VLM, the model was able to adequately represent the flight test data.

Research on Highly-Accurate Aerodynamic Parameter Identification [8]

Shenglu et al. [8] described system identification of a linear longitudinal model of a small UAV using the output-error method in the time domain. The UAV was instrumented with an altitude and heading reference system (AHRS), airdata probes and a sensor to measure control surface defection angle. The longitudinal dynamics were excited using a 2-1-1 elevator input command. The work empirically illustrated that the scatter of parameter estimates taken from separate flight maneuvers follows a Gaussian distribution centered at the mean parameter estimate. The work also showed that the standard Cramér-Rao bound for individual parameter estimates underpredict the error bounds due to the fact that the residuals from flight test data are typically colored [18]. The correction for colored residuals discussed in Morelli and Klein [1, 17, 18] was applied to the Cramér-Rao bounds

of the parameter estimates which better represented the scatter in the data of parameter estimation obtained from separate flight maneuvers.

2.5 Vortex Lattice Method (VLM)

The vortex lattice method (VLM) is a numerical method for the solution for flow over an arbitrary wing. It is based on the ideal flow model and the solution to Laplace's equation, and thus, carries the assumptions that the flow is incompressible, inviscid and that the aerodynamic angles remain small. The effect of wing thickness is also neglected [23]. The solution can be used to compute the pressure distribution and then estimate aerodynamic characteristics and stability and control derivatives of an aircraft. VLM is a generic method in the sense that it can be used to define a wide range of aircraft geometry where methods such as lifting line theory would not be applicable [24].

One formulation of VLM uses a series of horseshoe vortices of variable strengths Γ to model the surface of the wing. A panel on the surface of the wing is composed of a control point at the 3/4 chord of the panel and a vortex filament at the quarter chord of the panel which is bent 90° at the spanwise edge of the panel and extended infinitely trailing the wing. The induced velocity normal to the surface at each control point due to a vortex filament is calculated using the Biot-Savart law, Equation (2.59), where Γ is the strength of the vortex filament, $\boldsymbol{ds}$ is a differential length along the vortex filament, $\boldsymbol{r}$ is the distance to the control point and $\boldsymbol{dV}$ is the velocity induced by the vortex filament. The total normal velocity induced at a control point is calculated by summing the contributions from all horseshoe vortices on the wing. The strength of each horseshoe vortex is set by enforcing the condition that there is no component of velocity normal to the surface of the wing. This results in a linear system of equations that is solved for the strength of each vortex filament [25]. Another

version of the vortex lattice approach models the wing surface using a series of vortex ring elements using a similar implementation [26]. This approach has the added benefit that the boundary conditions on the wing surface can be satisfied exactly which allows more flexibility in wing shape, notably permitting the wing to be cambered.

$$\boldsymbol{dV} = \frac{\Gamma}{4\pi}\frac{\boldsymbol{ds}\times\boldsymbol{r}}{|\boldsymbol{r}|^3} \tag{2.59}$$

VLM requires attention to details in its implementation to produce good results. The total number of lines defining the surface outline should be minimized, the wing tips should be parallel to the streamwise direction, and the trailing vortices from a surface cannot collide with the control points of a trailing surface. Additionally, the effect of different panel distributions should be studied. Past results have shown that a good solution is obtained with a large amount of panels along the span compared to the number of panels along the chord [23].

The XFLR5 Analysis Tool

XFLR5 is an aerodynamics analysis program designed for use with subsonic, low Reynolds number aircraft [27]. XFLR5 has the the ability to implement XFOIL for airfoil analysis, and lifting line theory, vortex lattice methods (VLM) and 3D panel methods for wing and airplane analyses. This research effort is primary interested in XFLR5's capability to efficiently define aircraft geometry for implementation in VLM and its stability and control analysis using VLM.

The XFLR5 stability analysis code is based on the dynamic model postulated in Etkin and Reid [12], where longitudinal and lateral-directional modeling is considered independent. The code assumes a linear aerodynamic model shown in Equations (2.60)-(2.65) and is

designed for use with small perturbation theory. XFLR5 computes the following dimensional stability derivatives: X_u, X_w, Z_u, Z_w, Z_q, M_u, M_w, M_q, Y_v, Y_p, Y_r, L_v, L_p, L_r, N_v, N_p, N_r, and the associated non-dimensional stability derivatives. The control derivatives may also be calculated. The software also computes the longitudinal and lateral-directional state matrices and estimates of the dynamic modes of the aircraft [24]. The stability analysis capability models the wing using the ring vortex approach that was discussed above [26]. It is recommended in the code and guidelines to analyze the aircraft without the fuselage, i.e. typically only the wing and horizontal/vertical tail are defined for analysis. Omission of the body has been shown to have negligible effects on the results while avoiding potential numerical problems by including it [28]. The results from the stability analysis have been validated against those calculated with the Athena Vortex Lattice (AVL) software [29].

$$\Delta X = X_u \Delta u + X_w w + X_{\delta e} \delta e \tag{2.60}$$

$$\Delta Y = Y_v v + Y_p p + Y_r r + Y_{\delta a} \delta a + Y_{\delta r} \delta r \tag{2.61}$$

$$\Delta Z = Z_u \Delta u + Z_w w + Z_q q + X_{\delta e} \delta e \tag{2.62}$$

$$\Delta L = L_v v + L_p p + L_r r + L_{\delta a} \delta a + L_{\delta r} \delta r \tag{2.63}$$

$$\Delta M = M_u \Delta u + M_w w + M_q q + X_{\delta e} \delta e \tag{2.64}$$

$$\Delta N = N_v v + N_p p + N_r r + L_{\delta a} \delta a + L_{\delta r} \delta r \tag{2.65}$$

Chapter 3

Methods of Analysis

This chapter presents the procedures for the system identification process used in this research effort. The process began by measuring inertial and geometric properties of the experimental aircraft. This information was then used to develop a vortex lattice method (VLM) model of the aircraft to obtain preliminary information about the aircraft dynamics before flight experiments. Experimental flight test procedures were developed and implemented to collect an abundance of flight data. The raw flight test data was analyzed and conditioned to be used for system identification. A model structure was developed from the flight test data and parameter estimation was performed to develop the model of aerodynamic forces and moments on the aircraft. Methods were investigated to improve the parameter estimation results using information obtained from VLM and dividing the task of parameter estimation between different maneuvers. The model accuracy was finally analyzed to determine its validity and estimate its uncertainty. The general process is shown in Table 3.1.

3.1 Preliminary Data Collection and Analysis

As a prerequisite for formal system identification of an aircraft, properties of the aircraft must be measured and experimental data containing information of the relevant aircraft dynamics must be obtained. For system identification from flight test data, the

Table 3.1: Process used for system identification of the experimental UAV

Measurements of Inertial and Geometric Properties
↓
Vortex Lattice Method (VLM) Analysis
↓
Experimental Design
↓
Flight Test Data Collection
↓
Data Conditioning
↓
Kinematic Consistency Check
↓
Model Structure Identification
↓
Equation-Error Method Parameter Estimation
↓
Output-Error Method Parameter Estimation
↓
Model Validation and Uncertainty Analysis

mass and moments of inertia of the aircraft must be known or measured. For analysis using computational methods, additional geometric and inertial properties of the aircraft geometry must be accurately determined; this requires precise knowledge of the wing and tail dimensions, relative locations, incidence angles and mean camber lines, as well as the position of the aircraft center of gravity. Preliminary knowledge of the aircraft dynamics is useful for design and implementation of flight test experiments used for system identification. Quality data from flight testing which excites the dynamic modes of the aircraft may then be used to determine a mathematical model to describe the aircraft dynamics.

3.1.1 Properties of the Experimental Aircraft

The UAV used for this research effort was the HobbyKing™ Bix3 trainer [3]. The Bix3, pictured in Figure 3.1, is a small, fixed-wing UAV that has capability of modification for a variety of applications. The airframe used for research has a mass of 1.20 kg (2.65 lbs) and a wingspan of 1.54 m (5.05 ft). The Bix3 is powered by a propeller mounted behind the wing. The aircraft has traditional control surfaces with the standard elevator, ailerons and rudder. The Bix3 also has flaps, but they were not used or considered in the analysis. The cost of the stock aircraft is approximately $150 [3]. Important properties of the aircraft are shown in Table 3.2.

Figure 3.1: HobbyKing™ Bix3 aircraft

Table 3.2: Mass and geometric properties of the HobbyKing™ Bix3 aircraft

Property	Abbreviation	Value	Units
Mass	m	1.20	kg
Mean Aerodynamic Chord	$\bar{c}$	0.188	m
Projected Wing Span	b	1.54	m
Projected Wing Area	S	0.285	m^2

The aircraft was instrumented with a Pixhawk on-board flight computer [30]. The Pixhawk hosted sensors that were on-board the aircraft included an inertial measurement

unit (IMU), an attitude and heading reference system (AHRS), a global positioning system (GPS) and an airspeed sensor. Notably the aircraft lacked airdata probes used to measure aerodynamic angles (α, β) and the airspeed sensor was known from past experience to be unreliable. The Pixhawk contains an extended Kalman filtered (EKF) state estimation system that can improve accuracy and smooth measured data including orientation angles, earth-fixed velocity and position [31]. The pulse-width modulation (PWM) output signals from the control surface servos were also recorded. The important data fields used in analysis are shown in Table 3.3. The sampling rate of the raw IMU (accelerometers, rate gyros) and GPS data was 50 Hz; the sampling rate of the control signals, AHRS and EKF data was 25 Hz.

Table 3.3: Sources of key measurements from flight test data

Measurement Name	Source	Data Field	Abbreviations	Units
Body-Axis Accelerations	Accelerometers	IMU	a_x, a_y, a_z	m/s^2
Body-Axis Angular Velocities	Rate Gyros	IMU	p, q, r	$^\circ$/s
Earth-Fixed Velocities	GPS (EKF)	NKF1	V_N, V_E, V_D	m/s
Orientation Angles	AHRS (EKF)	NKF1	ϕ, θ, ψ	$^\circ$
Control Signals	PWM Signals	RCOU	δe, δa, δr	μs

Experimental Determination of the Moments of Inertia of the Bix3 airframe

Analyzing the dynamics of rotational flight requires knowledge of the aircraft moments of inertia. A common method for experimental determination of moments of inertia is swinging an aircraft on a pendulum. The moment of inertia about each axis is determined individually by positioning the axis of interest parallel to the axis of rotation of the pendulum. For large scale aircraft, a compound pendulum is used to calculate the moments of inertia about the roll and pitch axes, I_x and I_y, as well as the product of inertia, I_{xz}. Due to the size and handling difficulties of a large aircraft, a bifilar torsional pendulum is used to measure the moment of inertia about the yaw axis, I_z. The moment of inertia of the pendulum about

the axis of rotation can be determined from geometry, mass and the period of the system for each pendulum type. The known moment of inertia of the pendulum apparatus is then subtracted from the moment of inertia of the complete system resulting in a measurement of the moment of inertia of the aircraft about the pendulum axis of rotation. The moment of inertia about the parallel axis passing through the aircraft center of gravity can finally be determined using the parallel axis theorem [32].

For small-scale UAVs where it is possible to position the aircraft sideways, all moments of inertia can be determined using a single type of pendulum. In this application, a compound pendulum was used to measure all moments of inertia for consistency and ease of implementation. The method used here was very similar to the test performed in Arifianto and Farhood [4]. The formula for determining the moment of inertia of the bare compound pendulum apparatus about the pendulum's axis of rotation, I_p, is given in Equation (3.1). Here m_p is the mass of the bare pendulum, g is the gravitational acceleration, L_p is the distance between the pendulum's axis of rotation and the center of gravity of the pendulum, and T is the period of the pendulum. The moment of inertia of the apparatus about the axis intersecting its center of gravity parallel to the rotation axis is obtained by subtracting $m_p L_p^2$ from Equation (3.1) by making use of the parallel axis theorem. The moment of inertia of the bare pendulum about the axis of rotation and about the parallel axis intersecting its center of gravity were calculated to be 1.700 kg·m^2 and 0.0832 kg·m^2, respectively.

$$I_p = \frac{m_p g L_p T^2}{4\pi^2} \tag{3.1}$$

Three separate tests were performed to determine the moments of inertia about the roll, pitch and yaw axes. The experimental setup of these tests can be seen in Figure 3.2. The axis of interest was placed parallel to the axis of rotation and the distance of the center

of gravity of the aircraft to the axis of rotation was measured. The experiment was run in three trials for each of the three axes. The period of 25 small-angle oscillations was recorded for each trial and used to determine the average oscillation period for each axis T_i. Equation (3.2) was then used to calculated the moment of inertia about each aircraft axis, I_i. In this equation, m_a is the aircraft mass, L_i is the distance from the axis of rotation to the aircraft center of gravity, T_i is the average oscillation period of the system for the respective axis and all other variables corresponded to the pendulum apparatus which were defined previously [4]. The calculated moments of inertia about the roll, pitch and yaw axes can be seen in Table 3.4. The products of inertia I_{xy} and I_{yz} are zero because the aircraft is symmetric about the xz plane. The magnitude of product of inertia, I_{xz}, is finite but is assumed to be insignificant and thus is set to zero. Neglecting I_{xz} was expected to have little effect on the parameter estimation process [33].

$$I_i = \frac{g(m_p L_p + m_a L_i)}{4\pi^2/T_i^2} - I_p - m_a L_i^2 \tag{3.2}$$

(a) Empty Pendulum (b) Roll Axis (c) Pitch Axis (d) Yaw Axis

Figure 3.2: Moment of inertia tests of the Bix3 aircraft using a compound pendulum; rotation for the (b) roll, (c) pitch and (d) yaw axes are side-to-side along the plane of the page

The error bound in the moment of inertia about each axis was postulated to be

Table 3.4: Calculated moments of inertia of the HobbyKing™ Bix3 aircraft

Property	Abbreviation	Value	Units
Roll Axis Moment of Inertia	I_x	0.095	kg·m^2
Pitch Axis Moment of Inertia	I_y	0.045	kg·m^2
Yaw Axis Moment of Inertia	I_z	0.12	kg·m^2
Product of Inertia	I_{xz}	~ 0	kg·m^2

approximately 0.005 kg·m^2. Errors could result from inaccuracies in measurements or slight variation in the aircraft's inertial properties with different battery and sensor placements, but will still be close the the values displayed in Table 3.4. Measurement error of moments of inertia has been shown to have little effect on the average parameter estimates, but inaccuracies increase the standard error of the parameter estimates [33].

3.1.2 Preliminary Analysis Using the Vortex Lattice Method

After measurement of aircraft inertial properties and geometry, the vortex lattice method (VLM) was used to obtain a preliminary model of the Bix3 aircraft dynamics. As will be shown in Chapter 4, parameter estimation from flight test data only in certain situations is inadequate for identification of a useful and accurate flight dynamics model. In order to remedy this problem, VLM will be used to supplement the information gained from the flight test data. Additionally, flight test design benefits from knowledge of the aircraft dynamic modes for design of control inputs. VLM was used to provide estimates of the aircraft dynamic modes prior to flight experiments.

The XFLR5 program that was introduced in Section 2.5 was used to develop preliminary estimates of the aircraft dynamics [27]. Specifically, its stability analysis capabilities were used to determine estimates of the linear stability and control derivatives. Only the stability derivatives were used for analysis, however, because VLM typically overestimates the

control derivatives. When control surfaces are deflected, viscous effects not modeled in VLM become significant causing overprediction of control authority [23]. The stability analysis in XFLR5 also provides the linearized longitudinal and lateral-directional state matrices which will be used to provide a preliminary estimate of the dynamic modes of the Bix3 aircraft.

The Bix3 model that was created in XFLR5 is shown in Figure 3.3. As suggested by the XFLR5 documentation [24, 27, 28, 29], the wing and horizontal/vertical tail were defined and the fuselage was omitted. This simplification is not expected to affect the quality of the final results, but can eliminate numerical difficulties associated with including the fuselage [28]. Several key parameters needed to create the model are shown in Table 3.5. These parameters are in addition to those specified in Table 3.2 and the measured geometry of the wing, horizontal tail and vertical tail. The Clark Y airfoil was used as an approximation to the airfoil on the Bix3 wing. In VLM, the airfoil mean camber line is used as the camber of the flat surface defining the model. The use of a flat airfoil for the wing was also investigated which had little effect on the results. The horizontal and vertical tail were defined as flat surfaces because these surfaces on the aircraft did not have any camber. The final model contained 4762 mesh elements which was chosen because increasing the amount of mesh elements beyond this number had little to no effect on the results. A large number of spanwise panels were defined compared to the number of chordwise panels which has been shown to produce quality results [23].

Table 3.5: Summary of key geometric properties of the Bix3 aircraft needed for VLM

Property	Value	Units
CG_x Position (from wing root tip)	0.078	m
CG_z Position (below wing bottom)	0.028	m
Wing Incidence Angle	0.5	°
Horizontal Tail Incidence Angle	-3	°

The sensitivity of the VLM to slightly different geometry and mass properties as well

Figure 3.3: Bix3 aircraft (left), and the XFLR5 model of the Bix3 wing and tail (right)

as trimmed flight conditions were investigated to determine the effect on the final results. While the properties of the aircraft were measured as accurately as possible, there is still some uncertainty in its parameters. The parameters that were investigated were the position of the center of gravity, wing and tail incidence angles, wing airfoil, mass, moments of inertia, trim airspeed and trim angle of attack. The ranges of each of these parameters investigated is shown in Table 3.6. The changes in the stability derivative calculations due to variation of these model parameters will be shown with the results in Table 3.7.

Table 3.6: Model parameters varied in XFLR5 for investigation of sensitivity

Parameter	Nominal Value	Range Investigated	Units
CG_x Position (from wing root tip)	0.078	[0.067, 0.089]	m
CG_z Position (below wing bottom)	0.028	[0.025, 0.031]	m
Wing Incidence Angle	0.5	[-0.5, 1.5]	°
Horizontal Tail Incidence Angle	-3	[-4, -2]	°
Mass, m	1.202	[1.102, 1.302]	kg
Roll Moment of Inertia, I_x	0.095	[0.085, 0.105]	kg·m^2
Pitch Moment of Inertia, I_y	0.045	[0.035, 0.055]	kg·m^2
Yaw Moment of Inertia, I_z	0.12	[0.11, 1.13]	kg·m^2
Trim Airspeed, V_a	12	[10.1, 15.6]	m/s
Trim Angle of Attack, α	2.2	[0.7, 5.5]	°
Wing Airfoil	Clark Y	Clark Y to Flat	–

The stability derivatives calculated by XFLR5 are shown in Table 3.7. The nominal

case is middle center of gravity location (MID CG), a trim airspeed of 12 m/s and a trim angle of attack of 2.2° with all other parameters set to the nominal value shown in Table 3.6. The maximum range of sensitivity to different parameters as well as the corresponding parameter which perturbed each stability coefficient to its maximum variation are also displayed in Table 3.7. AFT CG_x or FWD CG_x refer to the conditions where the x center of gravity position is further toward the rear or nose of the aircraft, respectively, as compared to the nominal case of MID CG_x position. For the wing and tail incidence (In.) angles, (+) indicated a positive rotation from the nominal value and (−) indicated a negative rotation from the nominal value. It can be seen that most stability derivatives are generally unchanged with the variation of the VLM model parameters. Notably, C_{x_u}, C_{x_w}, C_{m_w}, C_{l_r} and C_{n_p} had a higher range of sensitivity to the different VLM model perturbations than the other parameters. The coefficients C_{z_u}, C_{m_u} also had a large range over variability, but their values are nearly zero so this effect can be ignored. Variation in the CG_x position, wing incidence angle, and tail incidence angle appeared to have the largest influence on the results. The airfoil variation also appears a few times, however, it appears in coefficients which are nearly zero, or coefficients which have a very low range of sensitivity so airfoil likely does not have a large effect on the overall results.

The XFLR5 output of the linearized longitudinal and lateral-directional state matrices were also used to estimate the dynamic modes of the Bix3 for flight test planning. The modal analysis for the same nominal flight conditions used above is shown in Table 3.8. The table displays the eigenvalue, natural frequency f, period T, damping ratio ζ and time to double or half amplitude ($t_{1/2}$ or t_2, depending on stability) for each mode. The results for the Short Period mode and Dutch Roll mode were used directly for control input design for the system identification flight tests. The Roll mode results were used indirectly to estimate the rolling response of the aircraft for input design. The Phugoid mode and Spiral mode were

Table 3.7: Stability derivatives of the Bix3 aircraft calculated using XFLR5

Coefficient	Nominal Value	Range of Sensitivity	Highest Parameter Sensitivities
C_{X_u}	-0.0182	$[-0.0370, -0.00705]$	AFT CG_x, $(-)$ Wing In. Angle
C_{X_w}	$+0.297$	$[+0.183, +0.425]$	$(+)$ Tail Incidence Angle, CG_x
C_{Z_u}	-1.4×10^{-5}	$[-2.8\times10^{-3}, +8.3\times10^{-5}]$	Airfoil, FWD CG_x
C_{Z_w}	-5.32	$[-5.34, -5.28]$	$(+)$ Tail In. Angle, CG_x
C_{Z_q}	-8.20	$[-8.85, -7.55]$	FWD CG_x, AFT CG_x
C_{m_u}	$+1.9\times10^{-6}$	$[+3.7\times10^{-5}, +3.1\times10^{-6}]$	Airfoil, $(-)$ Wing In Angle
C_{m_w}	-0.972	$[-1.25, -0.723]$	FWD CG_x, AFT CG_x
C_{m_q}	-12.2	$[-12.9, -11.7]$	FWD CG_x, AFT CG_x
C_{Y_v}	-0.225	$[-0.229, -0.223]$	$(-/+)$ Tail In. Angle
C_{Y_p}	-0.120	$[-0.127, -0.110]$	$(+)$ Tail In. Angle, Airfoil
C_{Y_r}	$+0.173$	$[+0.161, +0.186]$	$(+/-)$ Tail In. Angle
C_{l_v}	-0.0729	$[-0.0784, -0.0681]$	$(+/-)$ Wing In. Angle
C_{l_p}	-0.526	$[-0.529, -0.523]$	$(+)$ Tail In. Angle, AFT CG_x
C_{l_r}	$+0.132$	$[+0.0871, +0.177]$	$(-)$ Wing In. Angle, FWD CG_x
C_{n_v}	$+0.0535$	$[+0.049, +0.0569]$	AFT CG_x, FWD CG_x
C_{n_p}	-0.0692	$[-0.0981, -0.0432]$	AFT CG_x, $(-)$ Wing In. Angle
C_{n_r}	-0.0442	$[-0.0465, -0.0416]$	FWD CG_x, AFT CG_x

not considered for flight testing because their respective responses are too long in duration to be adequately investigated for an aircraft of this scale. The same model sensitivity analysis from Table 3.6 was used for the modal analysis. Due to the fact that the modes depend on the dimensional state matrices, the respective dynamic modes will vary with airspeed and atmospheric density. The largest sensitivity in the dynamic modes were caused by variations in airspeed and CG_x position. The range of sensitivity to different model parameters was used to develop the range of control inputs which will be discussed in Section 3.1.3 and will be displayed in Table 3.9.

3.1.3 System Identification Flight Test Design

A flight test plan was developed specifically for the Bix3 aircraft to collect experimental data to be used for system identification. The size of the aircraft and the fact the aircraft

Table 3.8: Modal analysis of the Bix3 XLFR5 model at V_a=12 m/s, θ=0°, MID CG

Mode	Eigenvalue	f (Hz)	T (sec)	ζ	$t_{1/2}$ or t_2 (sec)
Short Period	$-9.31 \pm 9.43i$	2.11	0.474	0.703	0.074 ($t_{1/2}$)
Phugoid	$0.00181 \pm 0.860i$	0.137	7.31	-0.0021	384 (t_2)
Dutch Roll	$-0.651 \pm 4.63i$	0.745	1.34	0.1392	1.06 ($t_{1/2}$)
Roll Mode	-13.3	–	–	–	0.052 ($t_{1/2}$)
Spiral Mode	0.0839	–	–	–	8.23 (t_2)

was flown by a pilot on the ground restricted the flight test maneuvers to be comprised of fast, simple maneuvers which did not require control coordination. The Short Period maneuver was selected to be used for identification of the longitudinal model; the Dutch Roll and Bank-to-Bank Roll maneuvers were selected for identification of the lateral-directional model. These three maneuvers were first introduced in Section 2.3.2 and were used previously in other UAV system identification experiments [4, 5]. The simpler doublet (1-1) and 1-2-1 control inputs, rather than the more complex inputs discussed in Section 2.3.2, were selected for simplicity because the plane was flown by a ground-based pilot and because the aircraft could very easily deviate from its initial flight condition. An elevator doublet was selected for the Short Period maneuver, a rudder doublet was selected for the Dutch Roll maneuver and a 1-2-1 aileron input was selected for the Bank-to-Bank Roll maneuver.

A test plan was developed to perform each of the aforementioned maneuvers at least 10 times each for half and full control inputs of both polarities (a total of 40 tests were planned for each maneuver). This large number of maneuvers was planned such that there would be enough maneuvers for model development and validation, while allowing the ability to discard a significant number of maneuvers due to poor inputs, poor trimmed flight conditions, wind gusts or any other undesirable situations which would corrupt the maneuver and the model identification. A very strict requirement for flight testing was a very low wind day with a limit of 0.9 m/s (2 MPH) wind gusts.

The time step of the control inputs for the Short Period and Dutch Roll maneuvers were chosen to be half of the estimated oscillation period of the Short Period mode and Dutch Roll mode. This was chosen so that the dominant frequency of the input was near the estimated frequency of the respective dynamic mode of the aircraft [1]. The time step for these maneuvers was audibly communicated to the pilot using a metronome set to play sound cues mimicking the designed maneuver inputs. An estimate of the expected frequencies was obtained using the VLM model of the Bix3 as discussed in Section 3.1.2. The estimates of these modes are the fast-responding, complex eigenvalues of the linearized, dimensional longitudinal and lateral-directional state matrices. Since the response of the modes change with airspeed, a range of inputs was developed to ensure the modes were properly excited. The time step of the aileron input for the Bank-to-Bank Roll maneuver was determined in flight to roll the aircraft to approximately 30° to 60° on each side. An optimal frequency input was not used for Bank-to-Bank Roll because the intent of this maneuver is to excite the Roll mode which is not an oscillatory mode like the Dutch Roll mode and Short Period mode [14]. All of the control inputs were designed to be square wave inputs and were performed at half and full control deflections of different polarity. Table 3.9 shows the control inputs designed for the maneuvers used for system identification. Figure 3.4 shows the target control inputs for each maneuver and corresponding control surface. The audible metronome frequency for the pilot to imitate in the control input was set nominally to 253 BPM for the Short Period maneuver and 89 BPM for the Dutch Roll maneuver. The input frequency was varied by default in the estimated frequency range due to favorable imperfections in pilot inputs.

Table 3.9: Control inputs used for the Bix3 system identification flight tests

Maneuver	Control Input	Mode Frequency (Hz)	Time Step (seconds)
Short Period	Elevator Doublet	2.1 ± 0.5	0.24 ± 0.06
Dutch Roll	Rudder Doublet	0.75 ± 0.1	0.67 ± 0.1
Bank-to-Bank Roll	Aileron 1-2-1	–	N/A, Roll to 30°-60°

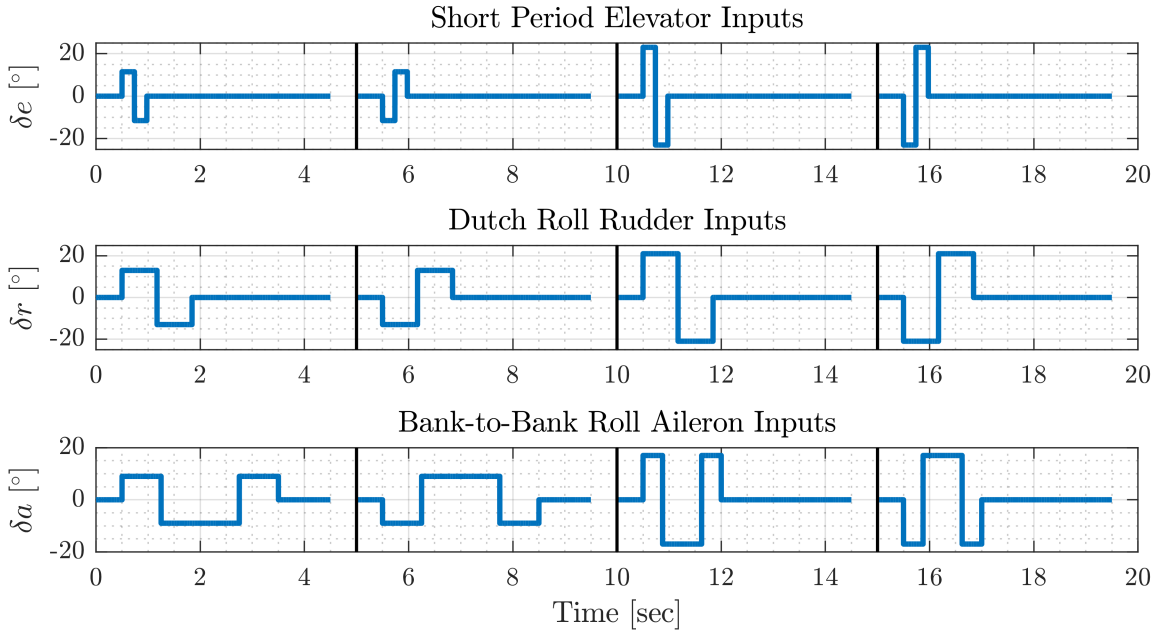

Figure 3.4: Control inputs designed for system identification of the the Bix3 aircraft

The maneuvers used for system identification were designed to have at least 3 seconds of a trimmed steady level flight condition at the start of each maneuver before performing the control input. After the scripted control input, the maneuvers were designed to have several seconds of free aircraft response which would ideally return the aircraft to the original flight condition. The thrust for each maneuver was to be held at a constant throttle setting and the inputs to the elevator, aileron and rudder were to be completely isolated. Additionally, each maneuver was to be performed open-loop, or bare airframe, such to best capture the natural motion of the aircraft. As discussed in Section 2.3.2, closed-loop feedback control is adverse to system identification because it can distort designed control inputs, cause data collinearity, and can silence the natural aircraft motion desirable for system identification [1].

Figure 3.5: The Bix3 aircraft performing a grass landing at the KEAS Laboratory

3.1.4 System Identification Flight Test Experiments

System identification flight testing for the Bix3 aircraft was performed at the Kentland Experimental Aerial Systems (KEAS) Laboratory in Blacksburg, VA. Flights were performed early in the morning in negligible wind conditions, eliminating nearly as much process noise as possible from atmospheric disturbances. The maneuvers discussed in Section 3.1.3 were performed repeatedly during the flights to collect as much data as possible in the allotted time limited by favorable wind conditions. The wind speed data taken from the Kentland Farm WeatherSTEM historical database [34] showed a steady wind speed and 10-minute gust wind speed of 0 MPH for the duration of all the flights used for system identification. The anemometer reports measurements at a resolution of 1 MPH (0.45 m/s) so it can be inferred that the wind speed during flights was likely below this bound and essentially unmeasurable; this supports the "negligible wind" qualitative assessment of the atmospheric conditions. A total of 53 Short Period maneuvers, 75 Dutch Roll maneuvers and 87 Bank-to-Bank Roll maneuvers were collected in negligible wind conditions. The flight test data was recorded on a Pixhawk flight computer and the raw data file output was converted to a Matlab compatible data file using the Mission Planner software [35]. Hunter McClelland, an Aerospace Engineering Ph.D. candidate at Virginia Tech, graciously assisted this effort by preparing

the Bix3 aircraft for flight and piloting all of the flight tests.

3.2 Flight Test Data Analysis

System identification routines require a specific data format where all signals must have the same time vector and generally must be smoothed and/or bias corrected before using the data. Aircraft states that are not measured directly must be computed from other measurements. Additionally, all of the data used for system identification must be kinematically consistent (see Section 2.3.3). Specific to the SIDPAC software, the data must be assigned to a standard flight data matrix or "fdata" matrix as discussed in Morelli and Klein [1]. A Matlab function was written to process and analyze the data for the Bix3 aircraft and create the "fdata" matrix for use with SIDPAC. The data analysis performed prior to using the SIDPAC system identification programs will be discussed in the remainder of this section.

3.2.1 Processing the Measured Flight Data

Smoothing and filtering is an important step prior to implementation of any system identification methods. Raw flight data contains undesirable noise which can compromise the accuracy of system identification. In addition, unmeasured states must be calculated using noisy measurements which can amplify the noise, especially if it requires numerical differentiation [1]. Reduction of noise is important, however, care must be taken to not over-smooth the data which will severely compromise the results because the data will no longer represent the actual deterministic movements of the aircraft.

The noisy signals in the flight test data were smoothed using the `smooth` function in

MATLAB [36]. The `smoothdata` and `filter` functions were also considered, but proved to be less reliable in reduction of noise while also maintaining the deterministic characteristics of the data. The `smooth` function contains several different algorithms which include moving averages, local linear and quadratic regressions, and the Savitzky-Golay filter [36]. The Savitzky-Golay filter is a type of moving average filter that uses an unweighted linear least-squares fit of a user specified degree of polynomial. The Savitzky-Golay filter can be more effective than other methods for data with rapid changes, which is the case for flight test data. The Savitzky-Golay filter was chosen to smooth the noisy flight test data based on these reasons and based on judgment comparing to all the methods listed when applied to the raw flight test data. The 5^{th} to 9^{th} order Savitzky-Golay filters were generally found to provide the best combination of noise reduction without altering the deterministic characteristics of the data compared to other polynomial orders of this filter.

Numerical differentiation of data is necessary for studying data compatibility and for calculating parameters that are not measured in the flight test data. This is challenging for noisy flight test data because numerical differentiation using a finite difference approach will amplify the noise in the derivative. An approach suggested in Morelli and Klein [1] is to compute numerical derivatives using differentiation of local polynomial regressions. The process they suggest is to numerically differentiate a local quadratic fit using the current data point and the two data points on either side of the current data point. It is also suggested that noisy data be smoothed prior to numerical differentiation using this technique.

The flight test data from the Bix3 was differentiated using multiple methods to determine the best option for numerical differentiation. The classical forward, backward and central difference formulas were found to yield noisy derivatives, as expected. Higher-order finite differences, which use more surrounding data points, were found to improve the results. Differentiation of local quadratic, cubic and quartic smoothing of the current time step and

the surrounding two, three and four points were also considered. In general for this data set, the most reliable numerical derivatives appeared to be calculated with a local quadratic fit of the current time step and the two neighboring data points on either side, which agrees with the method proposed by Morelli and Klein [1]. This was used as the default method of numerical differentiation in code developed to process the Bix3 flight test data. An exception to this method that occurred frequently was for the Euler yaw angle ψ which has a discontinuity when crossing $\pm 180°$. Here, a combination of forward and backward differences on either side of the discontinuity was used to maintain continuity in the derivative. The use of finite difference formulas here appeared to create little to no extra noise in the derivative because the Euler angles in the flight test data are generally smooth by default because they are calculated using an extended Kalman filter (EKF) for state estimation.

After all signals had been processed, it was necessary to make all signals conform to the same sampling frequencies and same time vector. Several interpolation methods were considered including, linear interpolation, cubic spline interpolation, and piecewise cubic Hermite interpolation polynomials [36]. The use of cubic splines was determined to be the preferred interpolation method. All data was converted to a sampling rate of 50 Hz for system identification.

3.2.2 Calculation of Unmeasured Parameters

Several variables crucial for system identification are not measured and must be calculated from other measured quantities. Aerodynamic forces and moments are not measured on an aircraft and must be calculated from other available measurements. Calculation of the non-dimensional aerodynamic force coefficients primarily requires the measured body-axis translational accelerations (a_x, a_y, a_z) and can be calculated using Equations (2.17)-(2.19).

Calculation of non-dimensional aerodynamic moment coefficients primarily requires the measured body-axis angular rates (p, q, r) and body-axis angular accelerations ($\dot{p}$, $\dot{q}$, $\dot{r}$). The angular accelerations are not measured and must be calculated from the body-axis angular rates using the smoothed numerical differentiation previously discussed. After this calculation, the aerodynamic moments can be calculated using Equations (2.20)-(2.22).

For the Bix3 aircraft system identification, a few simplifications were made to the equations to calculate the aerodynamic forces and moments: I_{xz} was assumed to be negligible, and thrust T was absorbed into the x body-axis force coefficient C_X. Since thrust was included in C_X, the quantification of aerodynamic forces and thrust force were not decoupled in model identification. This choice was made due to difficulty in identifying a reliable thrust model, and the fact that simulation results may be improved by identifying thrust and aerodynamic effects together [1]. The equations for the non-dimensional external forces and moments on the aircraft after the stated simplifications are shown in Equations (3.3)-(3.8). These equations are dependent on the additional quantities of dynamic pressure ($\bar{q} = \rho V_a^2/2$), aircraft inertial properties (m, I_x, I_y, I_z) and aircraft reference geometry ($\bar{c}$, b, S).

$$C_X = \frac{ma_x}{\bar{q}S} \tag{3.3}$$

$$C_Y = \frac{ma_y}{\bar{q}S} \tag{3.4}$$

$$C_Z = \frac{ma_z}{\bar{q}S} \tag{3.5}$$

$$C_l = \frac{1}{\bar{q}bS}\left(I_x\dot{p} + qr\left(I_z - I_y\right)\right) \tag{3.6}$$

$$C_m = \frac{1}{\bar{q}\bar{c}S}\left(I_y\dot{q} + rp\left(I_x - I_z\right)\right) \tag{3.7}$$

$$C_n = \frac{1}{\bar{q}bS}\left(I_z\dot{r} + pq\left(I_y - I_x\right)\right) \tag{3.8}$$

The body-axis velocity components (u, v, w) are not measured directly, but are used in the aircraft equations of motion and, as will be shown in Section 3.3.3, were used as regressors for modeling of aerodynamic forces and moments. On larger scale aircraft the body-axis velocity components are typically calculated using the airspeed V_a, angle of attack α, and angle of sideslip β. Since the aerodynamic angles α and β were not measured on the Bix3 aircraft, the body-axis velocity components must be calculated using the measured earth-fixed GPS velocities (V_N, V_E, V_D) and Euler angles (ϕ, θ, ψ). Equation (3.9) was used to calculate the body-axis velocity components. It is at this point that it must be assumed that there was no wind when the flight test data was taken. This is a reasonable assumption because the data was taken in conditions of unmeasurably low wind (see Section 3.1.4). An attempt was made to compute the air relative velocity of the aircraft, however, this approach seemed to degrade data quality rather than improve it. The amplitude of the noise in the airspeed sensor was greater than the magnitude of the wind during flight tests so its measurements were not used for system identification.

$$\begin{bmatrix} u \\ v \\ w \end{bmatrix} = \begin{bmatrix} \cos\theta\cos\psi & \cos\theta\sin\psi & -\sin\theta \\ \cos\psi\sin\theta\sin\phi - \cos\phi\sin\psi & \cos\phi\cos\psi + \sin\theta\sin\phi\sin\psi & \cos\theta\sin\phi \\ \cos\psi\sin\theta\cos\phi + \sin\phi\sin\psi & \sin\theta\cos\phi\sin\psi - \sin\phi\cos\psi & \cos\theta\cos\phi \end{bmatrix} \begin{bmatrix} V_N \\ V_E \\ V_D \end{bmatrix} \tag{3.9}$$

The Bix3 aircraft was not equipped with sensors to measure the control surface deflections directly in flight. The input and output pulse-width modulation (PWM) signals from the elevator, aileron and rudder servos were the only signals recorded related to control surface deflections. A mapping was developed from the output PWM signals to the actual control surface deflections to give the parameter estimates of the control derivatives physical meaning. The relationship between the control surface deflection and output PWM control signal was found to be approximately linear in the region of interest. The estimated control

surface deflection calculated from the mapping of the PWM signal was used as the control variables for system identification. The signal values were adjusted such that the nominal control deflections were zero.

3.2.3 Evaluation of the Flight Test Data Kinematic Consistency

As discussed in Section 2.3.3, determining if the data is kinematically consistent is critical prior to formally beginning the process of system identification. The kinematic consistency check involves integration of the aircraft kinematic relations (Equations (2.1)-(2.6), (2.31)-(2.33)) using the measured body-fixed translational accelerations and body-fixed angular velocities as inputs to obtain the flight path reconstruction (FPR). Flight data is said to be kinematically consistent if the integrated output parameters agree with their corresponding measurements. Drift in the outputs as time progresses is normal because the equations are considered unstable with respect to the input variables [1]. Excessive drift or disagreement between FPR and the measured flight data indicate that corrections must be made to fix instrumentation errors. The FPR analysis for the Bix3 was used to make corrections as well as determine the optimal smoothing and differentiation strategies to yield the best results.

As a beginning step in the process of data compatibility analysis and corrections, the aircraft kinematic equations were integrated using the measured inertial measurement unit (IMU) parameters of the translational accelerations and angular velocities as inputs. As stated in Morelli and Klein [1], accelerometers and rate gyroscopes are typically only corrupted by bias errors rather than scaling factor errors. The results indicated that there was a larger amount of bias in the measured translational accelerations and small, but non-negligible bias in the measured angular rates. The translational acceleration was calculated

for comparison using the measured and calculated parameters ϕ, θ, ψ, p, q, r, u, v, w, $\dot{u}$, $\dot{v}$ and $\dot{w}$ using Equations (3.10)-(3.12). The bias was calculated by finding the median difference in flight between the measured and calculated accelerations. In a similar fashion for the angular rates, the measured and calculated parameters ϕ, θ, ψ, $\dot{\phi}$, $\dot{\theta}$ and $\dot{\psi}$ were used to calculate the angular rates p, q and r using Equations (3.13)-(3.15). The median difference between the measured and calculated angular rates was the estimated bias in the measured quantities.

$$a_x = \dot{u} + qw - rv + g\sin\theta \tag{3.10}$$

$$a_y = \dot{v} + ru - pw - g\cos\theta\sin\phi \tag{3.11}$$

$$a_z = \dot{w} + pv - qu - g\cos\theta\cos\phi \tag{3.12}$$

$$p = \dot{\phi} - \dot{\psi}\sin\theta \tag{3.13}$$

$$q = \dot{\theta}\cos\phi + \dot{\psi}\sin\phi\cos\theta \tag{3.14}$$

$$r = \dot{\psi}\cos\phi\cos\theta - \dot{\theta}\sin\phi \tag{3.15}$$

3.2.4 Solution for Kinematically Inconsistent Flight Data

System identification was originally performed using the measured translational acceleration and angular rates from the IMU in the analysis. These quantities were all used to calculate the force and moment coefficients, and the measured angular rates were used as explanatory variables. The results were unsatisfactory and it was determined that there was a weakness in the analysis which was traced to using the measurements from the IMU. It was determined that the measured translational accelerations and angular rates, even after bias correction and smoothing, were subpar in quality. The IMU data, especially from the accelerometer, was found to have time-varying bias that could not be corrected systemati-

cally.

The choice was made to calculate the translational accelerations and angular rates from a more reliable data source for the purpose of system identification. A more reliable source of data is from the states ϕ, θ, ψ, V_N, V_E and V_D because the source of these signals is an extended Kalman filter (EKF) algorithm in the flight computer. The following quantities needed to be derived from these six reliable signals to proceed with the analysis: $\dot{\phi}$, $\dot{\theta}$, $\dot{\psi}$, p, q, r, $\dot{p}$, $\dot{q}$, $\dot{r}$, u, v, w, $\dot{u}$, $\dot{v}$, $\dot{w}$, a_x, a_y and a_z. The aerodynamic forces and moments were then calculated using these more reliable data signals. The path used to calculate these parameters is shown in Table 3.10. Note that the Euler heading angle ψ did not appear to be as accurate as the other EKF states, which can be attributed to the fact that it was estimated partially from a noisy magnetometer. However, analysis was proceeded with this knowledge because it was still the best known estimate of heading angle.

An example of FPR using the measured accelerations and angular rates compared to the method of deriving these quantities from the EKF states is displayed in Figure 3.6. The quantities p, q, r, a_x, a_y and a_z are the inputs into the FPR simulation, and the states ϕ, θ, ψ, u, v, w are used to assess the kinematic consistency. Recall that ϕ, θ, ψ, u, v, w are reliable signals sourced from an EKF. The figure is split into longitudinal maneuvering and lateral-directional maneuvering to assess kinematic consistency along the different axes. The data where the FPR signals follow most closely to the values of ϕ, θ, ψ, u, v, w from flight test data is considered the data that is more kinematically consistent and, therefore, best for system identification. It can be seen that the accelerations and angular rates calculated from the EKF states follow the actual flight path considerably better than the measured accelerations and angular rates with bias correction and smoothing. Analyzing the inputs into the FPR simulation, it can be seen in Figure 3.6 that the measurement of a_x is very poor, and the measurement of a_y is also flawed. The measurements of p, q, r and a_z appear to

Table 3.10: Optimal calculation strategies of important variables for system identification

Body-Axis Angular Rates	Body-Axis Velocity Components
ϕ, θ, ψ ↓ Smoothed Local Quadratic Differentiation ↓ $\dot{\phi}$, $\dot{\theta}$, $\dot{\psi}$ ↓ Equations (3.13)-(3.15) ↓ p, q, r	V_N, V_E, V_D, ϕ, θ, ψ ↓ Equation (3.9) ↓ u, v, w (raw) ↓ 5th order Savitzky-Golay filter ↓ u, v, w (smoothed)
Body-Axis Angular Acceleration	**Body-Axis Translational Acceleration**
p, q, r ↓ Smoothed Local Quadratic Differentiation ↓ $\dot{p}$, $\dot{q}$, $\dot{r}$	u, v, w (smoothed) ↓ Smoothed Local Quadratic Differentiation ↓ $\dot{u}$, $\dot{v}$, $\dot{w}$ ↓ Equations (3.10)-(3.12) ↓ a_x, a_y, a_z
Aerodynamic Moment Coefficients	**Aerodynamic Force Coefficients**
p, q, r; $\dot{p}$, $\dot{q}$, $\dot{r}$; $\bar{q}$, S, b, $\bar{c}$, I_x, I_y, I_z ↓ Equations (3.6)-(3.8) ↓ C_l, C_m, C_n	a_x, a_y, a_z; $\bar{q}$, m, S ↓ Equations (3.3)-(3.5) ↓ C_X, C_Y, C_Z

be relatively close to the respective values calculated from the EKF, however, there are still visible deviations which contribute to the kinematic inconsistency seen in using the measured IMU data. It is for this reason that the proceeding system identification analysis will be performed using the signals derived from the EFK state estimation. As just shown, the method of FPR is a powerful tool to assess the ability to use data for system identification purposes.

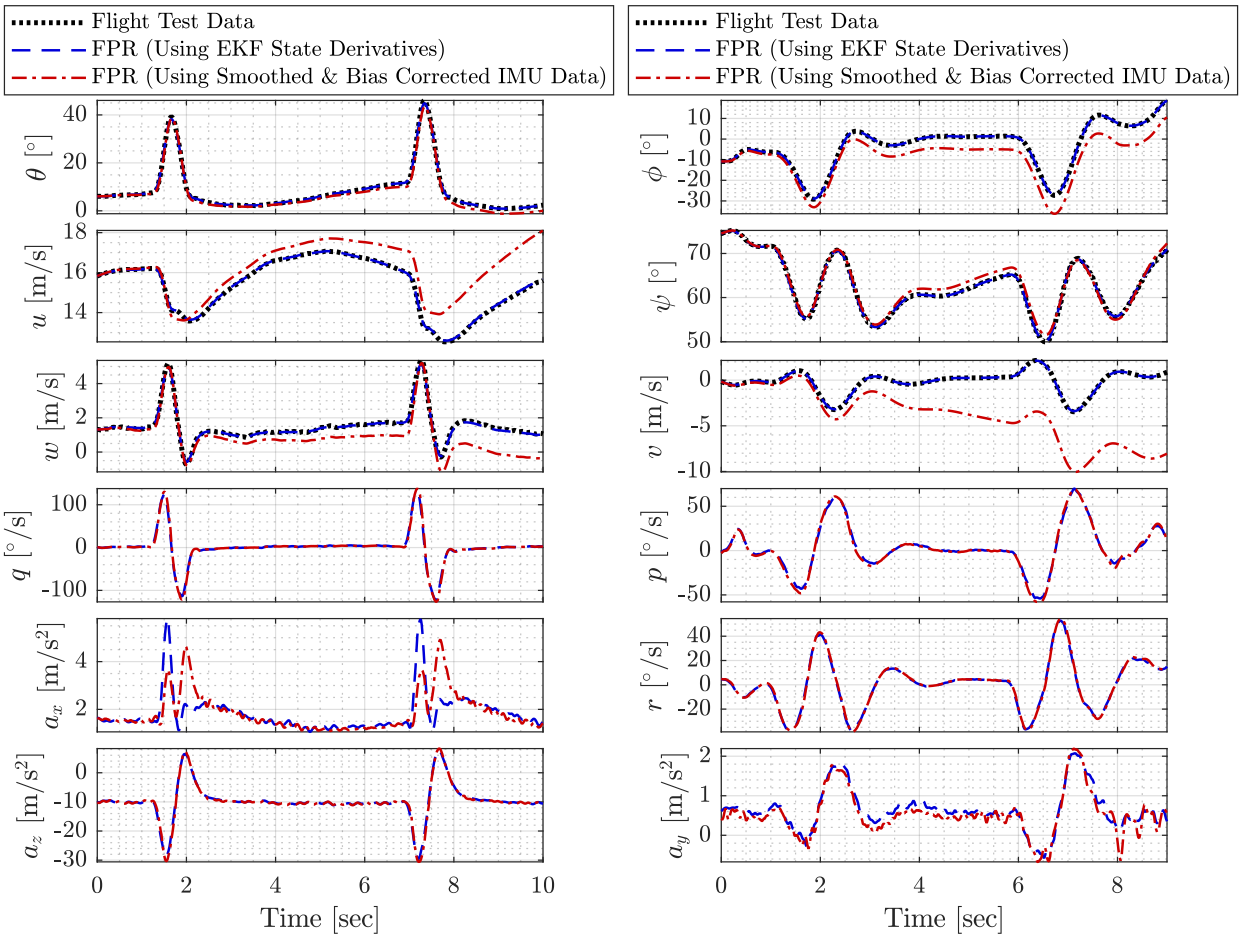

(a) Longitudinal Maneuvering (b) Lateral-Directional Maneuvering

Figure 3.6: Comparison of flight path reconstruction (FPR) results from measured and calculated translational accelerations and angular rates

3.3 Model Development Methodology

After the flight data has been experimentally obtained and processed, the formal model identification process may begin. This section will explain the model development methodology and techniques used to develop a flight dynamics model of the Bix3 aircraft using flight test data. Justification for using information from the vortex lattice method (VLM) to enhance parameter estimation from flight test data is provided, and procedures

for incorporating VLM information into the flight test data parameter estimation process are discussed. The results from these procedures will be displayed in Chapter 4. Recall that the goal of this system identification effort was to develop the best possible nonlinear flight dynamics model to capture a large portion of the Bix3 flight envelope with the intention of use for simulation purposes.

3.3.1 Justification for using VLM to Supplement System ID

Before proceeding further, the theoretical benefit of combining modeling information obtained from an independent source, such as VLM, with experimental flight test data (FTD) will be thoroughly explained. Analytical and numerical methods independently can be useful for cases including low angle of attack and low angular rates, but generally cannot be used for more aggressive dynamic maneuvering. Also, as stated previously, the control derivatives are generally overestimated if viscous effects are not included [23]. It should be noted that the best predictions of parameter estimates in many situations are obtained experimentally in the form of wind tunnel testing and/or flight testing [1]. This statement, however, assumes a certain quality standard in the experimental data. The quality of FTD is dependent on the amount of data, the number of different maneuvers, quality of maneuver execution, the number of sensors, the accuracy of sensors, and process noise from atmospheric aerodynamic disturbances. If the data quality is reduced by deficits in one or more of these categories, the accuracy of system identification from experimental data may be significantly reduced.

Data quality is usually a challenge that can be overcome for large-scale aircraft. The most prohibiting constraint for these aircraft is the allotted amount of flight testing time due to the high cost of flight testing and budget constraints. Data quality is a more significant challenge for a small, fixed-wing UAV. Firstly, due to their small size and weight, the effects

of even small atmospheric disturbances, such as turbulence or wind gusts, become more pronounced than they would be for a larger aircraft. This may make decoupling stochastic aerodynamic disturbances from deterministic signals of maneuvering flight difficult. Secondly, the available instrumentation on a small, low-cost UAV will typically be lower quality and may be limited in measurements due to cost and size considerations. This results in inaccuracy, uncertainty and omission of the measured quantities useful for system identification. Wind tunnel testing is a possible option to overcome these challenges for small UAVs, however, this option in many circumstances will be cost prohibitive.

A FTD set of a particular quality can only estimate a certain amount of parameters with accuracy. Also, for a given amount of FTD, as the number of parameters to be estimated increases, the accuracy of each parameter estimate decreases. For a given aircraft and instrumentation system, the number of parameters that can be estimated accurately can typically be increased by collecting data from more maneuvers and/or better maneuvers [1]. In aircraft system identification efforts where it is desired to develop a complex model, one approach is to first perform small perturbation maneuvers where the aerodynamics will be purely a function of the linear terms in the aerodynamic model and identify the corresponding linear parameter estimates. Subsequently, high amplitude maneuvering can be performed and the complex, nonlinear terms are estimated with the linear terms estimated from the small perturbation maneuvers held fixed.

The Bix3 aircraft falls into the category of a small UAV so, by default, it is highly susceptible to process noise from aerodynamic disturbances. For this reason, flight testing was performed in very calm conditions, but when testing in the real atmosphere these effects cannot be completely avoided. Notably, the Bix3 aircraft is significantly smaller, comparing both mass and wing-loading, than other small UAV system identification efforts [4, 5, 6, 7, 8] summarized in Section 2.4, so these effects will be more pronounced than in previous work.

Additionally, the Bix3 is categorized as being a low-cost UAV, so an expensive, high-quality instrumentation system was not practical. The low-cost instrumentation results in higher measurement noise levels and inaccuracies in sensor measurements. The instrumentation system also lacks the measurements of aerodynamic angles (α, β) and a reliable airspeed sensor.

The superposition of noise from external disturbances and measurement deficiencies made identification from FTD a challenge for the Bix3 aircraft. The high noise level also made identification from small perturbations from a reference flight condition unattainable because of the low signal-to-noise ratio that is present in using small perturbations maneuvering. Larger amplitude maneuvering was needed to increase the dominance of the deterministic signal over the noise. These larger amplitude maneuvers, however, perturb the aircraft outside of the range of a purely linear aerodynamic model. This means that the technique discussed to identify linear terms from small perturbation maneuvers, then fixing those terms to identify nonlinearity in the model from larger perturbation maneuvers cannot be utilized for this aircraft. The larger amplitude maneuvering requires the model structure to contain some nonlinearity to represent the aerodynamic forces and moments which increases the number of parameters to be estimated from a single maneuver. These nonlinear terms are also desired as parameter estimates because the goal of this system identification effort is to identify a model that is valid over a large portion of the flight envelope.

Consequent to the discussion above, VLM was used to supplement the collected FTD for the Bix3 aircraft in an attempt to overcome many of the challenges previously stated in this section. By incorporating certain VLM parameter estimates of the linear terms into the model, the number of terms to be identified from FTD decreases. This is hypothesized to increase the accuracy and lower the uncertainty of the individual parameter estimates because there are a fewer number of parameters to estimate. This is also hypothesized

to increase the overall modeling accuracy because of the increased accuracy of parameter estimation from FTD, while maintaining the desired and necessary complex model structure. This technique is postulated to be effective in scenarios were irreparable deficiencies exist in FTD which is a common problem with small, low-cost UAVs, or in scenarios where limited amounts of FTD is available for identification.

3.3.2 Selection of Data for System Identification

A large number of maneuvers were performed to allow for enough data for system identification and validation while also allowing the luxury to discard poor quality maneuvers. Maneuvers were discarded due to several different occurrences that could affect the system identification process. Maneuvers that had poor steady level trim conditions before control inputs or deviated significantly from their original flight conditions after the control inputs were removed from the system identification process. These conditions typically took the form of too much climb or descent before or after the maneuver, exceedingly high airspeed or approach to stall. Stall is detrimental to system identification because the aerodynamics become unsteady and highly nonlinear aerodynamics due to viscous instability. Excessively high airspeed was problematic because the designed control inputs were no longer valid for properly exciting the dynamic modes of the aircraft.

Another cause of maneuvers to be removed was subpar control inputs. This took the form of improper control execution, or more commonly, accidental deflection of auxiliary control surfaces that were supposed to remain stationary during the designed control inputs. This was a problem during the tests because the elevator/aileron and rudder/thrust controls were located on the same control stick on the R/C transmitter making it easy to unintentionally engage incorrect controls in a minimal but notable manner. Similarly, the pilot

assist switch was accidentally bumped during a few maneuvers rendering the data where this occurred unusable because the system identification maneuvers were designed to be open-loop. An additional cause of data to be removed from the system identification process was abnormally excessive measurement noise during the maneuver.

The flight test data was analyzed for evidence of all the phenomena discussed above before system identification. With the exception of any data that may have contained feedback control, all maneuvers were processed using the parameter estimation techniques which will be discussed in Section 3.3.4-3.3.5 to analyze the effect on parameter estimation from inferior maneuvers. The parameter estimates from poor maneuvers were typically significantly different than better quality maneuvers, as would be expected. The parameter estimates from maneuvers near stall were drastically different than quality maneuvers. This is an effective technique to validate the predictions of poor maneuvers to be removed from the system identification data. The identified poor maneuvers were removed from the system identification data before making final parameter estimates. Roughly half of the recorded maneuvers were used either for parameter estimation or validation, and the other half were discarded.

3.3.3 Model Structure Development

A model structure to represent the aerodynamic forces and moments on the aircraft must be developed or postulated before parameter estimation from flight test data. The non-dimensional force and moment coefficients C_X, C_Y, C_Z, C_l, C_m and C_n were used instead of the dimensional coefficients to eliminate the dependence on airspeed and density. C_X and C_Z were used instead of C_L and C_D because the Bix3 did not have an angle of attack sensor, in addition to the general reasons use of C_X and C_Z are favorable (see Section

2.2). The forces and moment coefficients were calculated from (3.3)-(3.8). Since the thrust force T was absorbed into the x body-axis force coefficient C_X, the identified model quantifies the combined influence of aerodynamics and thrust on the aircraft dynamics. Several attempts were made to develop a separate thrust model, but this approach was ultimately surrendered because of unquantifiable variations in performance of the low-cost propulsion system. For example, thrust changed as a function of variables such as the specific battery used for each flight or the duration of time into the flight for equivalent throttle setting and airspeed. The impact of this simplification on the final model was not expected to be adverse because modeling performance for simulation purposes may actually be improved by identifying combined aerodynamic and thrust effects [1]. This simplification is only expected to affect the parameter estimates for C_X.

The explanatory variables used to represent the aerodynamic forces and moments were the non-dimensional body-axis velocities ($\hat{u}$, $\hat{v}$, $\hat{w}$), the non-dimensional body-axis angular rates ($\hat{p}$, $\hat{q}$, $\hat{r}$) and the control surface deflections (δe, δa, δr) measured in radians. Equation (3.16) shows the non-dimensionalization of the state variables where V_o is a nominal reference airspeed chosen to be 12 m/s, $\bar{c}$ is the mean aerodynamic chord and b is the projected wingspan. This form is used instead of the alternate and perhaps more common form depending on non-dimensional airspeed $\hat{V}_a = V_a/V_o$, angle of attack α in radians and angle of sideslip β in radians, due to the lack of reliability in the airspeed sensor, and because there were no angle of attack or angle of sideslip sensors on the Bix3 aircraft. Methods have been developed to calculate angle of attack and angle of sideslip from IMU data for system identification, but this approach requires that the sensors have significantly increased accuracy [33]. Due to the lacking accuracy of the sensors on the Bix3, this approach was not practical.

$$\hat{u} = \frac{u}{V_o}, \quad \hat{v} = \frac{v}{V_o}, \quad \hat{w} = \frac{w}{V_o}, \quad \hat{p} = \frac{pb}{2V_o}, \quad \hat{q} = \frac{q\bar{c}}{2V_o}, \quad \hat{r} = \frac{rb}{2V_o} \tag{3.16}$$

The longitudinal force and moment coefficients, C_X, C_Z, C_m, were expressed as functions of the longitudinal states $\hat{u}$, $\hat{w}$, $\hat{q}$, and the control variable δe. The lateral-directional force and moment coefficients, C_Y, C_l, C_n, were expressed as functions of the lateral-directional states $\hat{v}$, $\hat{p}$, $\hat{r}$, and the control variables δa and δr. The decoupling of longitudinal and lateral-directional models in this way is a standard practice in aircraft system identification [1].

The stepwise regression method was used to develop a model structure for each aerodynamic force and moment coefficient individually using the explanatory variables discussed above. The stepwise regression method requires a set of possible regressor terms, which may be linear or nonlinear functions of the explanatory variables [1]. The stepwise regression method uses a linear regression, or the equation-error method, to assess the model structures where the force and moment coefficients are the dependent variables and the potential regressors terms are the independent variables. The data used for the stepwise regression was a series of different longitudinal maneuvers for C_X, C_Z and C_m and a series of lateral-directional maneuvers for C_Y, C_l and C_n. The Short Period maneuver was used to identify the longitudinal model structure, and the Bank-to-Bank Roll and Dutch Roll maneuvers were used to identify the lateral-directional model structure. Other system identification works and resources on aircraft dynamics modeling [1, 4, 12, 13, 16] were used as inspiration for possible terms to include in the aerodynamic model structure.

After a set of potential terms to represent each force and moment coefficient was developed, terms were brought into or taken away from the model of each force or moment coefficient one-by-one to assess the significance of including the respective term in the model. The success of the model at each iteration was analyzed by computing the least-squares fit of the force or moment coefficient as a function of the terms present in the model. Terms to bring into the model were determined by selecting the term with the largest relative partial

correlation to the response variable, r, of all terms that were not currently in the model. Terms were removed from the model if the partial F statistic, F_0, was low in comparison to the other terms. These metrics were discussed in Section 2.3.4. A bias was held toward including the linear terms first because it is considered favorable to model with linear terms over nonlinear terms if they can both equivalently describe the variation in the dependent variable [1]. The nonlinear terms were then used to quantify variation that was not captured by the linear terms in the model.

The effect of including a term in the model needed to be significant in order for it to be included in the final model. This was assessed by ensuring that the R^2 value was significantly increased by including the respective term in the model and that the qualitative fit of the model to the dependent variable was significantly improved. Care was taken to include the fewest number of model terms required to adequately model the dependence of the aerodynamic force and moment coefficients on the regressors terms. If a model term was found to be significant in a number of different maneuvers run through the stepwise regression procedure, then the term was included in the final model structure for the respective force or moment coefficient.

3.3.4 Parameter Estimation from the Equation-Error Method

The equation-error method in the form of a least-squares regression was used to obtain the first estimate of the unknown parameters in the aerodynamic model structure developed using a stepwise regression. The dependent variables were the non-dimensional aerodynamic force and moment coefficients, and the explanatory variables were non-dimensional states and control variables characterizing the model structure. The parameter estimates from this method were then used as the initial guess of parameter estimates used in the output-error

method, which was used to compute the final model.

At this stage in the analysis, the information from the vortex lattice method (VLM) began to be incorporated to supplement the information available in the flight test data (FTD). The equation-error method was used to assess the possible benefit of including parameter estimates from VLM to replace the corresponding estimate from FTD. A modified form of the stepwise regression method, developed specifically for this research effort, was used to assess the value in including this information. The method implemented held the previously identified model structure constant for each force and moment coefficient, but the source of certain parameter estimates were changed between FTD and VLM at each iteration. Using this procedure, the stability derivatives computed from VLM were brought into the model, or taken away from the model, one-by-one replacing the corresponding estimate from FTD and recomputing the least-squares parameter estimates from FTD for all other model terms not estimated from VLM. If including a single or multiple parameter estimate from VLM either improved modeling or appeared to make no change on the results, then the stability derivative(s) from VLM were considered as a possible set to replace these parameters from FTD. A set of VLM stability derivatives was deemed useful, even if it showed no improvement on the model because it meant that fewer terms needed to be estimated from FTD which could be a favorable result, as discussed in Section 3.3.1. This procedure was repeated for the model structure of each individual force and moment coefficient. The resulting viable combinations of VLM stability derivatives were recorded to be tested in the output-error method.

The equation-error method only played a minimum role in the majority of the final parameter estimation because a few of the assumptions associated with this method are severely violated. One assumption that is typically violated for aircraft parameter estimation is that residuals are uncorrelated which is hard to escape because estimation is typically

performed from a sequential measured time history. A more critically violated assumption is that there was no noise or error in the explanatory variables. This is a very poor assumption due to the elevated noise levels caused by the size of the Bix3 aircraft and the low-quality sensors.

3.3.5 Parameter Estimation from the Output-Error Method

The output-error method is computationally expensive but can provide better parameter estimates than the equation-error method. The output-error method has increased complexity because it is a nonlinear optimization problem that minimizes the difference between the measured and predicted outputs which requires integration of the aircraft equations of motion at each iteration. This scheme requires an initial guess of parameter estimates which was obtained from the equation-error method. Since the output-error method does not account for process noise due to wind and turbulence [16], the flight testing was performed on a very calm day with unmeasurable wind (see Section 3.1.4).

The output-error method was implemented to integrate the fully nonlinear aircraft equations of motion at each iteration using Equations (2.4)-(2.12). The only simplification to these equations is that, as previously stated, I_{xz} is assumed to be negligible. The navigation equations (Equations (2.1)-(2.3)) are omitted from the output-error implementation because the inertial positions x and y are not related to aircraft dynamics, and altitude $z = -h$ is only related to aircraft dynamics through atmospheric variation with altitude [1]. Thus, the method requires integration of nine coupled, nonlinear, first-order ordinary differential equations at each iteration. The parameter estimation was split up into longitudinal and lateral-directional dynamics. For the longitudinal maneuvers, the parameter estimates for C_X, C_Z, and C_m were estimated in parallel. The outputs for which the output error was to

be minimized for the longitudinal maneuvers were θ, u, w, q and a_z. The axial acceleration a_x was not included as an output because it contained a large amount of noise compared to the deterministic portion of the signal. For the lateral-directional maneuvers, the parameter estimates for C_Y, C_l, and C_n were estimated together. The outputs for which the output error was to be minimized for the lateral-directional maneuvers were ϕ, v, p, r and a_y. The heading angle ψ is not included as an output because is does not have a direct effect on the aircraft dynamics [1]. The axis respective angular accelerations $\dot{p}$, $\dot{q}$, $\dot{r}$ were not included as outputs due to noise accumulated in their calculation (see Table 3.10).

Parameter estimation from flight test data (FTD) alone showed that there was room for improvement in certain instances. Parameter estimates from VLM were used to supplement the parameter estimation from FTD in an attempt to improve the overall model of the flight dynamics as well as decrease the scatter in the parameter estimates from FTD alone. The sets of VLM terms shown to either improve the model or have equivalent modeling results using the equation-error method were implemented into the output-error method to investigate the effect on the final results. Additional justification for inclusion of terms from VLM was that the respective VLM parameter estimate had to be within the scatter of the respective population of parameter estimates calculated from FTD alone.

The final parameter estimates to include in the model were selected by taking the median value of the parameter estimates from all system identification maneuvers after removal of parameter estimates determined to be outliers. The parameter estimates with an abnormally large standard error (Cramér-Rao lower bound), and/or the parameter estimates with values that were significant outliers compared to the other estimates were removed from the data scatter. The MATLAB function `isoutlier` was used to make this decision quantitative rather than based on judgment. Several different outlier identification algorithms are available in this function which were all attempted. The best outlier removal method

found for this data set is based on the median absolute deviation (MAD), which is shown in Equation (3.17), where Θ is the population of the different estimates for the same parameter and n is the number of values in the population [36]. MAD is a robust measure of variance in a population of data that is less sensitive to outliers. Outliers were identified by being three scaled MAD ($\overline{\text{MAD}}$) from the median. $\overline{\text{MAD}}$ is calculated using Equation (3.18) where $\texttt{erfc}^{-1}()$ is the inverse complementary error function [36]. The scaled MAD is an estimate of the standard error σ of data which is normally distributed, but may be used for data which does not follow a normal distribution. Assuming that the data is normally distributed, three scaled MAD corresponds approximately to the 99.7% confidence interval.

$$\text{MAD} = \texttt{median}\left(|\Theta_i - \texttt{median}(\Theta)|\right), \; i = 1, 2, ..., n \tag{3.17}$$

$$\overline{\text{MAD}} = -\frac{1}{\sqrt{2}\,\texttt{erfc}^{-1}(3/2)}\,\text{MAD} \approx 1.4826 \times \text{MAD} \tag{3.18}$$

First, the `isoutlier` function was used to remove any parameter estimates that had standard errors larger than three $\overline{\text{MAD}}$ from the median standard error. Then, the `isoutlier` function was used to remove any values of the remaining parameter estimates that were three $\overline{\text{MAD}}$ from the median parameter estimate. The remaining parameter estimates were used to calculate the median parameter estimate which was the value of the parameter included in the final model. The parameter estimates that were removed were assumed to be due to excessive noise or a lack of convergence of the output-error method. This is not expected to affect the uncertainty analysis because these points were removed due to probable flaws in the data collection, not removing scatter from the data.

The process of parameter estimation for the longitudinal aerodynamic coefficients was expected to be relatively straight forward since it only included the Short Period maneuver and required estimation of fewer total aerodynamic coefficients. The lateral-directional

aerodynamic coefficients were expected to be more difficult to estimate since there were multiple maneuvers to consider, there were more parameters to estimate, and the inherent coupled dynamics between axes. Estimation of the Dutch Roll maneuvers and the Bank-to-Bank Roll maneuvers independently generally yielded different results for the shared stability derivatives. This is not an uncommon challenge when performing parameter estimation from lateral-directional maneuvers separately [37]. This is the reason that these maneuvers or similar maneuvers are often performed in succession to incorporate different lateral-directional dynamics and control surface inputs into one maneuver [1, 2, 37]. This approach was attempted for the Bix3 flight testing, but was ultimately not used for identification because of the difficulty in performing these maneuvers in succession with a ground-based pilot. Rather, Dutch Roll and Bank-to-Bank Roll maneuvers collected separately were used for parameter estimation. To overcome the challenge that parameter estimates from these two different maneuvers were not the same, a procedure was developed to synthesize information from the two different maneuvers into one unique set of parameter estimates to model all lateral-directional dynamics. The method for combining the best information of the two maneuvers together was found by analyzing the accuracy of parameter estimates calculated from the two different maneuvers in an iterative trial-and-error process. This will be discussed further in Chapter 4.

The dynamic mode of the Bix3 aircraft calculated from flight test data alone will be compared to the predictions that were used for flight testing input design. The aircraft equations of motion were linearized about a reference flight condition and the nonlinear terms in the aerodynamic model were neglected to obtain the longitudinal and lateral-directional state matrices. The stability properties of the eigenvalues, natural frequency, period, damping ratio and time to half or double in amplitude were computed and compared to the preliminary estimates obtained from VLM used for control input design. The Phugoid mode will not

be presented since this mode was not excited by the control inputs, the developed model structure does not contain certain terms required to model the Phugoid mode and the fact that this mode is too slow to be able to estimate for this scale of aircraft.

3.3.6 Model Validation and Analysis of Uncertainty

Uncertainty of the estimated model parameters from the output-error method was analyzed through error analysis of the parameter estimates of individual maneuvers and statistical analysis of the population of parameter estimates from all maneuvers. Model validation was performed using simulations intended to model maneuvers not used in the system identification process. Modeling performance was determined qualitatively and through use of multiple error metrics.

Uncertainty Quantification of Parameter Estimates

The uncertainty of the parameter estimates from single maneuvers were analyzed using the Cramér-Rao lower bound. The conventional error bound was calculated using Equation (2.54). This estimate was expected to be overly optimistic because it assumes that the residuals are not colored, which is typically the case in aircraft parameter estimation [1, 17]. The Cramér-Rao bound correcting for colored residuals was calculated using Equation (2.57) to account for this phenomena. These results will be presented in the form of error bar plots displaying the Cramér-Rao bounds for individual maneuvers. Ultimately, analyzing the spread in the population of parameter estimates obtained from different maneuvers appeared to be a better way of quantifying the true uncertainty in the parameter estimates.

The spread of the parameter estimates from all respective system identification maneuvers was analyzed by developing error bounds based on the median and scaled median

absolute deviation (MAD). Parameter estimates from the output-error method should approach a normal distribution with the mean being the actual value of the parameter as the number of estimates increases [17]. However, due to imperfections in the flight test data, lack of convergence of the output-error method or simply a lack of a large enough sample size, the population of some parameter estimates did not appear to be normally distributed, and contained outliers. The median and scaled MAD were used to account for this finding since they may be more effective for data which is not normally distributed and contains outliers compared to using conventional mean and t-distribution analysis. Notably, for data which is normally distributed, the values of these different sets of metrics are essentially equivalent. The 95% confidence interval (CI) was used to quantify the uncertainty in parameter estimates. This was calculated using two scaled MAD from the median parameter estimate. Assuming a normal distribution, the scaled MAD is equivalent to the standard error, thus, two scaled MAD approximates the 95% CI. Histograms are used to visualize the uncertainty characterized by the spread of parameter estimates, and the final parameter estimates are presented with error bounds approximating the 95% CI.

Comparison of Modeling Performance

The accuracy of the models created using different techniques were evaluated and compared through the differences in the individual measured outputs, $\boldsymbol{z}_i$, and the individual outputs predicted by the model, $\boldsymbol{y}_i$, for individual flight maneuvers. The differences were characterized qualitatively and through statistical error metrics. The different model's outputs for the predicted response of individual flight maneuvers were obtained through simulation of the developed model subject to the same initial conditions and control inputs as the measured flight test data for each individual system identification maneuver. The root-mean-square error (RMSE_i) and mean absolute error (MAE_i) of each individual out-

put's error ($\boldsymbol{z}_i - \boldsymbol{y}_i$) were calculated using Equations (3.19) and (3.20) respectively where N is the number of data points and k is the index of an individual data point. The main difference in these metrics is that RMSE assigns a higher penalty to larger levels of error than MAE. RMSE is typically better at quantifying differences in model predictive capability than MAE, however, RMSE is only appropriate when the model errors are normally distributed [38]. Both metrics will be used to assess model performance to provide a more complete error analysis.

$$\text{RMSE}_i = \sqrt{\frac{1}{N}\sum_{k=1}^{N}\left(\boldsymbol{z}_i(k) - \boldsymbol{y}_i(k)\right)^2} \tag{3.19}$$

$$\text{MAE}_i = \frac{1}{N}\sum_{k=1}^{N}\left|\boldsymbol{z}_i(k) - \boldsymbol{y}_i(k)\right| \tag{3.20}$$

A single metric to measure the total accuracy of a model was desired to characterize the overall model fit for comparison of different models intended to characterize the same dynamics. The MAE or RMSE for each signal cannot be added together because of the difference in units. The output errors of the non-dimensional outputs have the same units, but still cannot be added together due to the differences in magnitude of the signals. The MAE and RMSE of each output were normalized by the range of the respective measurement $\boldsymbol{z}_i$ to be able to combine these quantities together in an unbiased fashion. The range was chosen over the mean or median because these metrics are close to zero for some outputs which disproportionally weighs the error to the near zero mean/median outputs. Considering that the inputs for each flight maneuver were symmetric, short duration excitations, the range is the most appropriate simple normalization factor. The normalized root-mean-squared error (NRMSE) and the normalized mean absolute error (NMAE) for each important model output were then averaged to arrive at the averaged normalized root-mean-square error (ANRMSE) and averaged normalized mean absolute error (ANMAE). ANRMSE and ANMAE

provide a single metric to assess the total error across all relevant outputs present in the model predictions for each maneuver. Equations (3.21) and (3.22) show the formulas for ANRMSE and ANMAE where the index i is representative of a specific output quantity and n_o is the number of outputs.

$$\text{ANRMSE} = \frac{1}{n_o} \sum_{i=1}^{n_o} \frac{\text{RMSE}_i}{\texttt{range}(\boldsymbol{z}_i)} \tag{3.21}$$

$$\text{ANMAE} = \frac{1}{n_o} \sum_{i=1}^{n_o} \frac{\text{MAE}_i}{\texttt{range}(\boldsymbol{z}_i)} \tag{3.22}$$

Model accuracy was also analyzed by comparing each force and moment coefficient calculated from flight test data for each individual maneuver to the respective force and moment coefficient predicted in model simulation. The RMSE and MAE were used to compare errors between each force and moment coefficient calculated from measurements and those computed through simulation of the model.

The magnitude of all error metrics discussed will be dependent on the specific maneuver they are applied to as an independent event. To account for this fact, the results will be presented in percent change from a baseline model. Equation (3.23) shows the formula for percent change of a generic quantity, Λ, which in this case represents the individual error metrics discussed above. The analytical form of percent change is similar in form to percent error. For analysis, Λ will be replaced by the ANRMSE and ANMAE for the outputs, and the RMSE and MAE for the individual force and moment coefficients. A negative percent change indicates a lower measure of error for the quantity Λ_{new} which in this context may be inferred as a relative decrease in modeling error.

$$\%\ \text{Change} = 100 \times \frac{\Lambda_{new} - \Lambda_{baseline}}{\Lambda_{baseline}} \tag{3.23}$$

To assess improvement in model performance from a baseline case, the error statistics for each individual maneuver were pooled into a population of error measurements and hypothesis testing was performed between the models. A paired t-test and Wilcoxon signed-rank test were used to test the null hypothesis that the mean values of the respective error metrics were statistically the same for the different models. A paired t-test assumes that the samples come from a normal distribution which could be violated for these metrics. For this reason, the Wilcoxon signed-rank test was also used as an alternative to the paired t-test. The Wilcoxon signed-rank test tests the same hypothesis as the paired t-test, but is a non-parametric test meaning that it doesn't require any assumptions about the distribution of the data [36]. The one-sided variants of these tests were used to test if the new model was statistically significantly lower than the baseline model. These statistics were tested for maneuvers included in the parameter estimation process as well as validation maneuvers held outside the parameter estimation process. This is mainly to increase the sample population because more maneuvers were used for parameter estimation than left aside for validation. This was not expected to corrupt the results since the difference in modeling error between models is being assessed rather than quantification of the total modeling error.

Several flight maneuvers were not used in the identification process for the purpose of validation of the model developed from all other system identification maneuvers. Validation of the developed model from these maneuvers was evaluated through simulation. The control surface defections and initial conditions of the maneuvers not used for system identification were used as inputs and the aircraft equations of motion were integrated to compare the measured outputs from flight, $\boldsymbol{z}$, and the outputs predicted by the model, $\boldsymbol{y}$. A minimal difference between each measured and predicted output indicates good modeling performance.

Overall Modeling Performance of the Final Model

The final model was selected from the different models analyzed using the performance analysis techniques discussed above in this section. Simulations using the final model intended to replicate the validation flight maneuvers not included in the system identification process were performed and the response was compared to each validation flight maneuver. The inputs into the simulation were the initial conditions and control inputs of the flight test data for each validation maneuver. The full time histories of these maneuvers will be shown, including off-axis variables and the aircraft flight path for qualitative comparison of modeling performance. The overall modeling fit was characterized quantitatively through the goodness of fit (GOF) and Theil's inequality coefficient (TIC) [22] metrics by comparing the predicted model response to measured flight test data. GOF of each respective model response output denoted by index i was calculated using Equation (3.24) where $\boldsymbol{z}_{i_0}$ is the initial value of the measured time series and all other variables were defined previously in this section [5, 15]. A value of GOF closer to 1 indicates a good model fit [5]. TIC of each model response output with index i was calculated using Equation (3.25) [5, 6, 22]. The TIC metric may be corrupted when an output has a non-zero mean, so the TIC was computed by first subtracting the measured and modeled output by the mean value of the respective measurement vector [5, 22]. TIC will have a value between 0 and 1, where a value of 0 indicates a perfect model fit. A value of TIC 0.25-0.3 or lower indicates satisfactory modeling performance [2].

$$\text{GOF}_i = 1 - \frac{(\boldsymbol{z}_i - \boldsymbol{y}_i)^T(\boldsymbol{z}_i - \boldsymbol{y}_i)}{(\boldsymbol{z}_i - \boldsymbol{z}_{i_0})^T(\boldsymbol{z}_i - \boldsymbol{z}_{i_0})} \tag{3.24}$$

$$\text{TIC}_i = \frac{\sqrt{\frac{1}{N}(\boldsymbol{z}_i - \boldsymbol{y}_i)^T(\boldsymbol{z}_i - \boldsymbol{y}_i)}}{\sqrt{\frac{1}{N}\boldsymbol{z}_i^T\boldsymbol{z}_i} + \sqrt{\frac{1}{N}\boldsymbol{y}_i^T\boldsymbol{y}_i}} \tag{3.25}$$

Chapter 4

Results and Discussion

In this chapter, the results from the system identification experiments explained in Section 3.3 will be presented. Results from model structure identification are shown, then the parameter estimation results are presented for the longitudinal and lateral-directional dynamics. Results are presented using standard methods for parameter estimation from flight test data and using supplementary methods hypothesized to enhance parameter estimation results. The developed models are then compared through simulation, modeling error, and uncertainty in parameter estimation. Interpretation of the results will be presented in discussion sections following the results.

4.1 Model Structure Identification

The model structure was developed using the procedure discussed in Section 3.3.3. The stepwise regression method was implemented to develop a model structure for each individual force or moment coefficient. The longitudinal force and moment coefficients, C_X, C_Z, C_M, were considered functions of $\hat{u}$, $\hat{w}$, $\hat{q}$ and δe in the analysis. The lateral-directional force and moment coefficients, C_Y, C_l, C_n, were considered unknown functions of $\hat{v}$, $\hat{p}$, $\hat{r}$, δa and δr. All angles are in units of radians. The definition of non-dimensional state variables are given in Equation (4.1) where V_o =12 m/s is the reference airspeed, b is the projected

wingspan and $\bar{c}$ is the mean aerodynamic chord.

$$\hat{u} = \frac{u}{V_o}, \quad \hat{v} = \frac{v}{V_o}, \quad \hat{w} = \frac{w}{V_o}, \quad \hat{p} = \frac{pb}{2V_o}, \quad \hat{q} = \frac{q\bar{c}}{2V_o}, \quad \hat{r} = \frac{rb}{2V_o} \tag{4.1}$$

4.1.1 Longitudinal Model Structure

The Short Period maneuver was used to develop the longitudinal model structure. The terms considered were polynomial expansions of each state variable up to fourth order and the elevator deflection δe. The terms containing multiplication of multiple explanatory variable detailed in Grauer and Morelli [13] and shown in Equations (2.23), (2.25) and (2.27) (assuming $\hat{w} \approx \alpha$, $C_Z \approx -C_L$, $C_X \approx -C_D$) were also included in the potential model terms. An example of the stepwise regression method showing iterations of different model structures to arrive at the final model are shown in Figure 4.1. The stopping criteria for not including further terms in the model was when including more terms did not significantly improve the model of the respective force or moment coefficient. While complexity in the model structure was desired to model a significant portion of the flight envelope, simplicity was also considered equally important since parameter estimates become less accurate as the number of model terms increases [1]. Additionally, linear terms were preferred over nonlinear terms if both could equally characterize the same aerodynamic phenomena. As explained in Sections 2.3.4 and 3.3.3 there are several metrics to attempt to quantify the relative effectiveness of each model structure, however, the final decision comes down to engineering judgment. The final models were selected to included terms deemed significant in multiple different maneuvers of different control polarity and amplitude.

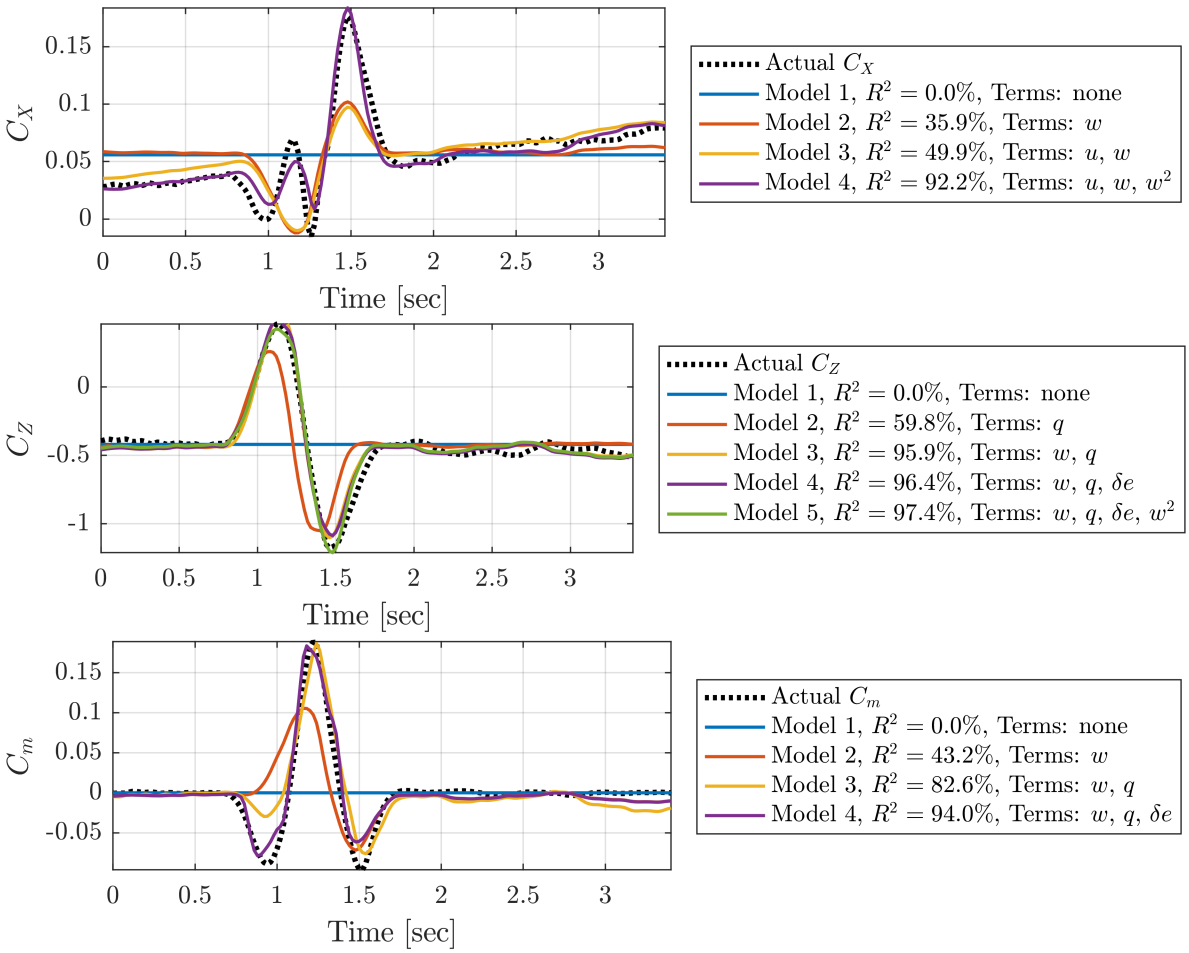

Figure 4.1: Stepwise regression iterations for C_X, C_Z, C_m using a Short Period maneuver

The model structures determined for C_X, C_Z and C_m are shown in Equations (4.2)-(4.4). Recall that C_X models the combined effects of both aerodynamics and thrust due to difficulty in reliably characterizing a separate thrust model and the fact that this approach can be better for the purposes of simulation [1]. C_X contains only $\hat{u}$ and $\hat{w}$ as the explanatory variables. The structure for C_X is nonlinear in the form of $\hat{w}^2$. C_Z and C_m both contain $\hat{w}$, $\hat{q}$ and δe as the explanatory variables. C_Z is nonlinear in the form of $\hat{w}^2$, and C_m is purely linear. The bias terms for C_X, C_Z, C_m are given as C_{X_o}, C_{Z_o}, C_{m_o} which contains

information about the trim conditions and aerodynamic bias [1].

$$C_X = C_{X_u}\hat{u} + C_{X_w}\hat{w} + C_{X_{w^2}}\hat{w}^2 + C_{X_o} \tag{4.2}$$

$$C_Z = C_{Z_w}\hat{w} + C_{Z_q}\hat{q} + C_{Z_{\delta e}}\delta e + C_{Z_{w^2}}\hat{w}^2 + C_{Z_o} \tag{4.3}$$

$$C_m = C_{m_w}\hat{w} + C_{m_q}\hat{q} + C_{m_{\delta e}}\delta e + C_{m_o} \tag{4.4}$$

4.1.2 Lateral-Directional Model Structure

The Dutch Roll and Bank-to-Bank Roll maneuvers were used to develop the lateral-directional model structure. The model terms considered were the explanatory state variable combinations detailed in Grauer and Morelli [13] and shown in Equations (2.24), (2.26) and (2.28), as well as the the aileron deflection δa and rudder deflections δr. Note that Grauer and Morelli [13] state that even for a complex model structure, C_Y and C_l can be sufficiently modeled by purely linear terms and C_n can be modeled by a polynomial expansion of $\hat{v} \approx \beta$ up to third order and linear terms of the remaining explanatory variables. An example of the stepwise regression method showing iterations of different model structures for both lateral-directional maneuvers to arrive at the final model are shown in Figures 4.2 and 4.3. The stopping criteria for not including further terms in the model was similar to the longitudinal case whereby only including terms which significantly improve the model. The final models were selected to included terms deemed significant in multiple of both different maneuvers of different control surface polarity and amplitude.

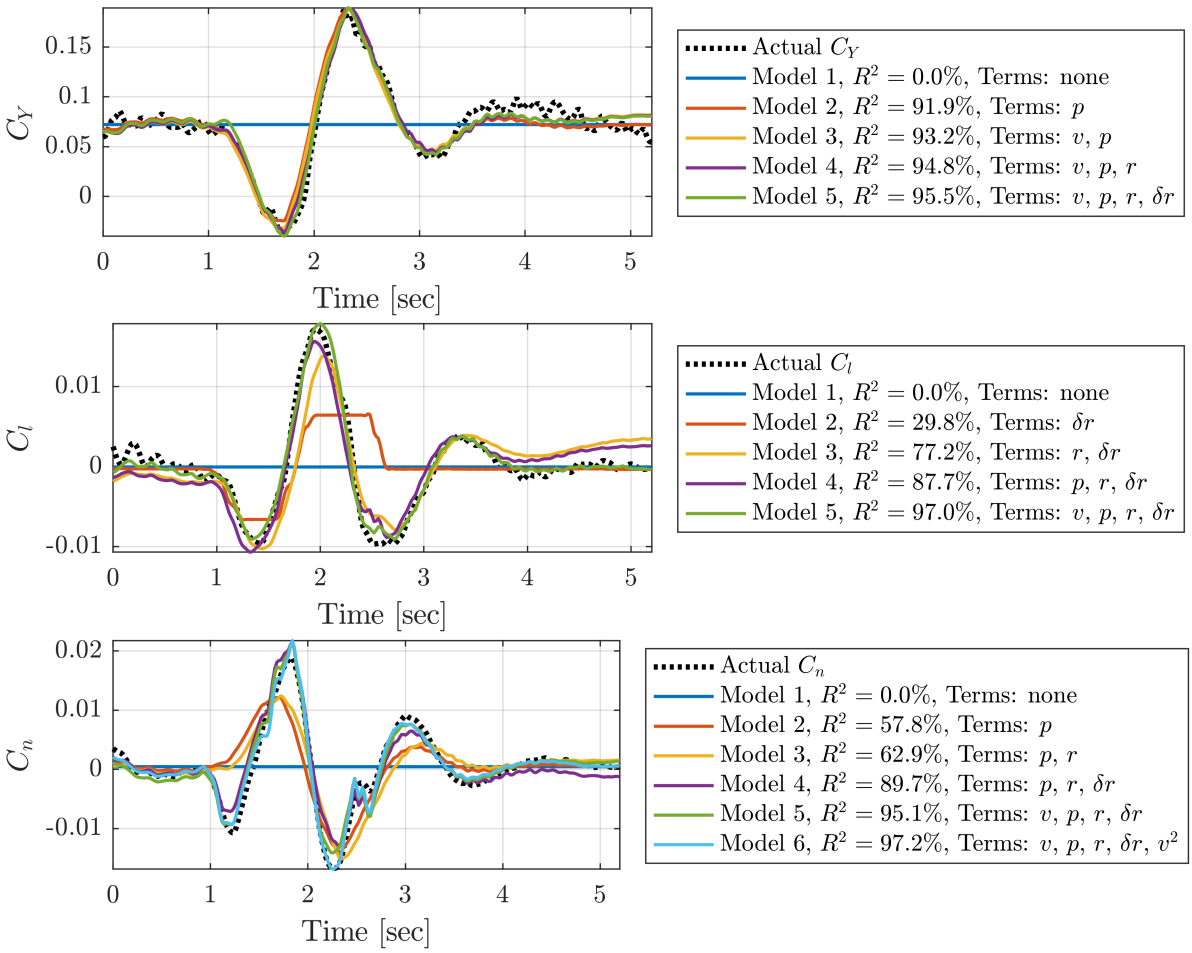

Figure 4.2: Stepwise regression iterations for C_Y, C_l, C_n using a Dutch Roll maneuver

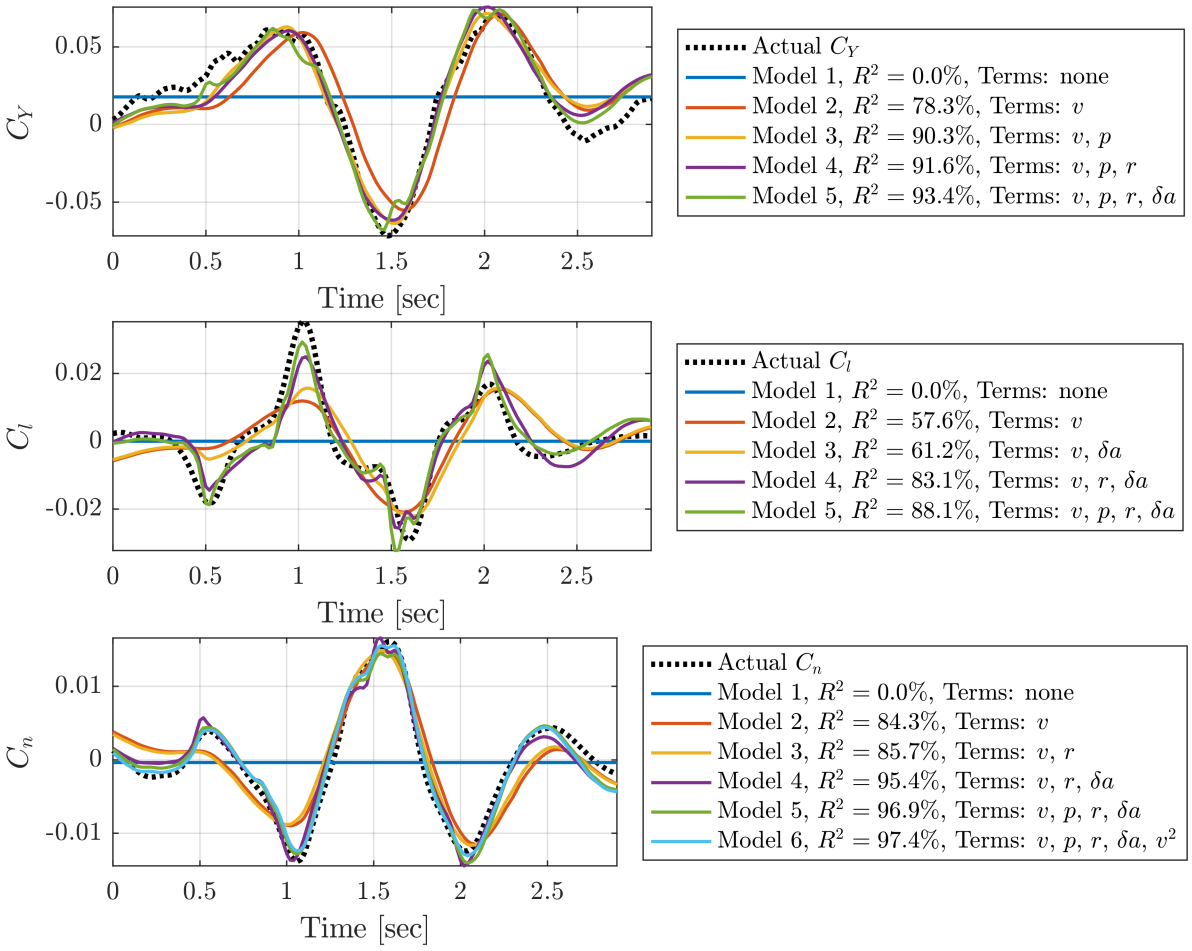

Figure 4.3: Stepwise regression iterations for C_Y, C_l, C_n using a Bank-to-Bank Roll maneuver

The best model structure determined for C_Y, C_l and C_n are shown in Equations (4.5)-(4.7). Each of these equation contain all the lateral-directional explanatory variables ($\hat{v}$, $\hat{p}$, $\hat{r}$, δa and δr). C_Y, C_l are purely linear equations; C_n is nonlinear in the form of $\hat{v}^2$ and linear in the remaining variables. The bias terms for C_Y, C_l, C_n are given as C_{Y_o}, C_{l_o}, C_{n_o} which characterize any aircraft asymmetries in aerodynamics or measurement error.

$$C_Y = C_{Y_v}\hat{v} + C_{Y_p}\hat{p} + C_{Y_r}\hat{r} + C_{Y_{\delta a}}\delta a + C_{Y_{\delta r}}\delta r + C_{Y_o} \tag{4.5}$$

$$C_l = C_{l_v}\hat{v} + C_{l_p}\hat{p} + C_{l_r}\hat{r} + C_{l_{\delta a}}\delta a + C_{l_{\delta r}}\delta r + C_{l_o} \tag{4.6}$$

$$C_n = C_{n_v}\hat{v} + C_{n_p}\hat{p} + C_{n_r}\hat{r} + C_{n_{\delta a}}\delta a + C_{n_{\delta r}}\delta r + C_{n_{v^2}}\hat{v}^2 + C_{n_o} \tag{4.7}$$

The final model structure developed contains nonlinearities which allow the model to characterize a larger portion of the flight envelope. At the same time, simplicity was emphasized such that to not over-parameterize the model.

4.2 Equation-Error Method Parameter Estimation

The equation-error method (EEM) was implemented by using the method of least-squares regression. The response variables were the external aerodynamic forces and moments on the aircraft, and the explanatory variables were composed of relevant aircraft states and control surface deflections. The full methodology was discussed in Section 3.3.4.

4.2.1 Equation-Error Method Modeling Performance

The model created from EEM parameter estimation of a single Short Period and Dutch Roll maneuver is displayed below as an illustrative example. The model for these single maneuvers was created from the least-squares fit of the relevant aerodynamic forces and moments which is shown in Figure 4.4. The fit to the aerodynamic forces and moments appears to be good overall at modeling the deterministic portion of the signal. Figure 4.5 shows the relevant outputs of a simulation of the model created for this single maneuver using both the equation-error method (EEM) and the output-error method (OEM) for comparison. This figure shows that the EEM model's representation of the system outputs are not as good as their representation of the forces and moments. Also, it can be seen that the OEM model significantly outperforms the EEM model. This same result was observed across all system identification maneuvers. When averaging the EEM parameter estimates across all

maneuvers, the overall modeling results will be worse than the figures shown here.

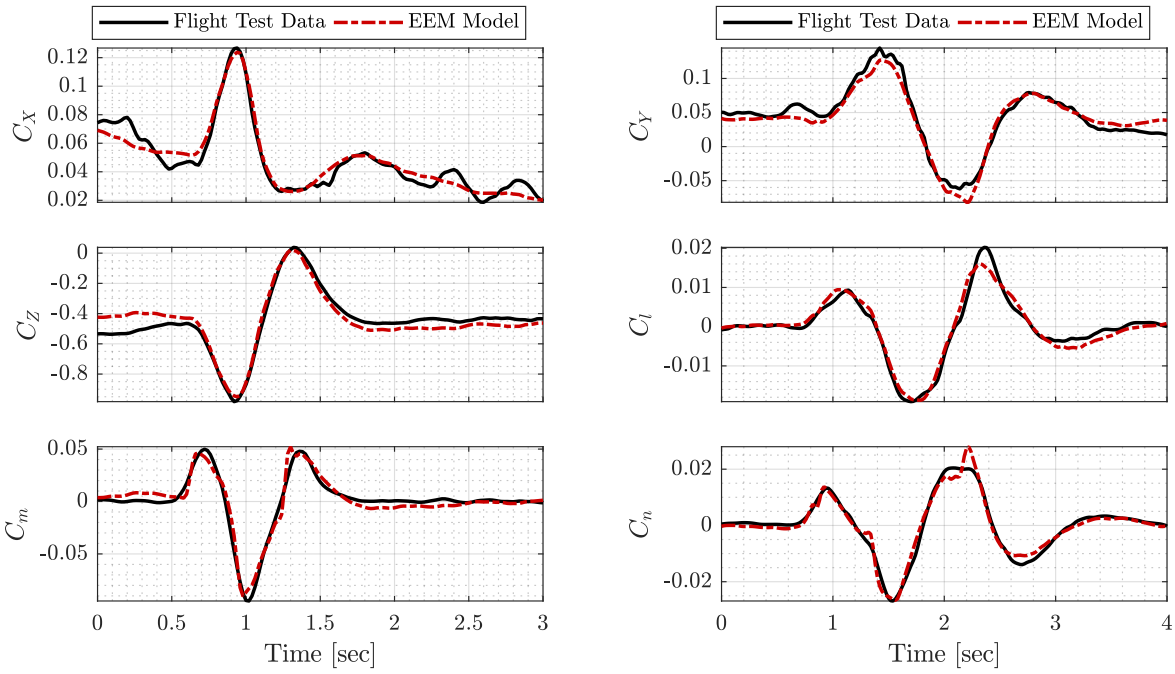

(a) Short Period (b) Dutch Roll

Figure 4.4: EEM least-squares fit: (a) C_X, C_Z, C_m for a Short Period maneuver, (b) C_Y, C_l, C_n for a Dutch Roll maneuver

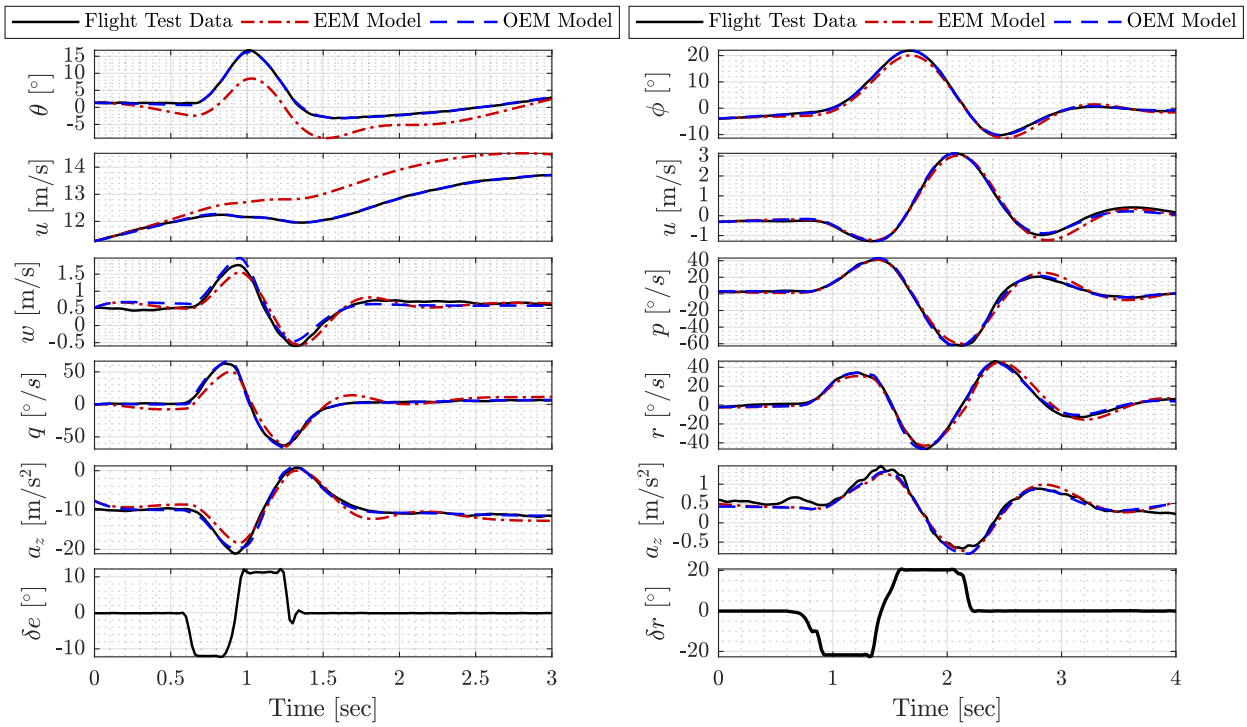

(a) Short Period (b) Dutch Roll

Figure 4.5: Simulation results from the EEM and OEM models creates for the same maneuvers as displayed in Figure 4.4; (a) Short Period maneuver, (b) Dutch Roll maneuver

4.2.2 Discussion of the Equation-Error Method

The parameter estimation results from the equation-error method (EEM) were deemed to be inadequate for model development for multiple reasons. Firstly, unsatisfactory performance in simulation of the models created from EEM parameter estimation was seen for all maneuvers similar to the presented example. One of the assumptions in this method is that the explanatory variables are known perfectly and contain no noise. This is a very poor assumption because the data obtained from the Bix3 aircraft is noisy and contains uncertainty in measurements due to low-cost sensors and the shear size of the aircraft. The fundamental formulation of the method used here also contains flaws due to the fact that optimal

prediction of the aerodynamic forces and moments are emphasized rather than prediction of aircraft outputs which are more important in practice. Additionally, the aerodynamic forces and moments for which the estimation is performed are lower quality signals because their calculation required multiple states and state derivatives which adds noise to these calculations.

One benefit of the equation-error formulation is its computational speed which is much faster than the output-error method. It is for this reason the equation-error method is used for the model structure identification process. The equation-error method would also be beneficial in scenarios of real-time parameter estimation. However, for all other reasons outlined in this section, the equation-error formulation was used only to assist in development of the model structure and to calculate an initial guess of parameter estimates for use in the output-error method. The output-error method is more appropriate for this system identification effort because it can account for measurement noise and places the focus on minimizing the model error with respect to more desirable states and state derivatives.

4.3 Longitudinal Model Parameter Estimation

The output-error method was used as the final parameter estimation method because it provided the most accurate results due to reasons discussed in the previous section. The output-error method required an initial guess of parameter estimates which was chosen to be the average value of each respective parameter estimate obtained from the equation-error method after removal of outliers. The longitudinal model parameter estimates for C_X, C_Z and C_m were developed from the Short Period flight maneuver. The methodology for the procedures used to develop these results was discussed in Section 3.3.5.

4.3.1 Longitudinal Parameter Estimation from FTD Only

The results from the parameter estimation of the longitudinal model from flight test data (FTD) alone are shown in Table 4.1. The median of the population of parameter estimates from all system identification Short Period maneuvers is reported as the predicted value. The error bounds are created from two scaled median absolute deviations (MAD) which would approach the 95% confidence interval for a normally distributed data set. This is used opposed to confidence intervals obtained from a t-distribution because of the MAD's robustness to outliers while reporting the same measure, and because this is a more appropriate measure of variability since the median was chosen as the best parameter estimate. Both metrics, as expected, yielded similar results for parameter estimates where the population scatter appeared to be approximately normally distributed.

Table 4.1: Longitudinal parameter estimates from flight test data (FTD) only

Coef.	Value	95% CI	Coef.	Value	95% CI	Coef.	Value	95% CI
C_{X_u}	-0.190	± 0.157	C_{Z_w}	-5.33	± 3.58	C_{m_w}	-0.286	± 0.421
C_{X_w}	$+0.345$	± 0.407	C_{Z_q}	$+16.7$	± 43.7	C_{m_q}	-3.89	± 5.47
$C_{X_{w^2}}$	$+0.681$	± 1.64	$C_{Z_{\delta e}}$	$+0.206$	± 0.928	$C_{m_{\delta e}}$	-0.350	± 0.172
C_{X_o}	$+0.248$	± 0.210	$C_{Z_{w^2}}$	$+4.83$	± 19.9	C_{m_o}	$+0.0146$	± 0.0198
			C_{Z_o}	-0.114	± 0.384			

Histograms of all longitudinal parameter estimates are displayed in Figure A.1 in Appendix A.1. The mean, median and confidence intervals created from two scaled MAD are displayed for each parameter. Many of the parameter estimates appear to roughly follow a Gaussian distribution as would be expected for maximum likelihood parameter estimates, however, some do not which confirms the validity of the use of the median and MAD rather than the mean and standard deviation which will be more biased toward outliers in the data. As can be seen in the figure, there is a particularly large scatter in the parameter estimates for the terms in C_Z, and a lesser, but still significant scatter in the parameter estimates for

C_X and C_m. Overall, the results show that there is significant room for improvement, of which method will be discussed in the next section.

The Cramér-Rao lower bound, or standard error, for each individual parameter Θ for each maneuver was calculated using the parameter covariance matrix which is computed as an intermediate step in the output-error method (see Equations (2.53)-(2.54)). The theory behind the output-error method assumes the residuals are white, Gaussian and zero mean, however, the residuals from FTD parameter estimation are usually colored due to process noise, modeling error and residual correlation [1, 17]. Error bar plots of the individual parameter estimates assuming white residuals are displayed in Figure 4.6a. The error bars represent twice the standard error (2σ) from the parameter estimate which is an attempted approximation of the 95% confidence interval for each individual parameter estimate. The figure shows that for this data set the residuals were colored as indicated by overly optimistic standard error calculations. The error bounds are clearly not representative of the scatter in the data across all maneuvers.

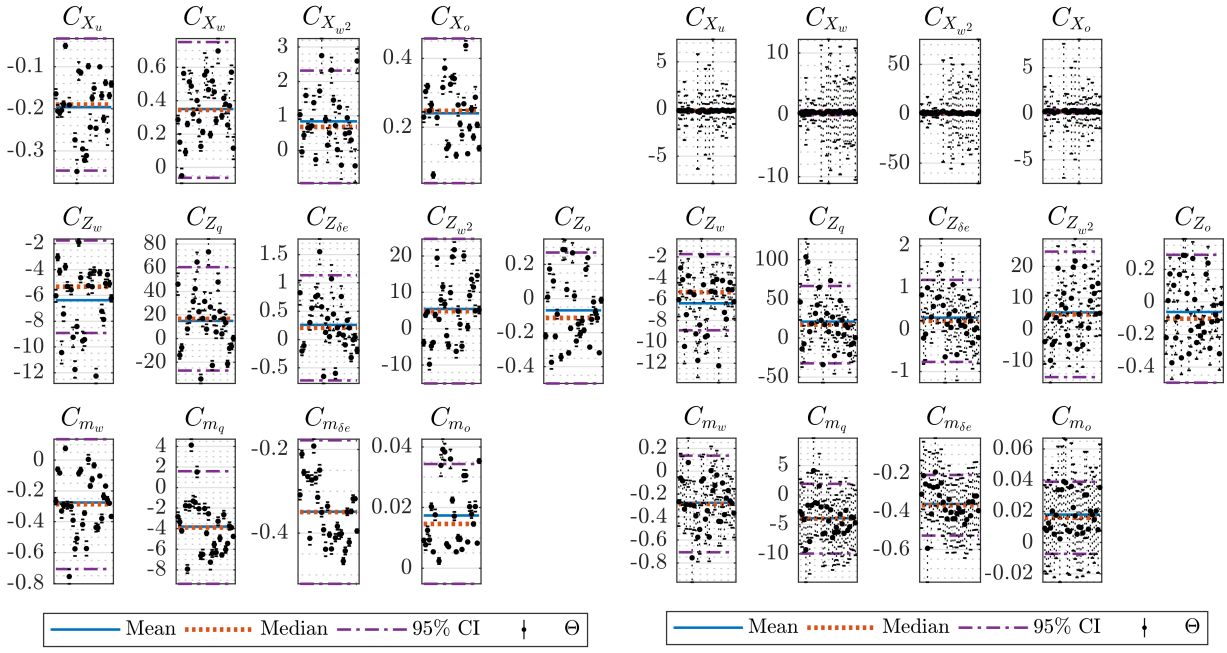

(a) White Residuals

(b) Colored Residuals Correction

Figure 4.6: Comparison of estimated error bounds of individual parameter estimates (Θ) assuming white residuals and correcting for colored residuals; error bars represent 2σ

The correction for colored residuals developed in Morelli and Klein [1] was applied to each maneuver to attempt to correct for residual coloring (see Equations (2.55)-(2.57)). Error bar plots after the correction for residual coloring had been applied can be seen in Figure 4.6b, where the error bounds represent 2σ or an approximation of the 95% confidence interval. However, it can be seen that the correction for colored residuals appeared to severely over-predict the error in the C_X parameters, while under-predicting the error for the C_Z parameters compared the spread in the population of parameter estimates. The correction appears to be representative of the scatter for the C_m parameter estimates. Due to the unreliable results for the residual coloring correction, the rudimentary "fudge factor" suggested in Jategaonkar [2], appeared to be just as accurate in correcting for residual coloring as the sophisticated correction presented in Morelli and Klein [1] for the longitudinal

parameter estimates. Due to the unreliable prediction of variance from individual maneuvers, it appears to be a superior technique to predict variance in the parameter estimates by analyzing a population of parameter estimates developed from a series of individual flight maneuvers.

The stability properties of the longitudinal dynamics were analyzed to compare to the vortex lattice method (VLM) results which were used for input design. The results from the analysis are shown in Table 4.2. The nonlinear aircraft equations of motion were linearized about a reference condition to calculate the longitudinal and lateral-directional linearized state matrices. The Phugoid mode is omitted due to the difficulty in estimating the mode accurately for an aircraft of this scale and because maneuvers to excite this mode were not performed. The stability properties calculated using VLM was displayed in Table 3.8. The estimated period of oscillation T from VLM was 0.474 seconds which is very close to the results from FTD parameter estimates. The predicted damping ratio from VLM was $\zeta = 0.703$ which is less damped than the results from parameter estimation from FTD.

Table 4.2: Longitudinal modal analysis of the Bix3 aircraft from flight test data at V_a=12 m/s, $\theta = 0°$

Mode	Eigenvalue	f (Hz)	T (sec)	ζ	$t_{1/2}$ (sec)
Short Period	$-12.5 \pm 4.61i$	2.12	0.471	0.938	0.055

4.3.2 Longitudinal Parameter Estimation from FTD & VLM

To attempt to improve the longitudinal model, information was incorporated from the vortex lattice method (VLM) parameter estimates developed in Section 3.1.2, using the procedures discussed in Section 3.3.5. The VLM parameters found to be most useful for this purpose were C_{X_w}, C_{Z_w} and C_{Z_q}. Combinations of these terms were fixed and the output-error method was run again holding a variable number of these VLM parameters constant.

The best combinations of VLM fixed parameter estimates appeared to be to fix C_{Z_w}; C_{Z_w} and C_{Z_q}; or C_{X_w}, C_{Z_w} and C_{Z_q}. The parameter estimates for these cases are shown in Tables 4.3-4.5, respectively. Similar to the results above, the reported values are based on the median and two scaled MAD.

Table 4.3: Longitudinal parameter estimates fixing the VLM value of C_{Z_w}, and then estimating the remaining terms from FTD

Coef.	Value	95% CI	Coef.	Value	95% CI	Coef.	Value	95% CI
C_{X_u}	-0.176	± 0.172	C_{Z_w}	-5.32	(VLM)	C_{m_w}	-0.245	± 0.177
C_{X_w}	$+0.298$	± 0.293	C_{Z_q}	$+1.61$	± 41.2	C_{m_q}	-4.28	± 4.38
$C_{X_{w^2}}$	$+0.717$	± 0.772	$C_{Z_{\delta e}}$	-0.00339	± 0.871	$C_{m_{\delta e}}$	-0.368	± 0.156
C_{X_o}	$+0.225$	± 0.201	$C_{Z_{w^2}}$	$+4.05$	± 11.1	C_{m_o}	$+0.0134$	± 0.013
			C_{Z_o}	-0.175	± 0.182			

Table 4.4: Longitudinal parameter estimates fixing the VLM values of C_{Z_w} and C_{Z_q}, and then estimating the remaining terms from FTD

Coef.	Value	95% CI	Coef.	Value	95% CI	Coef.	Value	95% CI
C_{X_u}	-0.167	± 0.172	C_{Z_w}	-5.32	(VLM)	C_{m_w}	-0.236	± 0.196
C_{X_w}	$+0.384$	± 0.261	C_{Z_q}	-8.20	(VLM)	C_{m_q}	-4.42	± 2.54
$C_{X_{w^2}}$	$+0.678$	± 2.05	$C_{Z_{\delta e}}$	-0.272	± 0.393	$C_{m_{\delta e}}$	-0.365	± 0.127
C_{X_o}	$+0.202$	± 0.200	$C_{Z_{w^2}}$	$+7.21$	± 5.59	C_{m_o}	$+0.0119$	± 0.0136
			C_{Z_o}	-0.178	± 0.243			

Table 4.5: Longitudinal parameter estimates fixing the VLM values of C_{X_w}, C_{Z_w} and C_{Z_q}, and then estimating the remaining terms from FTD

Coef.	Value	95% CI	Coef.	Value	95% CI	Coef.	Value	95% CI
C_{X_u}	-0.156	± 0.157	C_{Z_w}	-5.32	(VLM)	C_{m_w}	-0.240	± 0.195
C_{X_w}	$+0.297$	(VLM)	C_{Z_q}	-8.20	(VLM)	C_{m_q}	-4.49	± 2.13
$C_{X_{w^2}}$	$+0.960$	± 1.90	$C_{Z_{\delta e}}$	-0.308	± 0.351	$C_{m_{\delta e}}$	-0.364	± 0.119
C_{X_o}	$+0.197$	± 0.195	$C_{Z_{w^2}}$	$+7.02$	± 4.05	C_{m_o}	$+0.0134$	± 0.0149
			C_{Z_o}	-0.179	± 0.152			

The scatter of individual parameter estimates for the best cases where fixing VLM terms improved the model are displayed in Figures A.2-A.4 in Appendix A.1. Comparing to

the results from FTD alone, there is less scatter in the parameter estimates when VLM information was included. This is the improvement that was hypothesized since fewer parameters are being estimated from flight test data, and thus, the smaller number of parameters are estimated more accurately. Comparison of the created models will be explored further in the proceeding section.

4.3.3 Comparison of Modeling Performance and Uncertainty

In this section the model created from flight test data (FTD) only will be compared to the models created using both FTD and VLM. This will be done through validation of each model through simulation, modeling error analysis and uncertainty in individual parameter estimates.

Model Validation

Model validation was performed through simulation of maneuvers not included in the system identification process. Here, the simulation inputs were the initial conditions and the elevator inputs used in the Short Period maneuvers. Figure 4.7 shows the predictions of the longitudinal force and moment coefficients across three validation Short Period maneuvers with differing control amplitude and polarity. It can be seen that the models containing terms fixed from VLM outperform the model created from FTD alone, indicated by the model more closely following the measured FTD. C_X and C_Z show the most improvement when VLM parameter estimates are incorporated. The pitching moment coefficient C_m only shows marginal visual improvement. Overall, the models created from FTD and VLM in unison are able to better predict the aerodynamic force and moment coefficients than the model created from FTD alone.

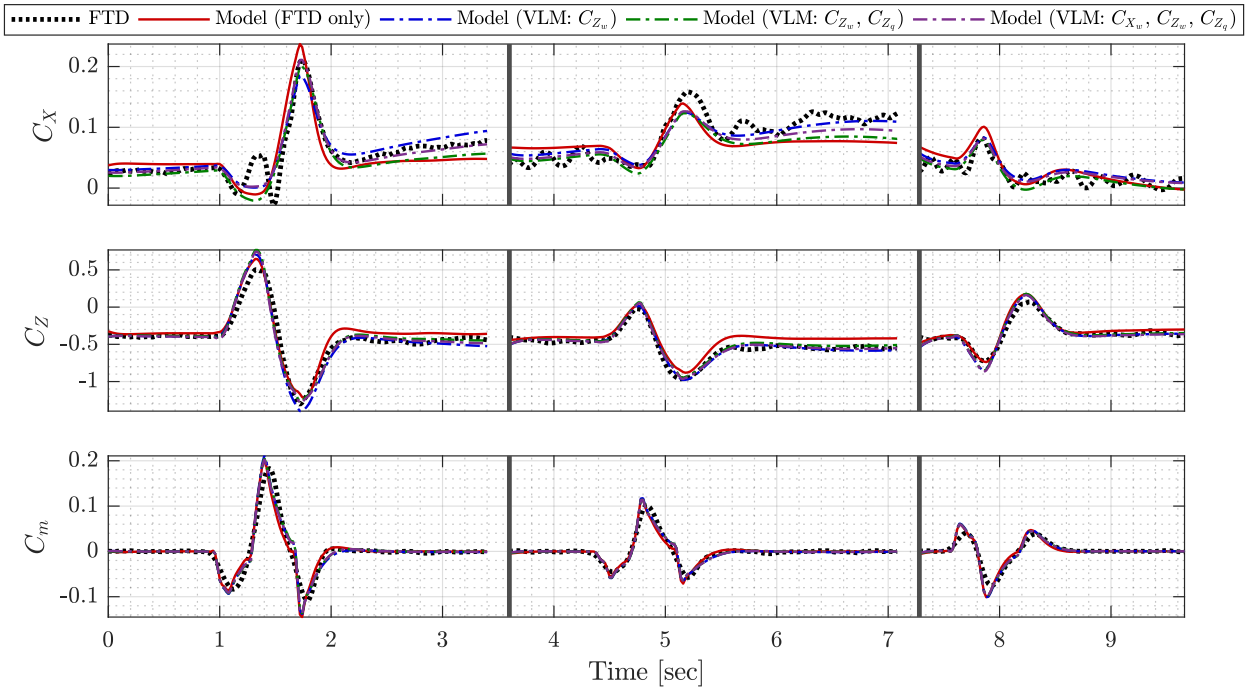

Figure 4.7: Comparison of C_X, C_Z, C_m simulation results for different longitudinal models for Short Period maneuvers not included in the system identification process

Figure 4.8 shows the important longitudinal outputs from simulation of the same validation Short Period maneuvers and models shown in Figure 4.7. It can be seen that the models created using information from VLM do a superior job of modeling the longitudinal dynamics. The most clear deficits in the model created from FTD only can be seen in the outputs of u and θ. There appears to be drift in the output of u in the model estimated from FTD alone, possibly caused by inaccurate bias terms. Even after correction of potential shortcomings, a similar behavior of drift is observed which can be attributed to overall modeling error in the model created from FTD alone.

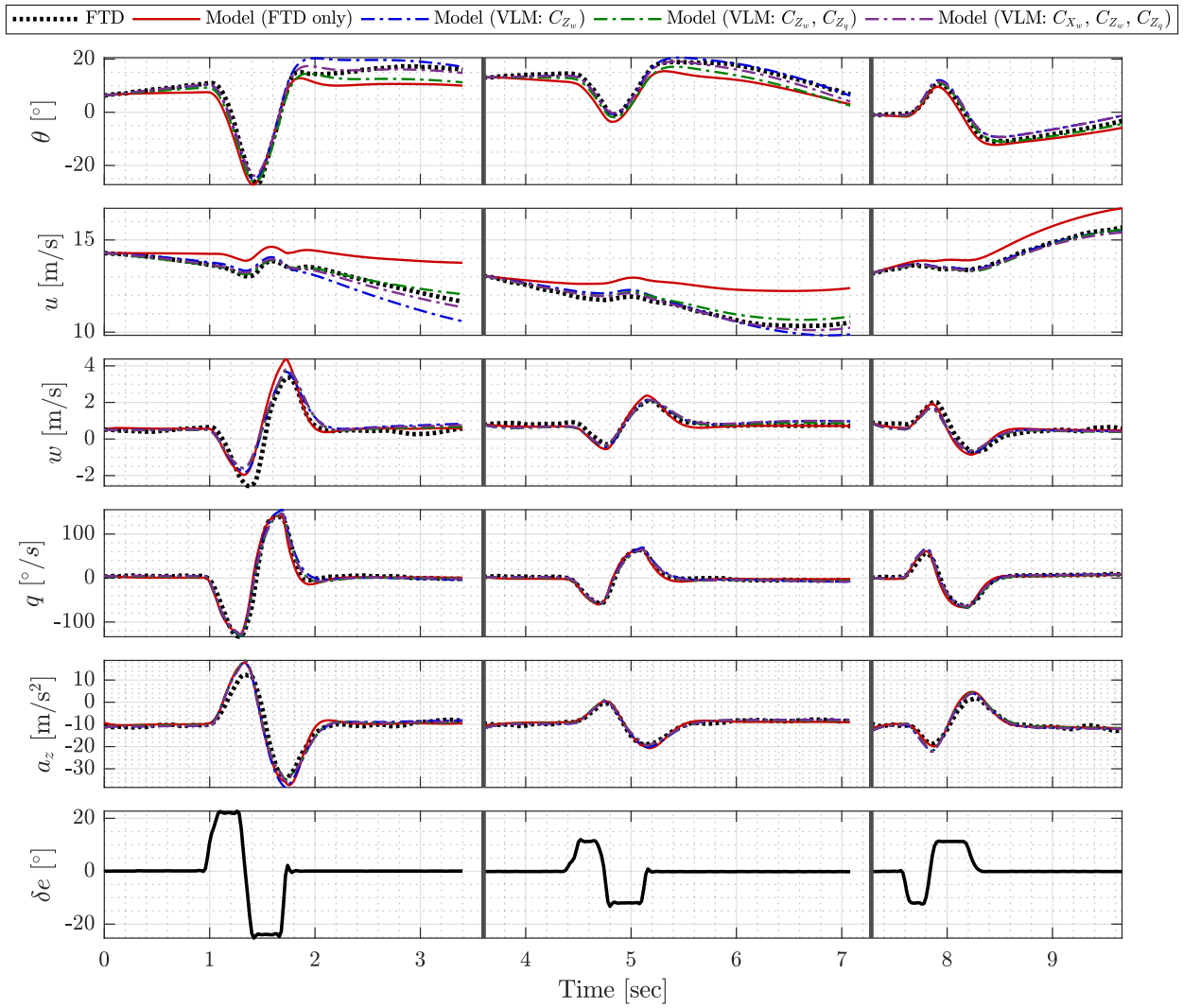

Figure 4.8: Comparison of output simulation results for different longitudinal models for Short Period maneuvers not included in the system identification process

Error Analysis

The results of the preceding sections will now be further analyzed over all collected longitudinal maneuvers. The overall modeling error can be quantified using the root-mean-square error (RMSE) and/or the mean absolute error (MAE) of important model output quantities (Equations (3.19)-(3.20)). Both will be presented due to the separate assumptions

present in each metric to better quantify the overall error [38]. The average normalized root-mean-square error (ANRMSE) and average normalized mean absolute error (ANMAE) of all the important output quantities were developed in Section 3.3.6 (Equations (3.21)-(3.22)). These metrics are a method of combining the modeling error of all model outputs into a single metric for each maneuver.

Figure 4.9 displays box plots of the percent change (Equation (3.23)) in ANRMSE and ANMAE in longitudinal outputs on a per-maneuver basis across all longitudinal maneuvers. In this figure, the modeling performance of models created by fixing certain VLM parameter estimates are compared to the performance of the model created from FTD alone, which is the baseline case. Significant percent change outliers have been removed to facilitate better presentation of the majority of results, using the criteria of 1.5 interquartile ranges beyond the 25^{th} or 75^{th} percentile constitutes an outlier (This corresponds to the 99.3% confidence interval assuming a normal distribution [36]). A high negative value in percent change of ANRMSE or ANMAE indicates a larger improvement over the baseline model created from FTD only. It can be seen that all models which incorporated parameter estimates from VLM displayed in the figure showed improvement over the baseline case of the model created from FTD alone. The best models based on these metrics appear to be models with C_{Z_w}; C_{Z_w} and C_{Z_q}; or C_{X_w}, C_{Z_w} and C_{Z_q}, held constant to the parameter estimates from VLM, which is why their results were presented in Tables 4.3-4.5 and Figures A.2-A.4.

A one-sided paired t-test and one-sided Wilcoxon signed-rank test (a non-parametric version of the paired t-test, see Section 3.3.6) were used to test the null hypothesis that the models created using VLM and FTD compared to the model created FTD alone had the statistically same mean values. Each separate flight maneuver is considered a paired, independent event. The tests for all VLM parameter combinations shown in Figure 4.9 rejected the null hypothesis with a p-value at a minimum of 7×10^{-5} indicating that the

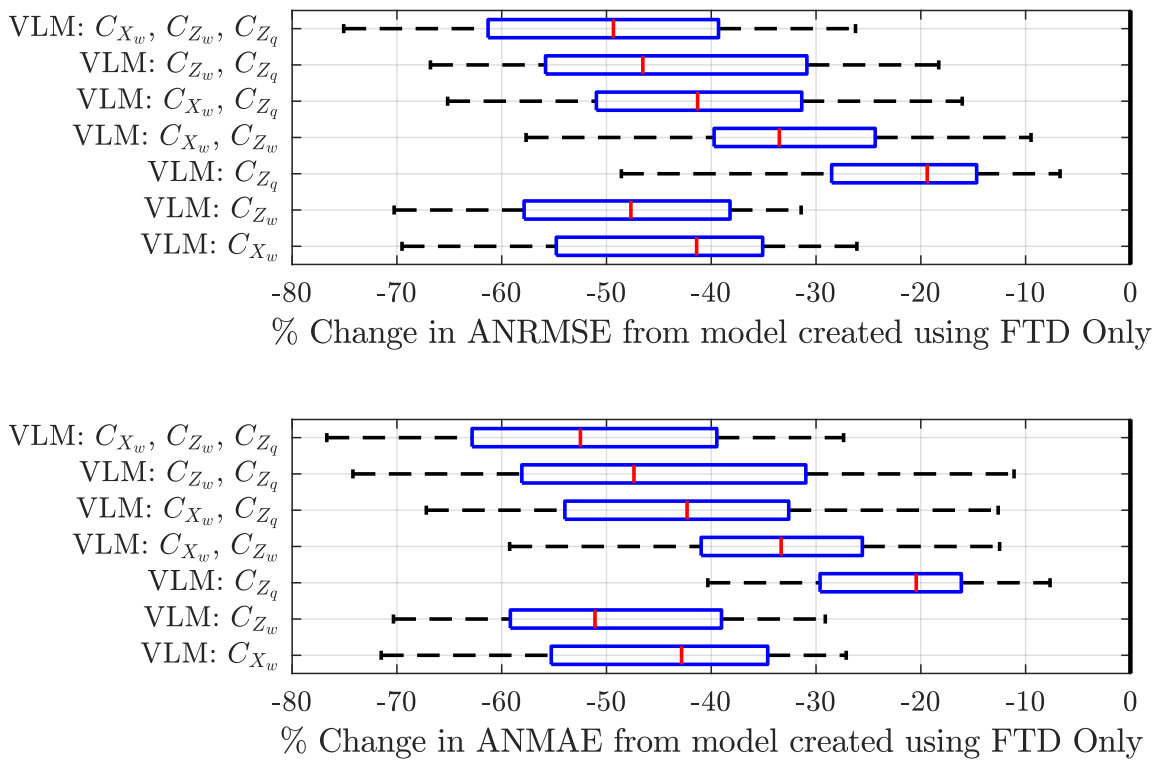

Figure 4.9: Percent change in ANRMSE (top) and ANMAE (bottom) of longitudinal output quantities calculated on a per-maneuver basis for models created by fixing the indicated terms to their VLM parameter estimates (a more negative value indicates a high model improvement over the baseline case)

models created using information from VLM showed statistically significant improvement in reduction of modeling error compared to using FTD alone.

The percent change in RMSE and MAE of C_X, C_Z, C_m on a per-maneuver basis were computed for models containing certain VLM parameter estimates and compared to the baseline model created from FTD only. These results are shown in box plots in Figure 4.10. A high negative value indicates a larger improvement in the error in C_X, C_Z, C_m when VLM parameter estimates were used as a supplement to FTD. It can be seen that the largest improvement is typically seen in the force coefficients C_X and C_Z. The pitching moment coefficient C_m also improves when information from VLM is included, but not as much in percent change in these error metrics. This again shows that models created by incorporating

VLM parameter estimates of C_{Z_w}; C_{Z_w} and C_{Z_q}; or C_{X_w}, C_{Z_w} and C_{Z_q}, generally appear to show the best performance.

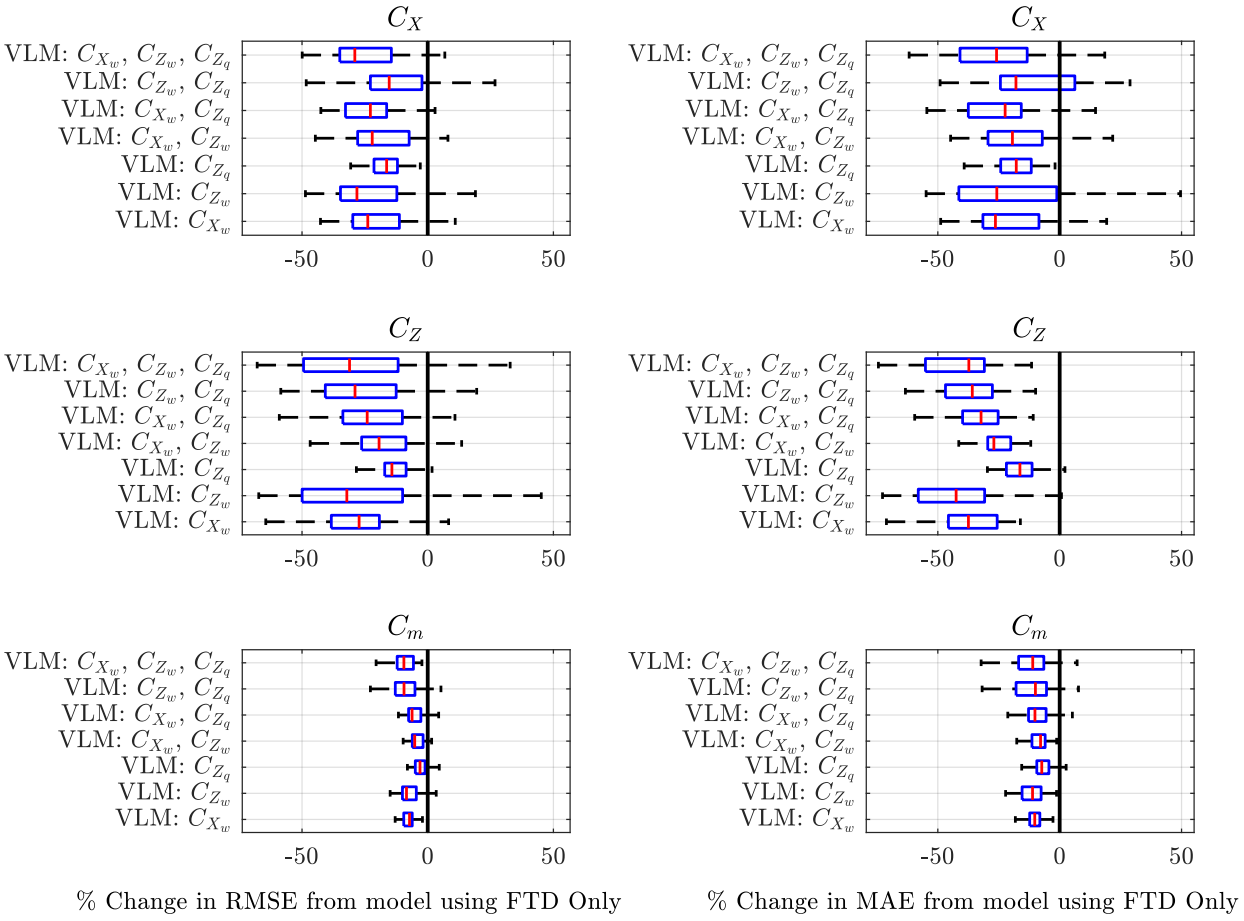

Figure 4.10: Percent change in RMSE (left) and MAE (right) of C_X, C_Z, C_m calculated on a per-maneuver basis for models created by fixing the indicated terms to their VLM parameter estimates (a more negative value indicates a high model improvement over the baseline case)

Uncertainty of Parameter Estimates

The error bar plots for each longitudinal parameter estimate from the best models which incorporated VLM parameter estimation and the model created from FTD alone are shown in Figure 4.11. The error bars are centered on the median parameter estimate, and the error bars themselves represent the 95% confidence interval calculated from two scaled

MAD. The terms which were fixed to a value estimated from VLM have no error bars. It can be seen that the parameter estimates from FTD alone have a larger uncertainty compared to the parameter estimates when certain terms estimated using VLM were held constant. All parameter estimates in C_Z and C_m generally decrease in their respective uncertainties when terms are incorporated from VLM. The terms in C_X did not generally appear to be affected much in their respective uncertainties regardless of whether VLM parameter estimates were included or not. C_X was the most noisy force or moment coefficient used in analysis which could provided an explanation for the large uncertainty in its parameter estimates.

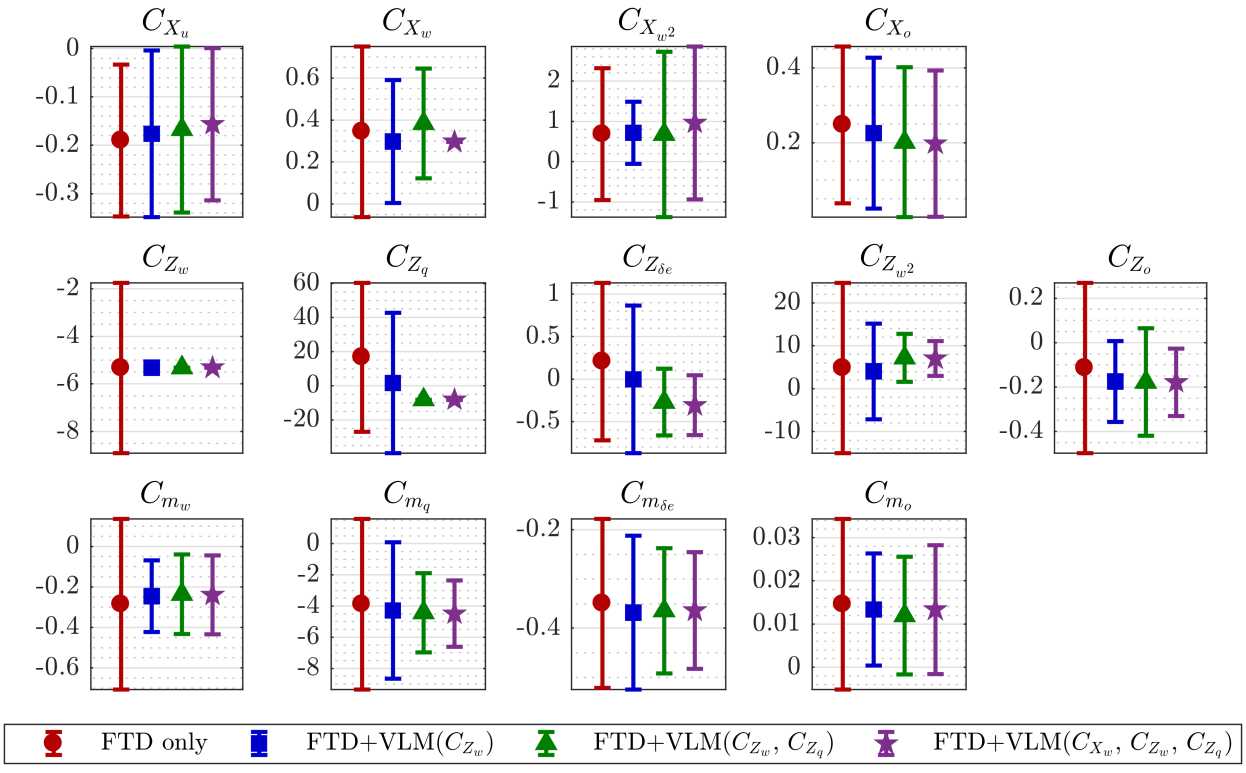

Figure 4.11: Uncertainty in parameter estimates calculated from FTD only and FTD with certain terms fixed to their indicated VLM parameter estimates

4.3.4 Discussion of Longitudinal Parameter Estimation

The results for longitudinal parameter estimation showed that estimation from FTD only had underwhelming modeling performance and a large uncertainty in individual parameter estimates. This shortcoming can be attributed to multiple different factors. Correlated measurement error and process noise both may have caused degradation in data quality. Due to the high noise levels, larger amplitude perturbations were needed to collect data with an acceptable signal-to-noise ratio needed for system identification. This required that the model structure be nonlinear and eliminated the possibility of using small perturbation maneuvers to identify a subset of linear terms (see Section 3.3.1). Also, the fact that the Short Period mode for the Bix3 was found to be well-damped may have caused difficulty in estimation because of the limited amount of identifiable free aircraft response after the control input.

Due to the nonlinear model structure needing to be estimated all at once, the noisy data, and nature of the longitudinal dynamics, there appeared to be a larger number of model parameters than could be accurately estimated using FTD alone. One illustrative example of this is in the parameter estimates of C_{Z_q} and $C_{Z_{\delta e}}$, where there is a very large error bound and the parameter estimates appear to have converged to the incorrect sign for a typical stable aircraft. One possible explanation for this is data collinearity, due to the pitch rate signal q being similar in shape to the elevator deflection signal δe, as a consequence of the well-damped Short Period dynamics. The estimator may have had difficulty in quantifying the separate effects of these signals on the aircraft response in parameter estimation. The average correlation coefficient between these two parameter estimates was found to be $\rho_{C_{Z_q} C_{Z_{\delta e}}} = 0.85$ which indicates some linear dependence in the parameter estimates. However, this value of the correlation coefficient is not above the tolerance which would indicate detrimental modeling effects requiring reformulation (see Section 2.3.5).

To perform longitudinal parameter estimation from FTD alone for this aircraft, an improved instrumentation system would likely be needed either to lower the noise level and/or provide more measurements. Other maneuvers could be performed to provide additional information about the longitudinal dynamics to aid in parameter estimate, however, the additional longitudinal maneuvers discussed in Section 2.3.2 are simply not practical for a ground-piloted aircraft of this scale. Changing the control input for the Short Period maneuver to a 3-2-1-1 or 2-1-1 may also improve results, but the time step in these inputs may become impractically small and difficult to implement due to the fast Short Period dynamics.

Due to the lack of performance of the model created from FTD alone, VLM was used to supplement the information content of the FTD such that fewer parameters needed to be estimated without removing any of the desired complexity in the model structure. The use of VLM significantly improved the modeling performance and decreased the uncertainty in the parameters identified. Again focusing on the parameters of C_{Z_q} and $C_{Z_{\delta e}}$ as an example, it can be seen that when the term C_{Z_q} is fixed from VLM, the estimated value of $C_{Z_{\delta e}}$ from FTD significantly decreases in uncertainty, and has the correct sign that would be anticipated. Incorporation of VLM allowed the creation of a model of acceptable quality for use in future applications. This shows that incorporation of accurate parameter information from sources other than FTD can be used to improve the resulting model.

A difficulty encountered in the overall parameter estimation for the longitudinal dynamics was that the aerodynamic bias terms (C_{X_o}, C_{Z_o}, C_{m_o}) appeared to change on a per-flight basis. This could be attributed to flaws in the measurement system, where the calibration of the measured parameters changes between flights, causing the aerodynamic bias terms to change. This could also be caused by slight changes in the weight distribution when the battery was changed between flights, even though the aircraft had the same weight

for all flights. Additionally, slight changes in control surface trims between flights may have led to the changing bias terms. These observations could also technically cause other model terms to change, but this did not appear to happen. The difficulty with estimation of the bias terms can be resolved by re-estimating these on all flights, but this is an inconvenient phenomena, especially if it is desired to model the aircraft in flights when these terms were not estimated. The phenomena of small changes in bias terms between maneuvers or flights is not an uncommon occurrence and can be seen in full-scale aircraft where the error can be attributed to measurement biases [1]. This effect, however, is likely more pronounced in this work than what would be seen for a full-scale aircraft.

4.4 Lateral-Directional Parameter Estimation

Similar to the longitudinal model, the output-error method was used to identify the final parameter estimates. The initial guess of parameter estimates used in the output-error method were again the average values obtained from the equation-error method parameter estimates after outliers were removed. The lateral-directional parameter estimates were developed from the Dutch Roll and Bank-to-Bank Roll maneuvers. The methodology for the procedures used to develop these results were discussed in Section 3.3.5.

4.4.1 Lateral-Directional Parameter Estimation from FTD only

Originally the parameter estimation was performed treating the two lateral-directional flight maneuvers separately. The two maneuvers provided estimates for all stability derivatives and the bias terms in the model. The Bank-to-Bank Roll maneuver was used to identify the aileron control derivatives ($C_{Y_{\delta a}}$, $C_{l_{\delta a}}$, $C_{n_{\delta a}}$) and the Dutch Roll maneuver was

used to identify the rudder control derivatives ($C_{Y_{\delta r}}$, $C_{l_{\delta r}}$, $C_{n_{\delta r}}$). This approach was, however, deemed inadequate because the two different maneuvers predicted differing values for several of the stability derivatives. A solution to this problem used in practice is performing these maneuvers back-to-back, such that all terms can be estimated in one maneuver. This could not be done in this system identification effort because of the difficulty in performing these maneuvers together without degrading the quality of the maneuvers.

The scatter of the results from identifying the maneuvers separately is shown in Figure 4.12. The parameter estimates of the individual maneuvers are shown with error bars created from the Cramér-Rao lower bound, or the predicted standard error, corrected for residual coloring [1]. Similar to the longitudinal parameter estimates, the conventional Cramér-Rao lower bound severely under-predicted the variance seen in the scatter of parameters estimated from individual maneuvers. The ends of the error bars are indicative of the 95% confidence interval predicted for each individual maneuver, which is calculated from two times the corrected Cramér-Rao lower bound (2σ). The plot shows that the Dutch Roll and Bank-to-Bank Roll predict different estimates of the stability derivatives C_{Y_v}, C_{Y_p}, C_{Y_r}, C_{l_v}, C_{n_v}, C_{n_p} and $C_{n_{v^2}}$. Also note that the correction for colored residuals for individual maneuvers appears to be representative of the maneuver specific scatter in the data, which was not the case for most longitudinal parameter estimates.

Due to the differing predictions of parameter estimates for the two lateral-directional maneuvers, a series of steps needed to be taken to identify one unique set of parameter estimates to describe all lateral-directional dynamics. As can be seen in Figure 4.12, the predicted variability in parameter estimates from the Bank-to-Bank Roll maneuvers is lower for the terms C_{Y_v}, C_{Y_p}, C_{Y_r}, C_{l_v}, C_{n_v} and $C_{n_{v^2}}$ compared to the respective parameter estimates from the Dutch Roll maneuver. The Bank-to-Bank Roll is a longer, less dynamically-coupled maneuver than the Dutch Roll, so it makes intuitive sense that Bank-to-Bank Roll appears

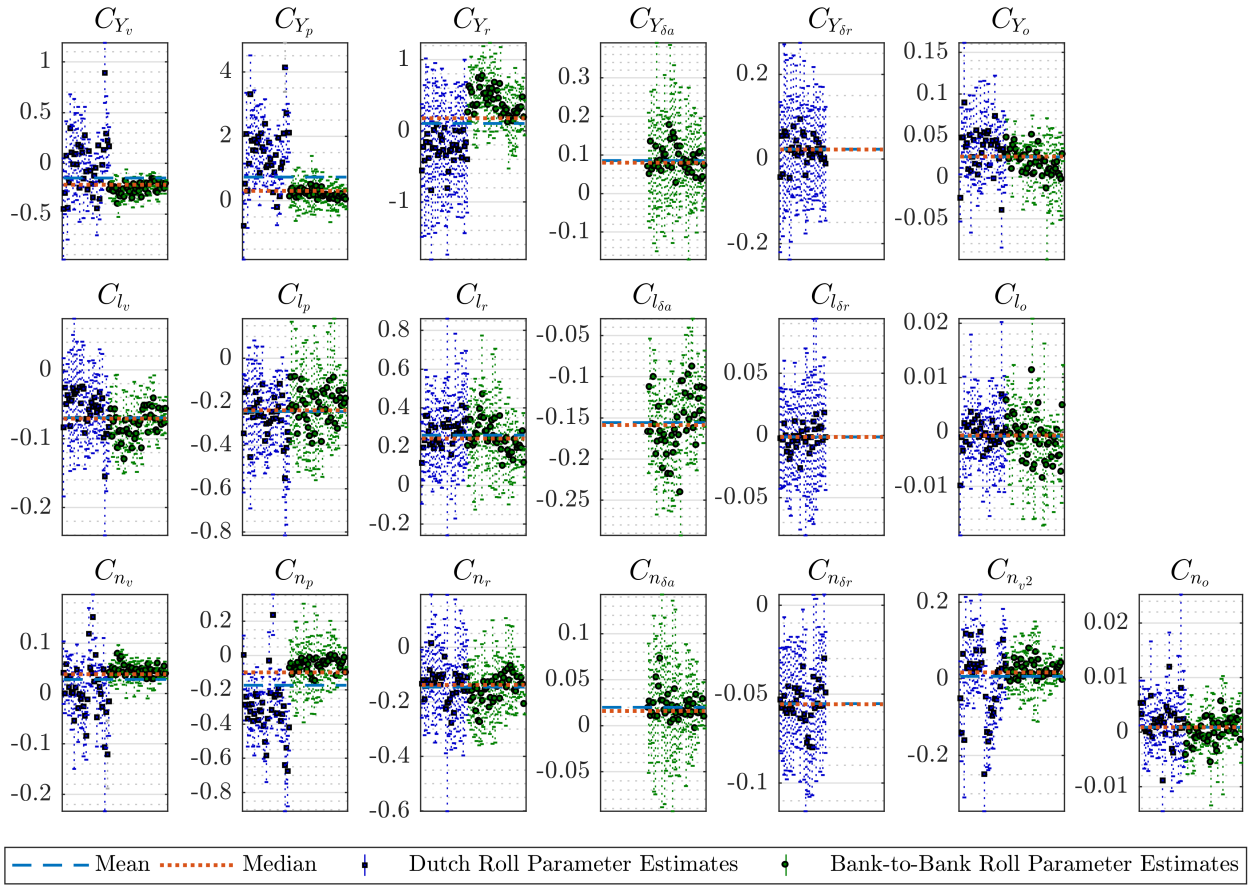

Figure 4.12: Error bar plots of parameter estimates from the individual Dutch Roll and Bank-to-Bank Roll maneuvers; error bars represent 2σ and account for residual coloring

to be more accurate at predicting several stability derivatives. The first step in the process to create a unique set of parameter estimates was to estimate the terms better predicted from the Bank-to-Bank Roll using only that maneuver. Note that the term C_{n_p} also appears to have lower variability in the Bank-to-Bank Roll estimates, however, this term was found to be better estimated from the Dutch Roll maneuver, so it is omitted from this step.

After C_{Y_v}, C_{Y_p}, C_{Y_r}, C_{l_v}, C_{n_v} and $C_{n_{v^2}}$ had been estimated from the Bank-to-Bank Roll maneuver, these terms were fixed and the remaining terms were estimated from the Dutch Roll maneuver. At this step, it was found to be beneficial to fix the terms C_{l_p}, C_{n_p} and C_{n_r} from the Dutch Roll parameter estimates, and then re-identify the C_{l_r}, the

aileron control derivatives and bias terms from the Bank-to-Bank Roll maneuver. Finally, all stability derivatives were held fixed and the rudder control derivative and bias terms for the Dutch Roll maneuver were re-identified. This set of steps in displayed in Table 4.6. This set of steps, while likely not completely unique, was found to produce the best modeling results using one set of parameter estimates to describe all lateral-directional dynamics.

Table 4.6: Steps for combining information from the Bank-to-Bank Roll and Dutch Roll maneuvers into a single set of lateral-directional parameter estimates

Iteration	Maneuver	Estimated Model Terms
1	Bank-to-Bank Roll	C_{Y_v}, C_{Y_p}, C_{Y_r}, C_{l_v}, C_{n_v}, $C_{n_{v^2}}$
2	Dutch Roll	C_{l_p}, C_{n_p}, C_{n_r}
3	Bank-to-Bank Roll	C_{l_r}, $C_{Y_{\delta a}}$, $C_{l_{\delta a}}$, $C_{n_{\delta a}}$, C_{Y_o}, C_{l_o}, C_{n_o}
4	Dutch Roll	$C_{Y_{\delta r}}$, $C_{l_{\delta r}}$, $C_{n_{\delta r}}$, C_{Y_o}, C_{l_o}, C_{n_o}

The parameter estimates for the lateral-directional model created with the 4-step procedure described above is shown in Table 4.7. The median parameter estimate is shown with error bounds calculated from two scaled MAD which reflects the 95% confidence interval. The methodology for using these metrics was discussed in Sections 3.3.5 and 4.3.1. Figure A.5 in Appendix A.2 shows the distribution of parameter estimates in a histogram with the sample mean, median, and 95% confidence interval (CI). The histograms for each individual parameter estimate are taken from the corresponding step where each term was estimated, as indicated in Table 4.6.

Table 4.7: Lateral-directional parameter estimates from FTD using the steps in Table 4.6

Coef.	Value	95% CI	Coef.	Value	95% CI	Coef.	Value	95% CI
C_{Y_v}	-0.251	± 0.119	C_{l_v}	-0.0756	± 0.0459	C_{n_v}	$+0.0408$	± 0.0158
C_{Y_p}	$+0.170$	± 0.199	C_{l_p}	-0.319	± 0.0933	C_{n_p}	-0.242	± 0.150
C_{Y_r}	$+0.350$	± 0.377	C_{l_r}	$+0.183$	± 0.126	C_{n_r}	-0.166	± 0.0998
$C_{Y_{\delta a}}$	$+0.103$	± 0.0603	$C_{l_{\delta a}}$	-0.170	± 0.0325	$C_{n_{\delta a}}$	-0.0416	± 0.023
$C_{Y_{\delta r}}$	$+0.0157$	± 0.0482	$C_{l_{\delta r}}$	-0.0117	± 0.0220	$C_{n_{\delta r}}$	-0.0618	± 0.0177
C_{Y_o}	$+0.0286$	± 0.0382	C_{l_o}	-3×10^{-5}	± 0.00832	$C_{n_{v^2}}$	$+0.0126$	± 0.0269
						C_{n_o}	-9×10^{-5}	± 0.0048

The stability properties of the lateral-directional dynamics identified from the developed 4-step procedure were analyzed in order to compare to the VLM stability analysis used for input design. The dynamic modes of the aircraft were calculated from the lateral-directional linearized state matrices and are shown in Table 4.8. The stability properties calculated using VLM were displayed in Table 3.8. The oscillation period for the Dutch Roll mode was calculated to be 1.34 seconds from VLM which is slightly longer than the period of 1.07 seconds calculated from FTD. The damping ratio of the Dutch Roll mode calculated from VLM was $\zeta = 0.14$ which is less damping than shown in the FTD where that damping ratio was calculated to be $\zeta = 0.32$. The Roll mode calculated from VLM had an eigenvalue of $\lambda = -13.3$ and a time to half amplitude of $t_{1/2} = 0.052$ seconds; the Roll mode calculated from FTD had a slower response than predicted by VLM. The Spiral mode calculated from VLM had an unstable eigenvalue of $\lambda = +0.084$ and a time to double amplitude of $t_2 = 8.2$ seconds; the Spiral mode calculated from FTD had a stable eigenvalue and a slightly faster response, although this mode is likely not accurately estimated because it was not directly excited and is a longer duration mode which would be difficult to estimate for an aircraft of this scale.

Table 4.8: Lateral-directional modal analysis of the Bix3 aircraft from flight test data at V_a=12 m/s, $\theta = 0°$

Mode	Eigenvalue	f (Hz)	T (sec)	ζ	$t_{1/2}$ (sec)
Dutch Roll	$-1.89 \pm 5.57i$	0.936	1.07	0.322	0.366
Roll Mode	-7.77	–	–	–	0.0892
Spiral Mode	-0.118	–	–	–	5.8597

4.4.2 Modeling Performance and Uncertainty from FTD Only

In this section, the model created using the 4-step procedure listed in Table 4.6, will be compared to the model created from parameter estimation of the two lateral-directional

maneuvers separately and averaging the results. Model validation through simulation, error analysis and model uncertainty analysis will be presented to compare the two approaches.

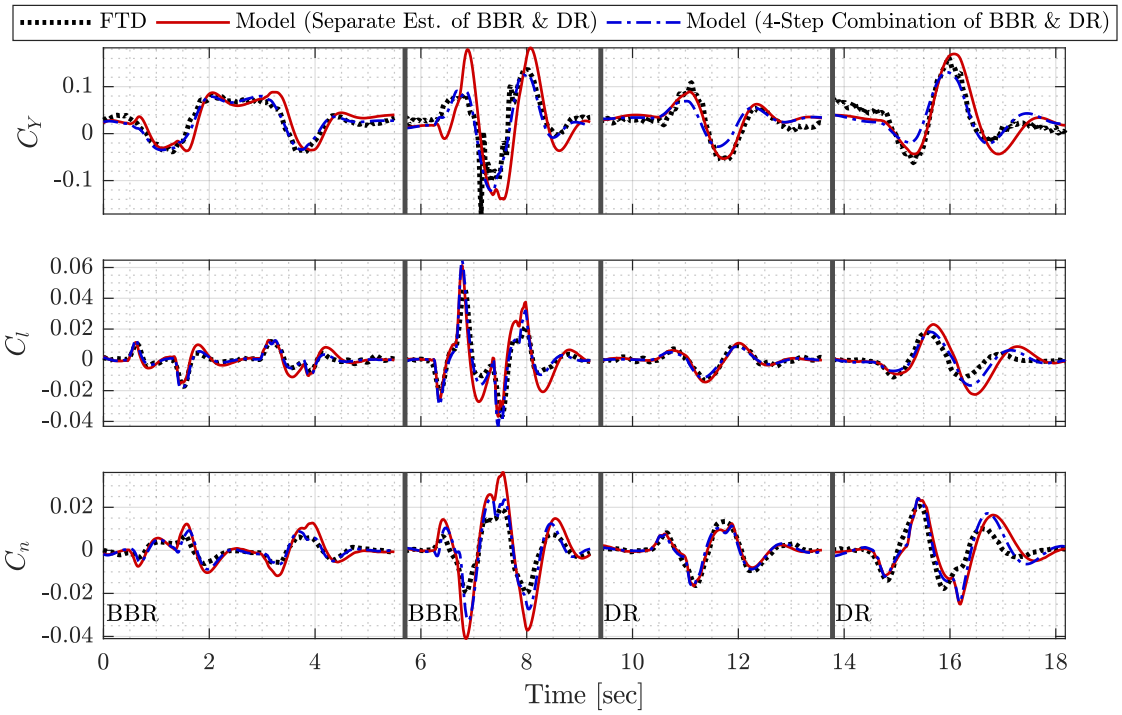

Figure 4.13: Comparison of C_Y, C_l, C_n simulation results from the model created identifying DR and BBR separately, and the model created by combining the parameter estimates using the steps listed in Table 4.6; BBR and DR maneuvers not included in the system identification process were used for this analysis

Model Validation

Model validation was performed through simulation of lateral-directional maneuvers not included in the system identification process. The simulation inputs were the initial conditions from flight test data (FTD) and the control inputs in flight. An aileron input is used for the Bank-to-Bank Roll (BBR) maneuvers, and a rudder input is used for the Dutch Roll (DR) maneuver. Figure 4.13 shows the lateral-directional force and moment coefficients for two BBR maneuvers and two DR maneuvers with differing control amplitude and polarity. It appears that the model using the 4-step procedure to combine parameter

estimates better matches C_Y, C_l, C_n calculated from the measured FTD.

Figure 4.14 shows the simulation outputs of the same models and maneuvers displayed in Figure 4.13. It can be seen that the model created from the 4-step process described in Table 4.6 outperforms the parameter estimates from identification of the two maneuvers separately. The 4-step procedure developed indicates it can model the full lateral-directional dynamics adequately with one unique set of parameter estimates.

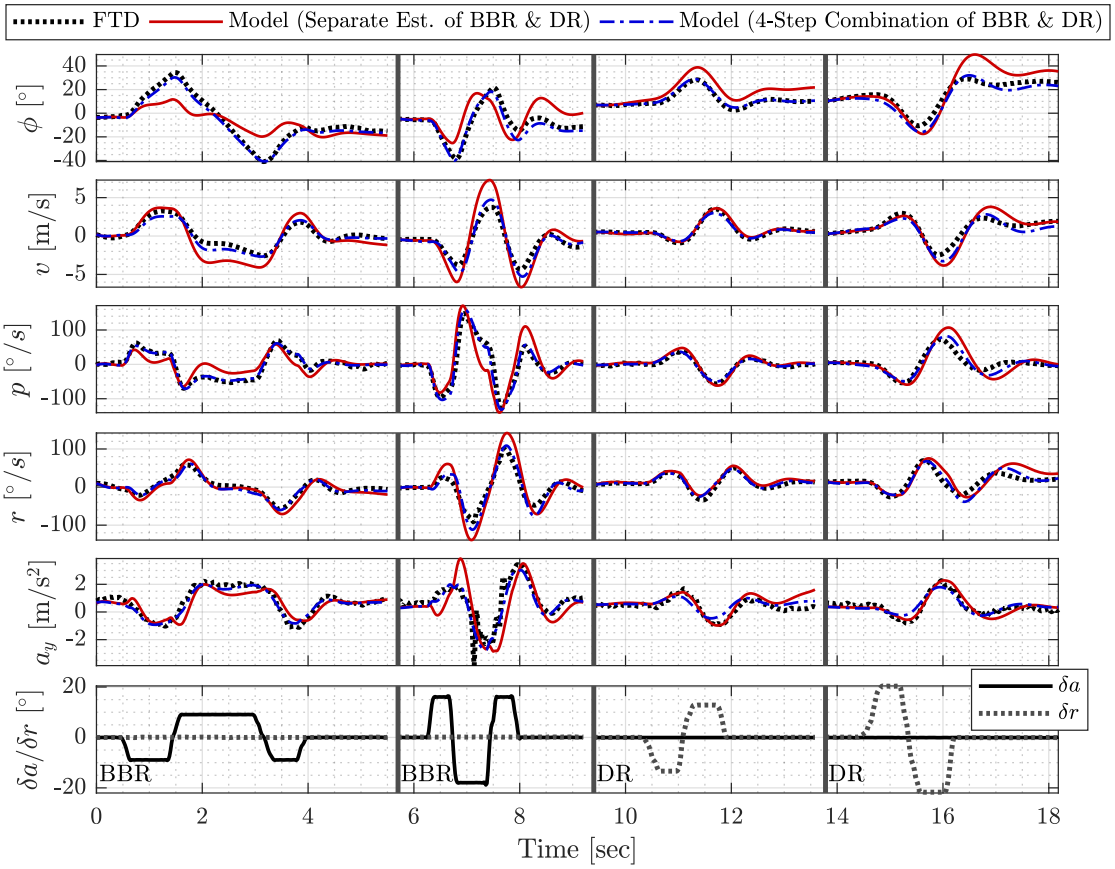

Figure 4.14: Simulation results of the lateral-directional outputs comparing the model created from identifying DR and BBR separately and the model created combining the parameter estimates using the steps listed in Table 4.6; BBR and DR maneuvers not included in the system identification process were used for this analysis

Error Analysis

The same error metrics discussed above in Sections 3.3.6 and 4.3.3 were applied to compare the results for the two lateral-directional parameter estimation approaches. The error in the simulation outputs is quantified by the average normalized root-mean-squared error (ANRMSE) and average normalized mean absolute error (ANMAE). Figure 4.15 displays box plots of the percent change in ANRMSE and ANMAE in lateral-directional outputs on a per-maneuver basis across all Dutch Roll (DR) and Bank-to-Bank Roll (BBR) maneuvers. Significant outliers have been removed to aid in clearly showing the overall data distribution. A high negative value indicates a larger improvement of the model created using the developed 4-step process over the baseline case, which here is the model created parameter estimation of BBR and DR maneuvers separately. It can be seen that there is significantly less overall modeling error by using the developed 4-step procedure for combining parameter estimates from DR and BBR maneuvers.

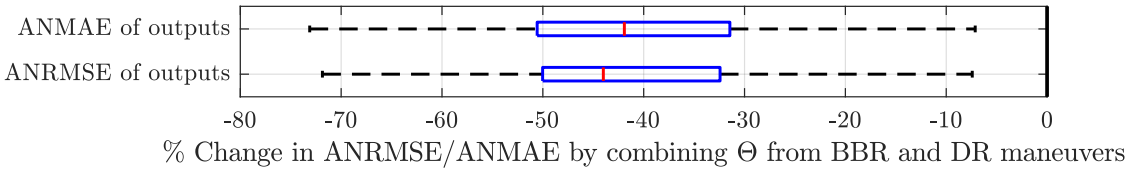

Figure 4.15: Percent change in ANRMSE and ANMAE of output quantities calculated on a per-maneuver basis by using the steps listed in Table 4.6 (a more negative value indicates a high model improvement over the baseline case identifying DR and BBR separately)

A one-sided paired t-test and one-sided Wilcoxon signed-rank test (see Section 3.3.6) were used to test the null hypothesis that the different modeling approaches had the statistically same mean values of ANRMSE and ANMAE treating each separate maneuver as a paired, independent quantity. The tests both rejected the null hypothesis with a p-value at a minimum of 10^{-14} indicating that the models created using the developed 4-step procedure in Table 4.6 produced statistically significant improvement in reduction of modeling error

compared to identification of parameter estimates from BBR and DR maneuvers separately.

The percent change RMSE and MAE of C_Y, C_l, C_n on a per-maneuver basis was computed for the 4-step combined parameter estimation model compared to the baseline model of averaging the results of separate parameter estimation of BBR and DR. These results are plotted in Figure 4.16. A high negative value indicates a larger improvement in the error in C_Y, C_l, C_n when the 4-step procedure is used to combine parameter estimates from DR and BBR. It can be seen that C_Y, C_l and C_n all show significant improvement in percent change of the error metrics over the baseline model.

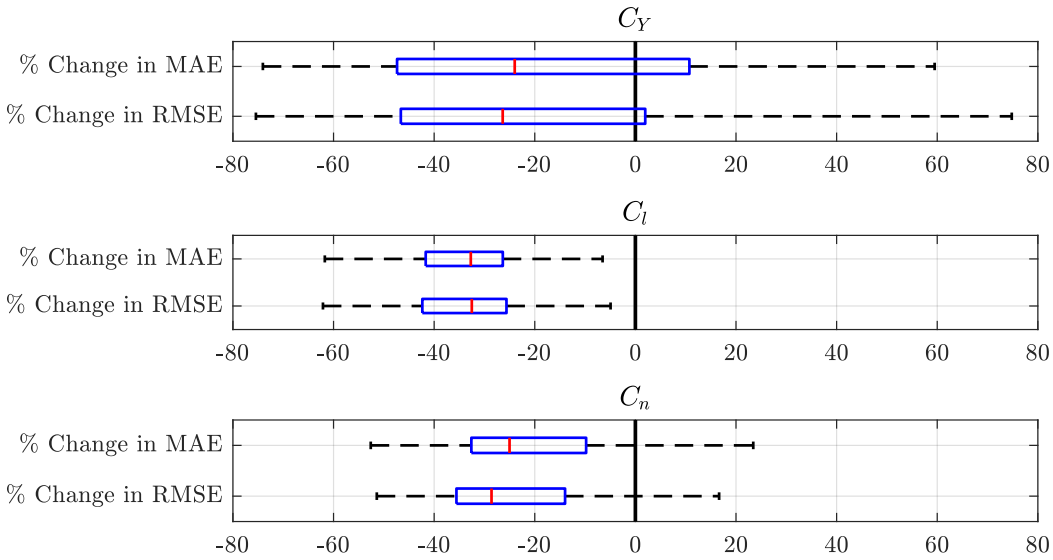

Figure 4.16: Percent change in ANRMSE and ANMAE of output quantities calculated on a per-maneuver basis by using the steps listed in Table 4.6 (a more negative value indicates a high model improvement over the baseline case of identifying DR and BBR separately)

Uncertainty Analysis

The error bar plots for each lateral-directional parameter estimate Θ from the different model creation techniques are shown in Figure 4.17. Error bars represent the 5^{th} and 95^{th} percentile in the scatter of the parameter estimates. It can be seen that the parameter

estimates from the 4-step process developed in Table 4.6 have a lower uncertainty than those developed from identifying BBR and DR maneuvers separately. All parameter estimates of the stability derivatives significantly decrease in uncertainty and most of the control derivatives decrease in uncertainty. The uncertainty in the bias terms remained relatively constant between the methods. Several of the different parameter estimates significantly change values between the models which can explain the differences in modeling performance.

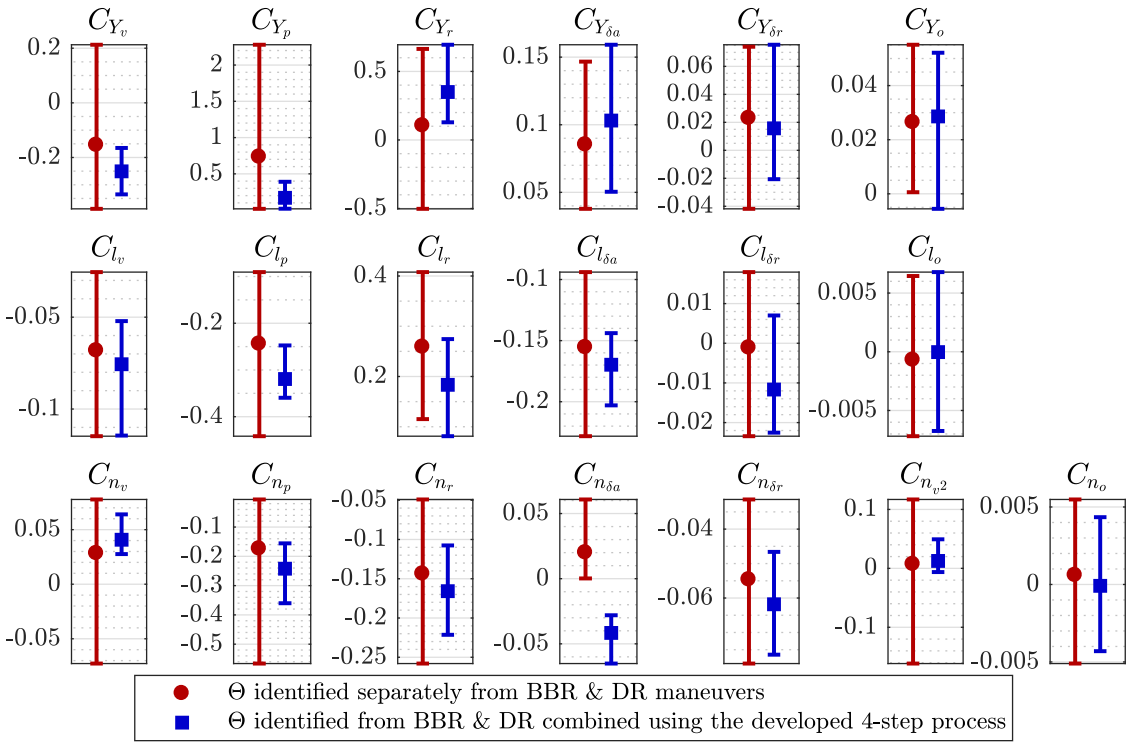

Figure 4.17: Uncertainty in lateral-directional parameter estimates from the different methods using FTD only

Analysis of Lateral-Directional Parameter Estimation from FTD only

The previous analysis in this section has shown that parameter estimation from flight test data alone appears to be adequate to model the lateral-directional dynamics of the Bix3 aircraft. This is contraindicative of the longitudinal parameter estimation where VLM

parameter estimates were needed to develop a model with acceptable accuracy. For completeness, the next section will investigate whether parameter estimation from VLM can be beneficial to lateral-directional parameter estimation.

4.4.3 Lateral-Directional Parameter Estimation from FTD & VLM

To attempt to improve the lateral-directional model, information was incorporated from the vortex lattice method (VLM) parameter estimates developed in Section 3.1.2, using the procedures discussed in Section 3.3.5. The VLM parameters found to be suitable for this purpose were C_{Y_v}, C_{Y_p}, C_{Y_r}, C_{l_v} and C_{n_v}. Combinations of these terms were fixed and the output-error method was run again holding a certain number of VLM parameters constant. The 4-step process listed in Table 4.6 of combining parameter estimates from the two different lateral-directional maneuvers was again used in this process. The best combinations of VLM parameter estimates to hold fixed appeared to be C_{Y_v} and C_{Y_r}; or C_{Y_v}, C_{Y_r} and C_{l_v}. These parameters were best in that the error remained nearly the same compared to estimation from flight test data (FTD) only. Unlike the longitudinal parameter estimation, there did not appear to be any notable improvement in modeling error or uncertainty which will be explored below. The parameter estimates for these cases are shown in Table 4.9 and Table 4.10, respectively. The reported values are based on the median and two scaled MAD, which estimates the 95% confidence interval.

The scatter of individual parameter estimates for the two best cases using certain VLM parameter estimates held constant are displayed in Figures A.6 and A.7 in Appendix A.2. Contrary to the results from the longitudinal parameter estimation using VLM, no obvious benefit is apparent from examining these figures and comparing to the results from FTD only. This will be explored further in the next section.

Table 4.9: Lateral-directional parameter estimates from fixing the values of C_{Y_v} and C_{Y_r} then using the steps in Table 4.6 to estimate the remaining parameters from FTD

Coef.	Value	95% CI	Coef.	Value	95% CI	Coef.	Value	95% CI
C_{Y_v}	-0.225	(VLM)	C_{l_v}	-0.0771	± 0.0399	C_{n_v}	$+0.0406$	± 0.0158
C_{Y_p}	$+0.0985$	± 0.357	C_{l_p}	-0.326	± 0.0958	C_{n_p}	-0.243	± 0.145
C_{Y_r}	$+0.173$	(VLM)	C_{l_r}	$+0.183$	± 0.13	C_{n_r}	-0.166	± 0.0977
$C_{Y_{\delta a}}$	$+0.111$	± 0.0767	$C_{l_{\delta a}}$	-0.174	± 0.0308	$C_{n_{\delta a}}$	-0.0423	± 0.0236
$C_{Y_{\delta r}}$	-0.0204	± 0.0362	$C_{l_{\delta r}}$	-0.0122	± 0.0224	$C_{n_{\delta r}}$	-0.0619	± 0.0179
C_{Y_o}	$+0.0290$	± 0.0381	C_{l_o}	-2×10^{-5}	± 0.00855	$C_{n_{v^2}}$	$+0.0145$	± 0.0293
						C_{n_o}	-0.00019	± 0.00488

Table 4.10: Lateral-directional parameter estimates from fixing the values of C_{Y_v} , C_{Y_r} and C_{l_v} then using the steps in Table 4.6 to estimate the remaining parameters from FTD

Coef.	Value	95% CI	Coef.	Value	95% CI	Coef.	Value	95% CI
C_{Y_v}	-0.225	(VLM)	C_{l_v}	-0.0729	(VLM)	C_{n_v}	$+0.0418$	± 0.0152
C_{Y_p}	$+0.106$	± 0.257	C_{l_p}	-0.312	± 0.0933	C_{n_p}	-0.241	± 0.150
C_{Y_r}	$+0.173$	(VLM)	C_{l_r}	$+0.170$	± 0.110	C_{n_r}	-0.169	± 0.0964
$C_{Y_{\delta a}}$	$+0.112$	± 0.0662	$C_{l_{\delta a}}$	-0.166	± 0.0331	$C_{n_{\delta a}}$	-0.0395	± 0.0225
$C_{Y_{\delta r}}$	-0.0203	± 0.0414	$C_{l_{\delta r}}$	-0.0132	± 0.0217	$C_{n_{\delta r}}$	-0.0624	± 0.0194
C_{Y_o}	$+0.0292$	± 0.0374	C_{l_o}	-0.000134	± 0.00892	$C_{n_{v^2}}$	$+0.0128$	± 0.0254
						C_{n_o}	$+2 \times 10^{-5}$	± 0.00497

4.4.4 Modeling Performance and Uncertainty from FTD & VLM

In this section the model created from the developed 4-step procedure from FTD only will be compared to the models created by holding certain terms estimated from VLM constant, then using the same 4-step procedure to estimate the remaining terms from FTD. Simulation results to validate the models, modeling error analysis and uncertainty analysis will be presented to compare the results.

Model Validation

Model validation was performed through simulation of maneuvers not included in the system identification process. Here the simulation inputs were the initial conditions and con-

trol inputs for the Dutch Roll (DR) and Bank-to-Bank Roll (BBR) maneuvers. Figure 4.18 shows the models' predictions of the lateral-directional force and moment coefficients for two BBR and two DR validation maneuvers with varying control polarity and amplitude. Figure 4.19 shows the relevant lateral-directional outputs from simulation of the same validation maneuvers. It can be seen from the two figures that the modeling performance between the different models created appears to be very similar.

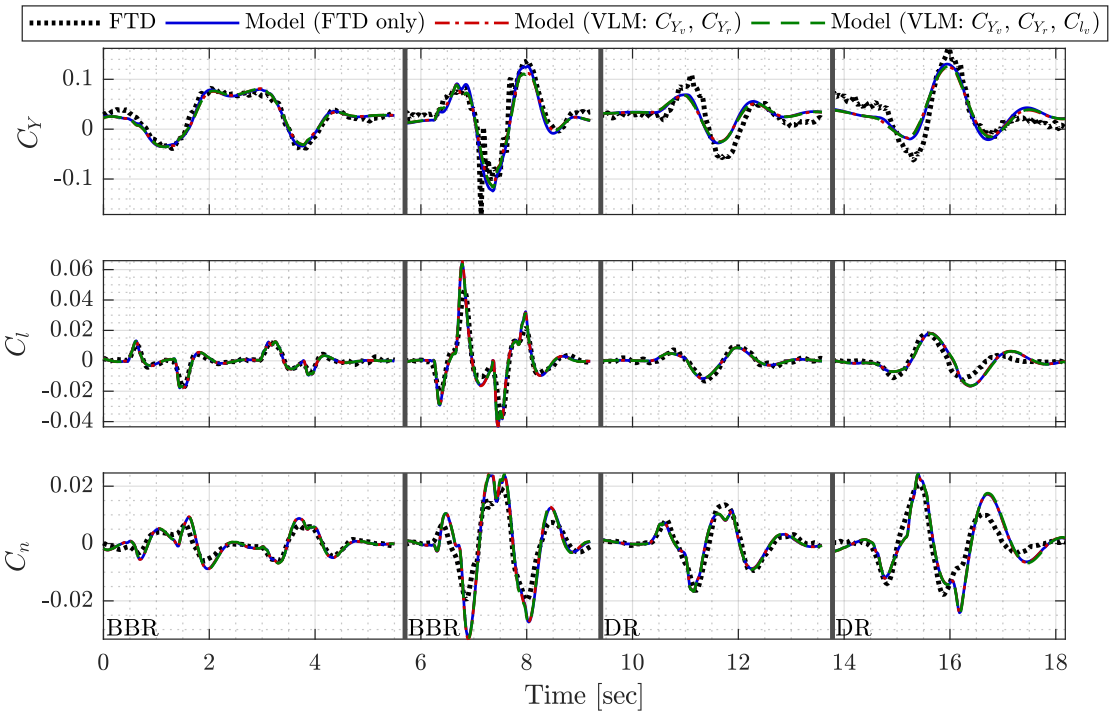

Figure 4.18: Comparison of C_Y, C_l, C_n simulation results between using FTD only and used a combination of FTD and VLM for parameter estimation; BBR and DR maneuvers not included in the system identification process were used for this analysis

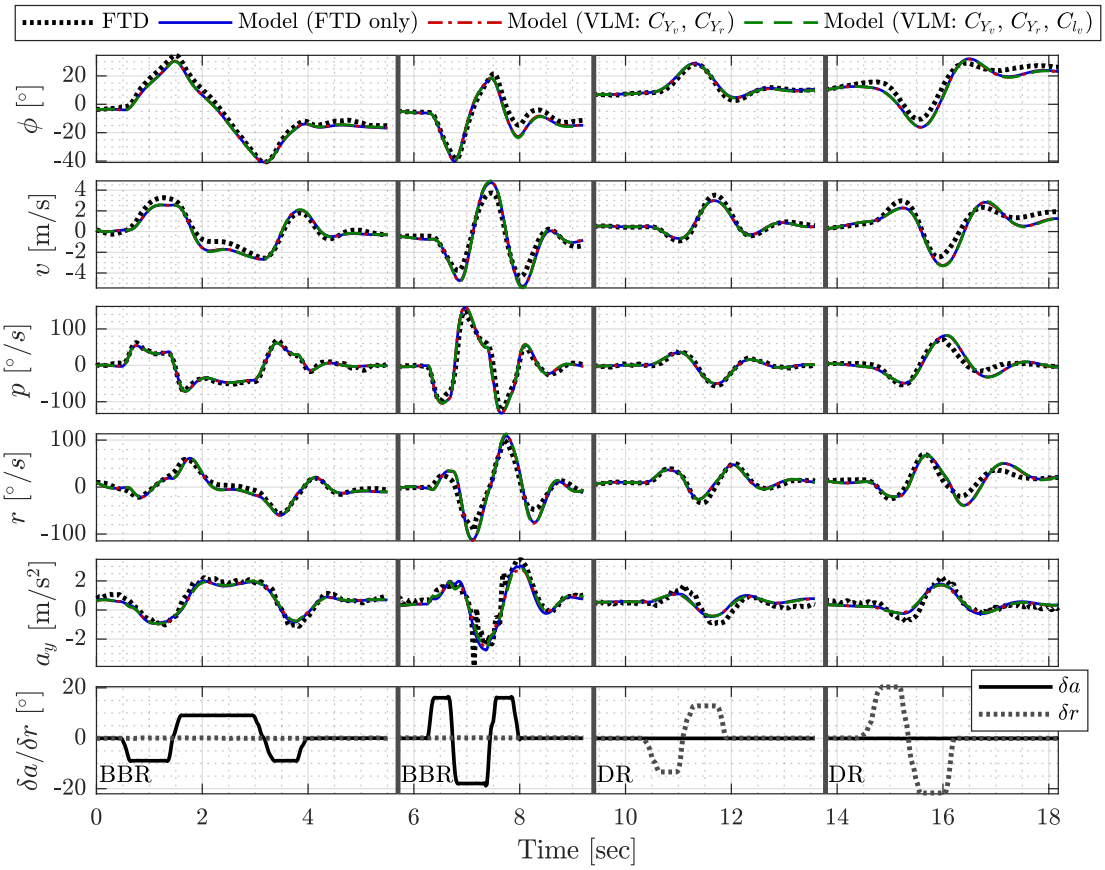

Figure 4.19: Simulation results of lateral-directional output quantities comparing models created using FTD only and using a combination of FTD and VLM for parameter estimation; BBR and DR maneuvers not included in the system identification process were used for this analysis

Error Analysis

To analyze the modeling performance over all maneuvers, modeling error was quantified by a series of error metrics discussed previously in Sections 3.3.6 and 4.3.3. The average normalized root-mean-square error (ANRMSE) and average normalized mean absolute error (ANMAE) for relevant lateral-directional outputs were used to assess the modeling performance of different models. Recall that this is a method to compare the modeling error of all model outputs using a single parameter for each maneuver. Figure 4.20 displays box plots

of the percent change (Equation (3.23)) in ANRMSE and ANMAE in lateral-directional outputs on a per-maneuver basis across all lateral-directional maneuvers. Significant outliers have been removed using a cutoff of 1.5 interquartile ranges beyond the 25^{th} and 75^{th} percentile. A negative value indicates an improvement over the baseline case, which here is the model created from FTD only using the developed 4-step procedure discussed in Section 4.4.1. It can be seen that the models displayed incorporating various model terms from VLM showed nearly no improvement or degrading model performance over the baseline case of the model created from FTD alone. It can be seen that the best models developed based on these metrics appear to be the models with C_{Y_v} and C_{Y_r}; or C_{Y_v}, C_{Y_r} and C_{l_v}, held constant to the parameter estimates from VLM.

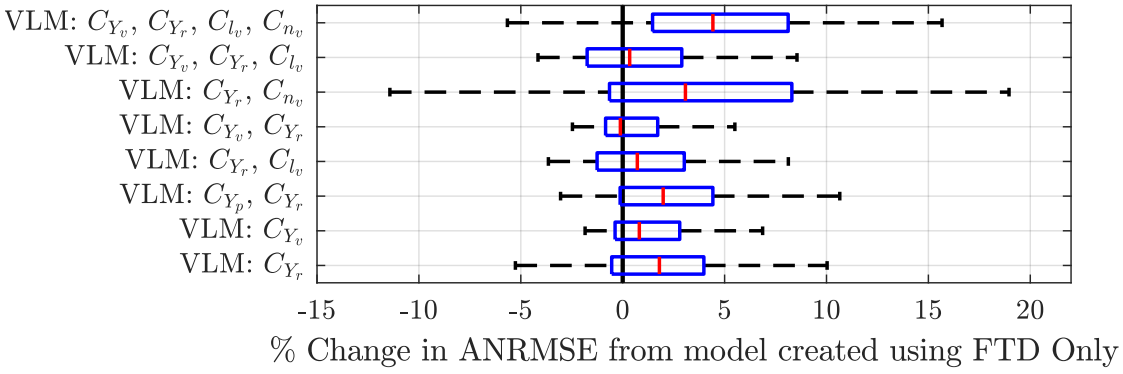

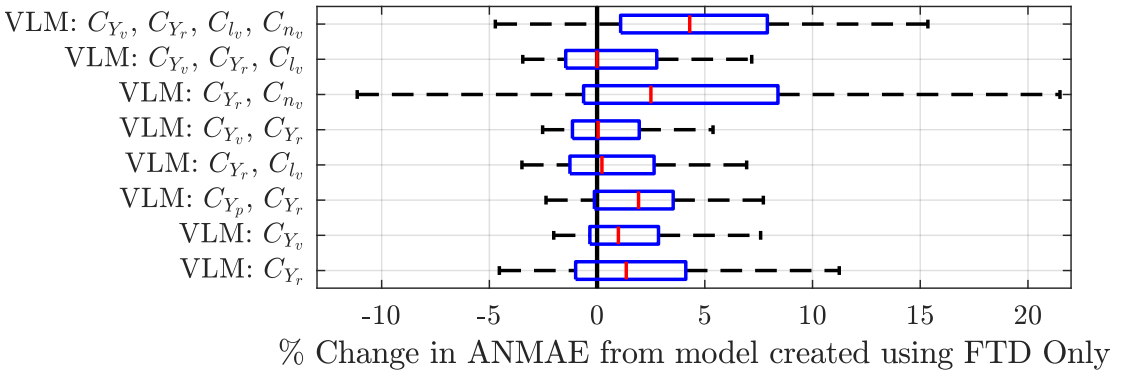

Figure 4.20: Percent change in ANRMSE (top) and ANMAE (bottom) of lateral-directional output quantities calculated on a per-maneuver basis for models created by fixing the indicated terms to their VLM parameter estimates (a more negative value indicates a high model improvement over the baseline case)

The percent change RMSE and MAE of C_Y, C_l, C_n on a per-maneuver basis was computed for models containing information from VLM compared to the model created from FTD only. These results are plotted in Figure 4.21. A negative value indicates an improvement in the error in C_Y, C_l or C_n when VLM parameter estimates were used as a supplement to FTD. It can be seen that a few cases show marginal improvement in modeling C_l, modeling performance of C_Y appears to remain about the same for most cases, and modeling performance appears to degrade for C_n for all cases displayed. These results confirm that the modeling performance when incorporating parameter estimates from VLM appears to remain about the same or slightly degrade.

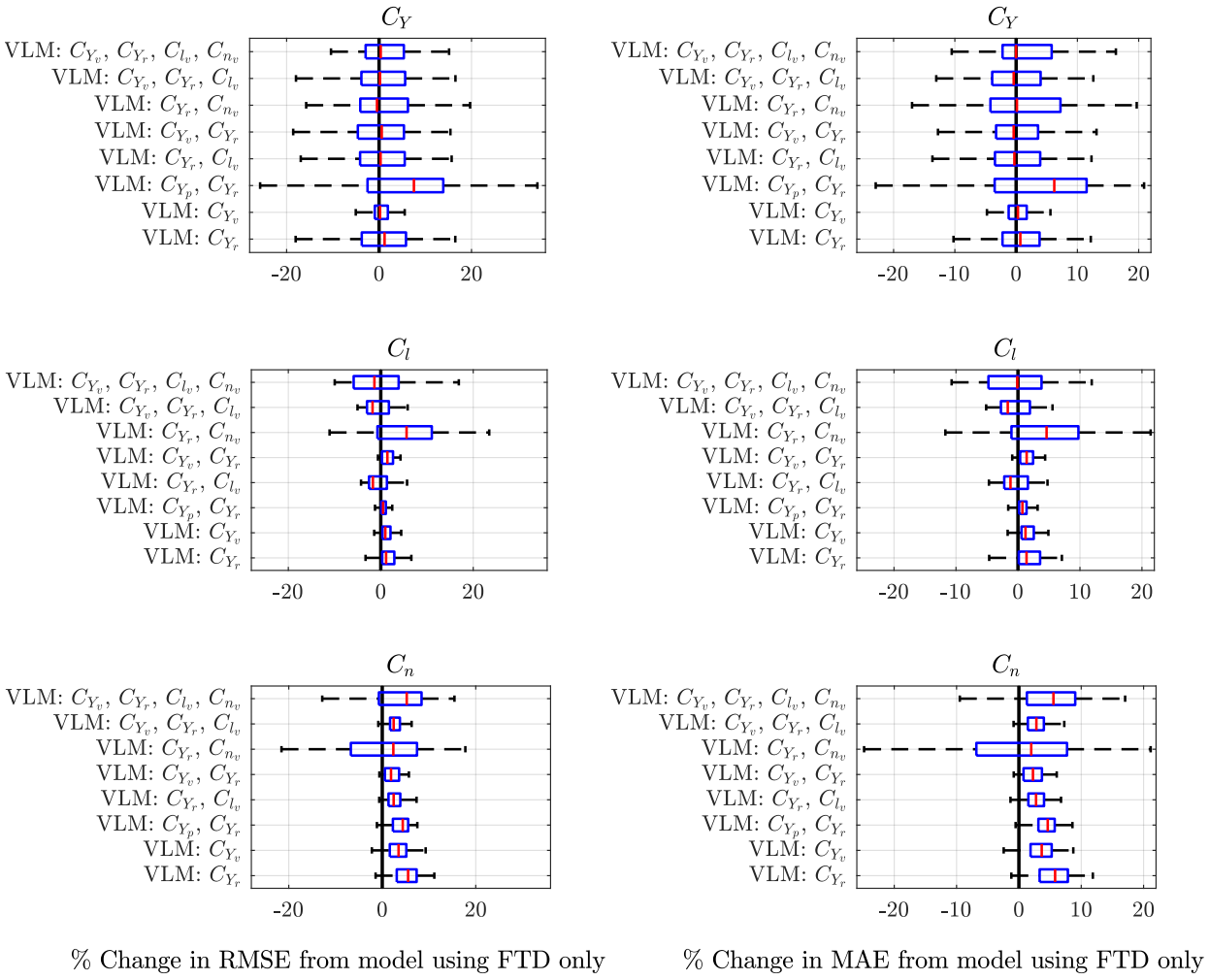

% Change in RMSE from model using FTD only

% Change in MAE from model using FTD only

Figure 4.21: Percent change in RMSE (left) and MAE (right) of C_Y, C_l, C_n calculated on a per-maneuver basis for models created by fixing the indicated terms to their VLM parameter estimates (a more negative value indicates a high model improvement over the baseline case)

Uncertainty of Parameter Estimates

The error bar plots for each lateral-directional parameter estimate from different models discussed above are shown in Figure 4.22. It can be seen that the parameter estimates from FTD only have similar levels of uncertainty compared to the parameter estimates where certain terms from VLM were held constant and the remaining terms were estimated from FTD. Clearly, this confirms the previous results that there appears to be no benefit from

incorporating VLM parameter estimates into the lateral-directional parameter estimation process.

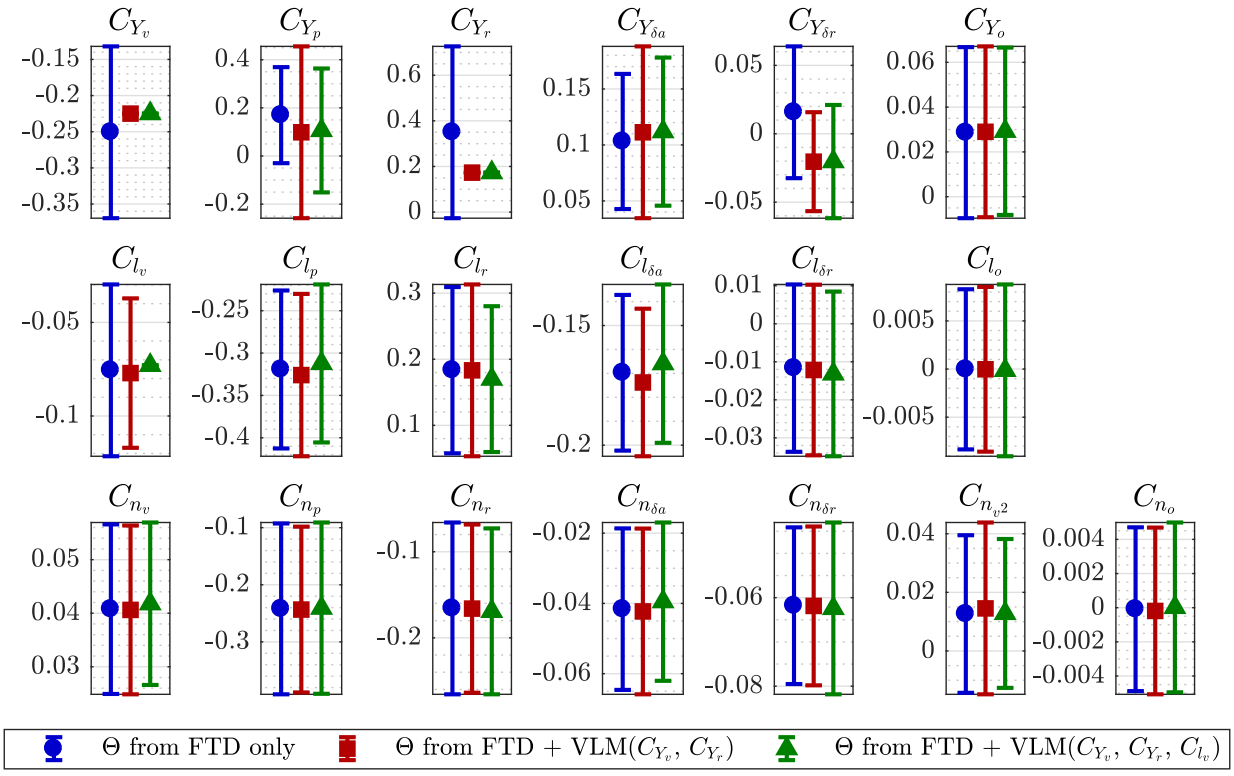

Figure 4.22: Uncertainty in lateral-directional parameter estimates (Θ) calculated from FTD only and FTD with with certain terms fixed to their indicated VLM parameter estimates

4.4.5 Discussion of Lateral-Directional Parameter Estimation

The results showed that the parameter estimation from the Bank-to-Bank Roll and Dutch Roll maneuvers separately resulted in differing estimates in shared lateral-directional stability derivatives. This is not an uncommon problem when the estimation is done separately for lateral-directional maneuvers [37]. Since these maneuvers could not be adequately performed immediately following one another in flight testing, a successful 4-step procedure was developed to create a unique set of parameters to model all lateral-directional dynamics.

This method provided a model sufficient to adequately model the lateral-directional dynamic of the aircraft.

With the knowledge of success in improving the longitudinal model by using vortex lattice method (VLM), the same approach was applied to the lateral-directional dynamics. Contrary to the results for the longitudinal model, incorporation of VLM parameter estimates for the lateral-directional dynamics did not prove successful in improving the model or decreasing uncertainty in parameter estimates. The level of error of the lateral-directional modeling, however, did not significantly degrade, showing that the VLM terms considered appeared to be accurate.

The approach of incorporating terms from VLM could have been unsuccessful in improving modeling for multiple reasons. Firstly, if the information content is available, the best parameter estimates are obtained from experimental methods. This is because when creating a model to describe the aircraft dynamics in flight, it is best to derive the data directly from the aircraft in flight rather than a simplified model implemented into a computational algorithm or using analytical methods [1]. For the lateral-directional model, enough data appeared to be present to develop a model without incorporation of information from other sources. The information content for the lateral-directional dynamics appeared to be richer compared to the longitudinal dynamics because multiple maneuvers were used to develop the lateral-directional parameter estimates. If one maneuver had a weakness in estimation of shared parameter, the other maneuver could be used to estimate that term and vice versa. Having multiple maneuvers to describe the dynamics filled in the gaps in information that, perhaps, could not have been filled if there was only one maneuver that could be successfully attempted.

Similar to the longitudinal parameter estimation, difficulty was encountered in the lateral-directional parameter estimation of the aerodynamic bias terms (C_{Y_o}, C_{l_o}, C_{n_o}) be-

cause these appeared to change on a per-flight basis. Note that these terms would be expected to be zero for a perfectly symmetric aircraft, but aerodynamic asymmetries and/or measurement system offsets were observed causing these terms to be finite. In particular, the term C_{Y_o} consistently was estimated to have a significant positive value whereas C_{l_o} and C_{n_o} were typically closer to zero. As previously discussed, the variable bias terms could be attributed to changes in the bias of the measurement system, slightly different control surface trims, or slight changes in the weight distribution between flights. Like the longitudinal parameter estimation, this problem was resolved by re-estimating the bias terms on all flights, but this is an inconvenient problem if it is desired to model the aircraft in flights where these terms were not estimated. As stated previously, a similar phenomena of slight changes in bias terms between maneuvers or flights can be seen in full-scale aircraft [1], however, it is likely not as pronounced of an effect as was seen in this work.

4.5 Selection and Validation of the Final Model

The final model of the Bix3 aircraft was selected to be comprised of the longitudinal model parameter estimates listed in Table 4.5 and the lateral-directional model parameter estimates listed in Table 4.7. The longitudinal model selected was the set of parameter estimates developed by fixing C_{X_w}, C_{Z_w} and C_{Z_q} to their values estimated from VLM and estimating the remaining parameters from flight test data (FTD). This model has the largest favorable change in ANRMSE and ANMAE of the outputs as compared to the baseline model created from FTD alone and showed good qualitative modeling performance. The lateral-directional model chosen was the set of parameter estimates developed from FTD only using the procedures listed in Table 4.6 to combine parameter estimation from the two different lateral-directional maneuvers. This model showed significant improvement over the baseline

model created from FTD with parameter estimation from the different lateral-directional maneuvers performed separately. Parameter estimation by including terms from VLM did not show any performance increases, and thus, was not chosen to be used for the final model.

Validation of the final model was performed through simulation of all the nonlinear aircraft equations of motion (Equations (2.1)-(2.13)) using both the longitudinal and lateral-directional models identified. The inputs into the simulation were the initial conditions and control inputs present in the FTD for the validation maneuvers not included in the system identification process. The results of these simulations are presented in Appendix A.3 where the full complement of both on- and off-axis measured and predicted signals are shown along with the measured and predicted flight path. Note that the off-axis aerodynamics bias terms appearing in the model had to be corrected for each maneuver because, as previously described, these changed on a per-flight basis and were not estimated on the flights where validation was performed. The on-axis aerodynamic bias terms were corrected on a per-flight basis, but this information was available from the parameter estimation process. The on-axis aerodynamic biases for the longitudinal model are C_{X_o}, C_{Z_o} and C_{m_o}, and the on-axis aerodynamic biases for the lateral-directional model are C_{Y_o}, C_{l_o} and C_{n_o}.

The validation time series plots for the Short Period maneuvers shown in Figure A.8 shows good model predictive performance for the on-axis, longitudinal signals and an acceptable fit to the off-axis lateral-directional signals. Note that in the off-axis signals, the model response is being compared to noisy measurement signals because these quantities were not directly excited in the flight maneuver. The flight path predicted for the Short Period maneuvers shown in Figure A.9 generally shows a decent fit to the FTD.

The validation time series plots for the Bank-to-Bank Roll and Dutch Roll maneuvers shown in Figures A.10-A.11 shows good modeling performance for the on-axis lateral-directional signals and an acceptable fit to the off-axis longitudinal signals. The flight path

predicted for the lateral-directional maneuvers shown in Figure A.12 generally illustrates an acceptable fit to the FTD, however, some drift in aircraft heading is observed. This could be attributed to measurement error in the Euler yaw angle ψ which was known to be a less reliable measurement, as previously discussed.

The modeling performance was quantitatively analyzed using the goodness of fit (GOF) metric and Theil's inequality coefficient [22], which were introduced in Section 3.3.6. These are used to assess model prediction of measured outputs relevant to the maneuver being analyzed. Recall the outputs for longitudinal maneuvering were defined as θ, u, w, q and a_z, and the outputs for the lateral-directional maneuvers were defined as ϕ, v, p, r and a_y. The GOF and TIC metrics were computed for the modeling response for all validation maneuvers, and the average values are reported in Tables 4.11-4.12. The high values of GOF in all output quantities indicates good modeling performance. The values of TIC are also below the threshold of 0.25-0.3 defined to indicate a good modeling fit [2]. Overall, the model validation indicates good performance of the final model.

Table 4.11: Average values of the goodness of fit (GOF) and Theil's inequality coefficient (TIC) metrics for outputs of the model response for longitudinal validation maneuvers

	θ	u	w	q	a_z
GOF	0.963	0.991	0.864	0.984	0.940
TIC	0.097	0.086	0.195	0.063	0.112

Table 4.12: Average values of the goodness of fit (GOF) and Theil's inequality coefficient (TIC) metrics for outputs of the model response for lateral-directional validation maneuvers

	ϕ	v	p	r	a_y
GOF	0.916	0.923	0.951	0.919	0.828
TIC	0.136	0.136	0.101	0.136	0.221

4.6 Discussion of Overall Modeling Quality

The final longitudinal and lateral-directional models appear to adequately model the respective dynamics for the simulation results presented. The models also contain nonlinearities which can effectively model a large portion of the operational envelope. However, even after the procedures taken to improve the parameter estimates, there is still a significant uncertainty in their values characterized by the error bounds of each parameter estimate. This uncertainty developed in the estimation process is due to non-random, correlated measurement noise and error due to the limited and low-cost instrumentation system, as well as the increased effect of process noise due to the small size of the platform. These effects are largely unescapable for a small, low-cost UAV. Also, the aerodynamic bias parameters were found to change in value on a per-flight basis, which makes modeling a new flight difficult without first re-estimating the bias parameters. An additional limitation of the model developed is that, as presented, it is only valid for maneuvers with constant thrust because the combined effects of thrust and aerodynamics were characterized in the x-body axis force coefficient C_X. This means that throttle position cannot be used as a control input.

Considering the discussed limitations, the model could still have many practical uses. The model itself and the developed error bounds could be used for risk assessment for the UAV. For example, a Monte Carlo simulation could be used to vary the various parameters to evaluate the likelihood of a crash. The model could also be used for flying qualities analysis, path planning or preliminary control system design among other applications which would tolerate the inherent uncertainty and render the model useful. The model will not be as useful in situations where a model with very high accuracy is desired, or in situations where information on the bias parameters is necessary and cannot be estimated on a new flight where the model is intended to be used. This may limit the model's usefulness for wind sensing, or accurately modeling complex dynamics over an extended period of time. These

limitations will most likely be present for any system identification effort of an aircraft of this scale and cost range. Ultimately, as the cost and scale of the aircraft decreases, the deterministic portion of the aircraft flight data also decreases, which will result in a lower-quality model with a high uncertainty and lower range of applicability.

Chapter 5

Conclusions and Future Research

System identification for small, low-cost, fixed-wing, UAVs has many associated challenges making the process different than for full-scale aircraft. Choice of an appropriate flight test plan for this effort was limited by the small-size of the Bix3 aircraft and the difficulty of piloting from the ground. A flight test plan was developed from three short-duration maneuvers. The vortex lattice method (VLM) was used to develop estimates of the optimal control inputs for system identification which proved to be a useful approach. Due to the low-cost nature of the aircraft, sensors were inherently limited and of lower quality which made the system identification process difficult from the beginning. Careful choices of the most reliable signals and meticulous calculation of signals was necessary to ensure lower noise and kinematically consistent data. Ultimately, the best system identification results were obtained using states and state derivatives derived from an extended Kalman filter. Effective experimental data collection and data analysis is a prerequisite requirement which cannot be bypassed to produce quality modeling results.

After careful data analysis and processing, the flight test data may then be used for model development. The model structure must be chosen not to over-parameterize the model, yet be able to model all dynamics present in the flight test data. This is a challenge for small UAVs with high noise data, because larger perturbation inputs must be used to produce an adequate signal-to-noise ratio for identification which results in a nonlinear modeling structure. The nonlinear model structure results in more parameters to estimate and the

associated challenge to accurately estimate all model terms from individual flight maneuvers. Remedies to these challenges were developed by incorporating computational aerodynamics and synthesizing the best information from different flight maneuvers to improve modeling performance.

For the longitudinal model, estimation from flight test data alone proved to be inadequate. Certain parameter estimates from VLM were held fixed in the model, then all remaining terms were estimated from flight test data. This approach proved to significantly improve modeling performance and decreased uncertainty in most parameters estimated from flight test data. This approach was successful because it effectively reduces the number of model terms which needed to be estimated while retaining the desired complex model structure to model all variations in the data. Since the accuracy of parameter estimation decreases as the number of terms increases [1], this is a significant finding that it is possible to use information from other sources to effectively reduce the parameter space without sacrificing model complexity.

For the lateral-directional model, estimation from two separate flight maneuvers resulted in a different set of parameter estimates for each maneuver. An attempt to average the parameter estimation results between both maneuvers proved to be inadequate. Steps were developed to identify a subset of terms from each maneuver which were found to be more accurately represented by that respective maneuver. This resulted in identification of an accurate model from experimental flight test data alone. VLM parameter estimates were also used to try to improve the model, but was shown to yield equivalent or decreased accuracy. The use of information from multiple maneuvers reduced the effective number of parameters needed to be estimated from each maneuver which explains why an adequate model was able to be obtained from only flight test data contrary to the longitudinal model.

The results show that in certain situations there is a benefit to combination of flight

test data with information obtained from other sources, which in this case was VLM. Future research could implement a higher-fidelity computational fluid dynamics (CFD) method to improve parameter estimation results used to supplement flight test data which may lead to higher accuracy in parameter estimation and lower overall uncertainty. Results from wind tunnel testing could also be combined with flight test data leading to a similar benefit. Future research could also be performed on larger-scale UAVs or full-scale aircraft to investigate whether benefits can be gained by using a another method to supplement parameter estimation from flight test data.

The results from this research could be improved by performing more flight testing to obtain a larger population of parameter estimates for better uncertainty analysis. This would also allow the ability to be even more selective on maneuvers to remove from the data set. This could involve performing a larger number of maneuvers, maneuvers with different control input sequences, or perhaps different/hybrid maneuvers. Another possibility is to develop an autopilot algorithm specifically for system identification using the same maneuvers. This would be challenging to implement because the system should ideally be switched to open-loop during system identification maneuvers and have programmed random variation in the control inputs for the best results, while including fault tolerance algorithms to avoid departure. An additional strategy could be to use minimally intrusive first-person view (FPV) technology, to improve the pilot's ability to visualize the aircraft's motion. This may allow for higher quality system identification maneuvers by increasing the quality of trimmed flight conditions and allowing the pilot to have a better perception of the success in execution of each maneuver.

Results could also be improved by upgrading the instrumentation system either by utilizing higher quality sensors and/or recording more measurements such as angle of attack and angle of sideslip. Ultimately, this would reduce measurement error, however, the aircraft

would still be highly sensitive to process noise in the form of atmospheric disturbances. The filter-error method could be used instead of the output-error method which could improve results because the filter-error method is resistant to process noise. However, to implement the filter-error method would likely involve more computational resources than were available for this research effort. Finally, accurate characterization of a thrust model would help simulation efforts if throttle position could be used as another control input rather than being restricted to be constant.

System identification of a small, low-cost, fixed-wing UAV is a challenging process which requires keen attention to detail and careful execution of all procedures. It has been shown that it is possible to develop a useful nonlinear aerodynamic model which could be used for a variety of different applications. However, it is important to understand that models for any aircraft of this scale will not be flawless and should be treated as such when choosing an application for the model. Inexpensive instrumentation systems for these small unmanned aircraft make it difficult for the flight data to have high quality measurements of the aircraft states. Additionally, a meaningful portion of their actual flight mechanics are governed by stochastic atmospheric disturbances. This renders the expectation of a purely deterministic model an unrealistic task and understanding that there will be modeling uncertainty must be stated clearly. System identification can be performed successfully for a small, low-cost aircraft to develop a model useful for a variety of applications, but the potential user must be aware of the inherent limitations present in modeling this type of system.

Bibliography

[1] E. A. Morelli and V. Klein, *Aircraft system identification: theory and practice*, 2nd ed. Williamsburg, VA: Sunflyte Enterprises, 2016.

[2] R. Jategaonkar, *Flight vehicle system identification: a time domain methodology*, 2nd ed. Reston, Virginia: American Institute of Aeronautics and Astronautics/Aerospace Press, 2015.

[3] "Hobbyking™ bix3 trainer/fpv epo 1550mm mode 2 (ready-to-fly)," *HobbyKing.com*. [Online]. Available: https://hobbyking.com/en_us/hobbykingtm-bix3-trainer-fpv-epo-1550mm-mode-2-ready-to-fly.html

[4] O. Arifianto and M. Farhood, "Development and modeling of a low-cost unmanned aerial vehicle research platform," *Journal of Intelligent & Robotic Systems*, vol. 80, no. 1, pp. 139–164, 2015.

[5] D. J. Grymin and M. Farhood, "Two-step system identification and trajectory tracking control of a small fixed-wing uav," *Journal of Intelligent & Robotic Systems*, vol. 83, no. 1, pp. 105–131, 2016.

[6] A. Dorobantu, A. Murch, B. Mettler, and G. Balas, "System identification for small, low-cost, fixed-wing unmanned aircraft," *Journal of Aircraft*, 2013.

[7] S. Park, "Modeling with vortex lattice method and frequency sweep flight test for a fixed-wing uav," *Control Engineering Practice*, vol. 21, no. 12, pp. 1767–1775, 2013.

[8] Z. Shenglu, X. Ran, W. Liaoni, and D. Xiuxin, "Research on highly-accurate aerodynamic parameter identification," *The Institution of Engineering & Technology*, 2015.

[9] A. K. Tangirala, *Principles of system identification: theory and practice*. Crc Press, 2014.

[10] K. J. Keesman, *System identification: an introduction*. Springer Science & Business Media, 2011.

[11] N. V. Hoffer, C. Coopmans, A. M. Jensen, and Y. Chen, "A survey and categorization of small low-cost unmanned aerial vehicle system identification," *Journal of Intelligent & Robotic Systems*, vol. 74, no. 1-2, p. 129, 2014.

[12] B. Etkin and L. D. Reid, *Dynamics of flight: stability and control*. Wiley New York, 1996, vol. 3.

[13] J. A. Grauer and E. A. Morelli, "A generic nonlinear aerodynamic model for aircraft," in *AIAA Atmospheric Flight Mechanics Conference*, 2014, p. 0542.

[14] *U.S. Naval Test Pilot School Flight Test Manual, Fixed Wing Stability and Control*. Patuxent River, MD: Naval Air Warfare Center Aircraft Division, 1997.

[15] J. Oliveira, Q. Chu, J. Mulder, H. Balini, and W. Vos, "Output error method and two step method for aerodynamic model identification," in *AIAA Guidance, Navigation, and Control Conference and Exhibit*, 2005, p. 6440.

[16] L. E. Hale, M. Patil, and C. J. Roy, "Aerodynamic parameter identification and uncertainty quantification for small unmanned aircraft," *Journal of Guidance, Control, and Dynamics*, vol. 40, no. 3, pp. 680–691, 2016.

[17] E. A. Morelli and V. Klein, "Accuracy of aerodynamic model parameters estimated from flight test data," *Journal of Guidance, Control, and Dynamics*, vol. 20, no. 1, pp. 74–80, 1997.

[18] ——, "Determining the accuracy of maximum likelihood parameter estimates with colored residuals," *NASA Contractor Report*, 1994.

[19] E. Morelli, "System identification programs for aircraft (sidpac)," in *AIAA Atmospheric Flight Mechanics Conference*, 2002, p. 4704.

[20] M. Hepperle, "Javaprop - design and analysis of propellers." [Online]. Available: https://www.mh-aerotools.de/airfoils/javaprop.htm

[21] M. Sri-Jayantha and R. F. Stengel, "Determination of nonlinear aerodynamic coefficients using the estimation-before-modeling method," *Journal of Aircraft*, vol. 25, no. 9, pp. 796–804, 1988.

[22] H. Theil, *Economic forecasts and policy*, 2nd ed. Amsterdam, Netherlands: North Holland Publishing Company, 1961.

[23] W. H. Mason, "Configuration aerodynamics," *Lecture Notes, Virginia Tech*, 2009.

[24] A. Deperrois, "Xflr5 analysis of foils and wings operating at low reynolds numbers," *Guidelines for XFLR5*, 2009.

[25] D. Anderson John, *Fundamentals of aerodynamics*, 3rd ed. New York, NY: McGraw-Hill, 2001.

[26] J. Katz and A. Plotkin, *Low speed aerodynamics*, 2nd ed. New York, NY: Cambridge University Press, 2001.

[27] A. Deperrois, "Xflr5: a tool for the design of airfoils, wings and planes operating at low reynolds numbers," *Software Package*, 2017.

[28] ——, "About xflr5 calculations and experimental measurements," *Presentation document*, 2009.

[29] ——, "About stability analysis using xflr5," *Presentation document*, 2010.

[30] L. Meier, "Pixhawk," *pixhawk.org*. [Online]. Available: https://www.pixhawk.org/

[31] "Ekf2 estimation system," *Ardupilot*. [Online]. Available: http://ardupilot.org/dev/docs/ekf2-estimation-system.html

[32] M. P. Miller, "An accurate method of measuring the moments of inertia of airplanes," *NACA Technical Note*, 1930.

[33] J. Grauer and E. Morelli, "Dynamic modeling accuracy dependence on errors in sensor measurements, mass properties, and aircraft geometry," in *51st AIAA Aerospace Sciences Meeting including the New Horizons Forum and Aerospace Exposition*, 2013, p. 949.

[34] "Kentland farm weather station," *WeatherSTEM*, 2016. [Online]. Available: http://montgomery.weatherstem.com/kentlandfarm

[35] M. Oborne, "Mission planner," 2016. [Online]. Available: http://ardupilot.org/planner/docs/mission-planner-overview.html

[36] *MATLAB Documentation, version 9.2 (R2017a)*. Natick, Massachusetts: The MathWorks Inc., 2017.

[37] G. B. Gilyard, "Flight-determined derivatives and dynamic characteristics of the cv-990 airplane," *NASA Technical Note*, 1972.

[38] T. Chai and R. R. Draxler, "Root mean square error (rmse) or mean absolute error (mae)?–arguments against avoiding rmse in the literature," *Geoscientific model development*, vol. 7, no. 3, pp. 1247–1250, 2014.

Appendices

Appendix A

Additional Figures

A.1 Histograms of Longitudinal Parameter Estimates

This section contains additional figures to accompany the longitudinal parameter estimation results presented in Section 4.3.

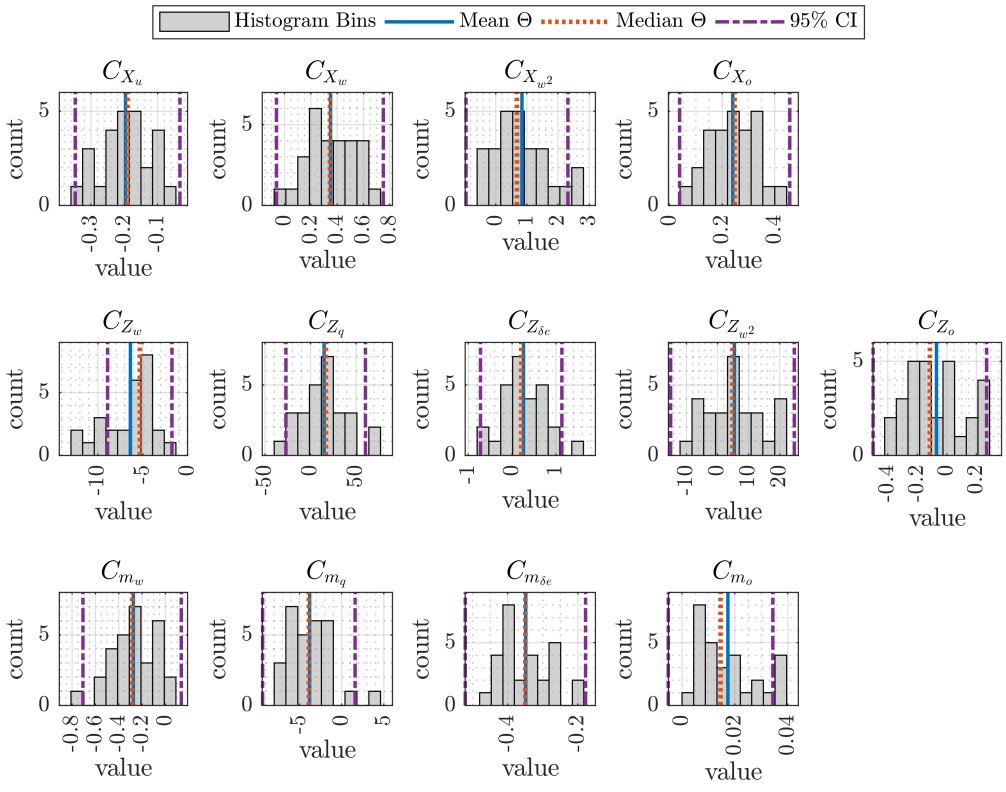

Figure A.1: Histograms of longitudinal parameter estimates (Θ) from individual maneuvers from flight test data only

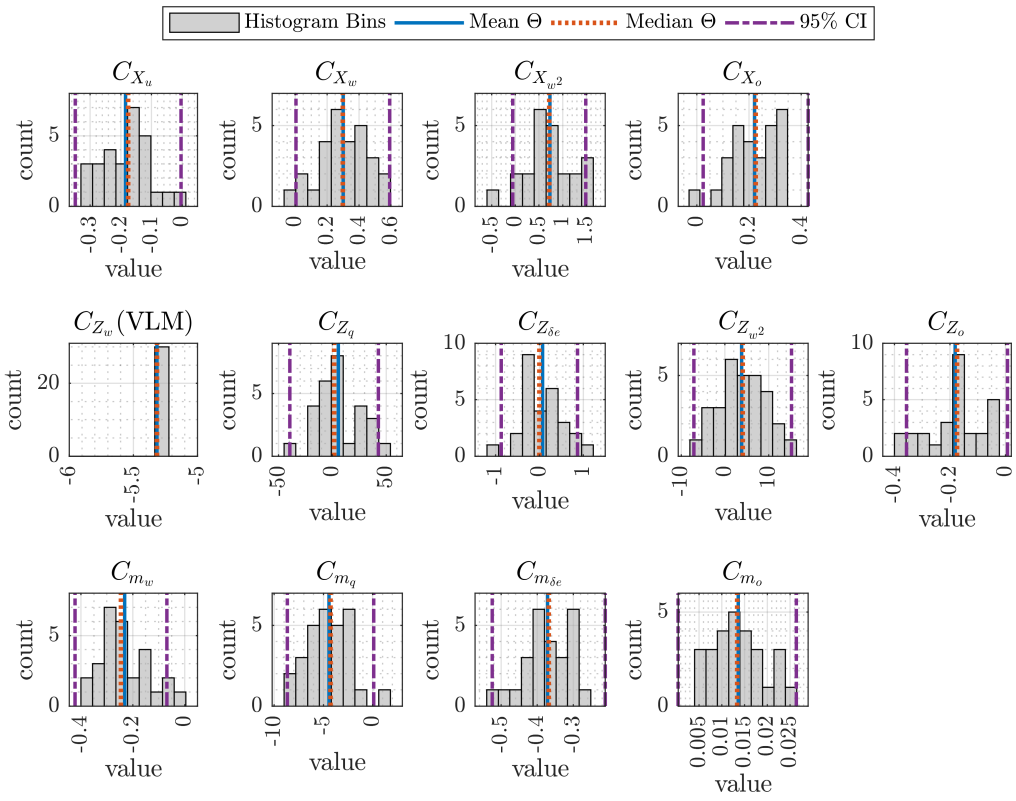

Figure A.2: Histograms of longitudinal parameter estimates (Θ) from individual maneuvers fixing the VLM value of C_{Z_w}, and then estimating the remaining terms from flight test data

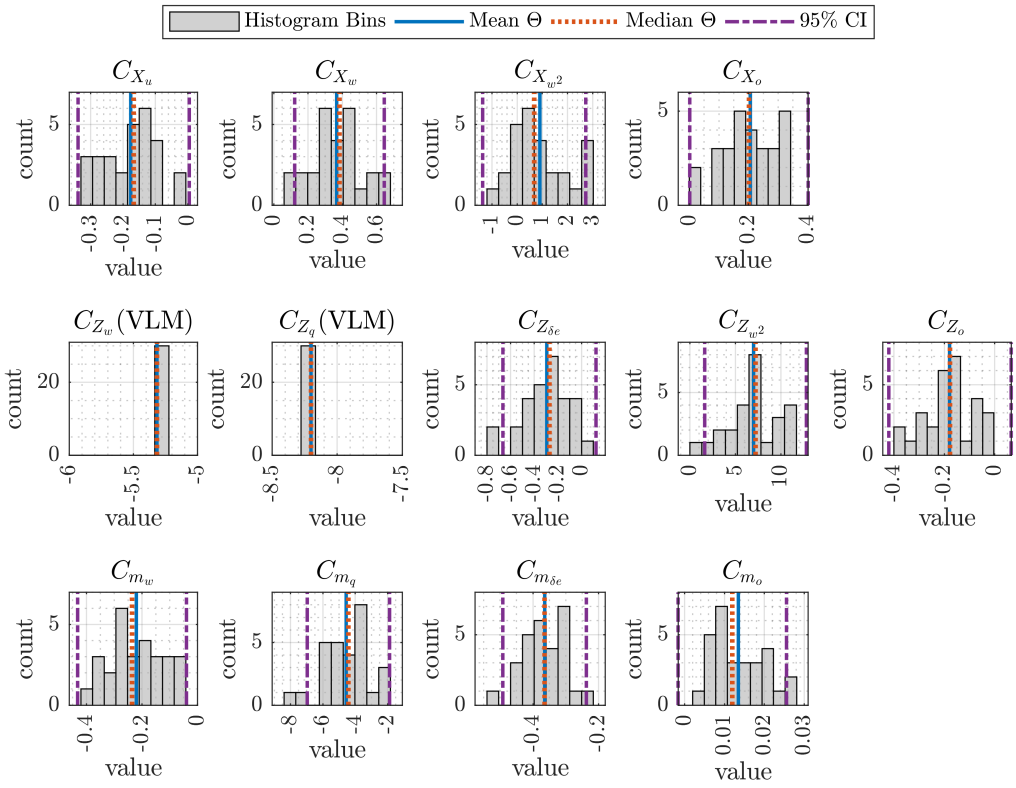

Figure A.3: Histograms of longitudinal parameter estimates (Θ) from individual maneuvers fixing VLM values of C_{Z_w} and C_{Z_q}, and then estimating the remaining terms from flight test data

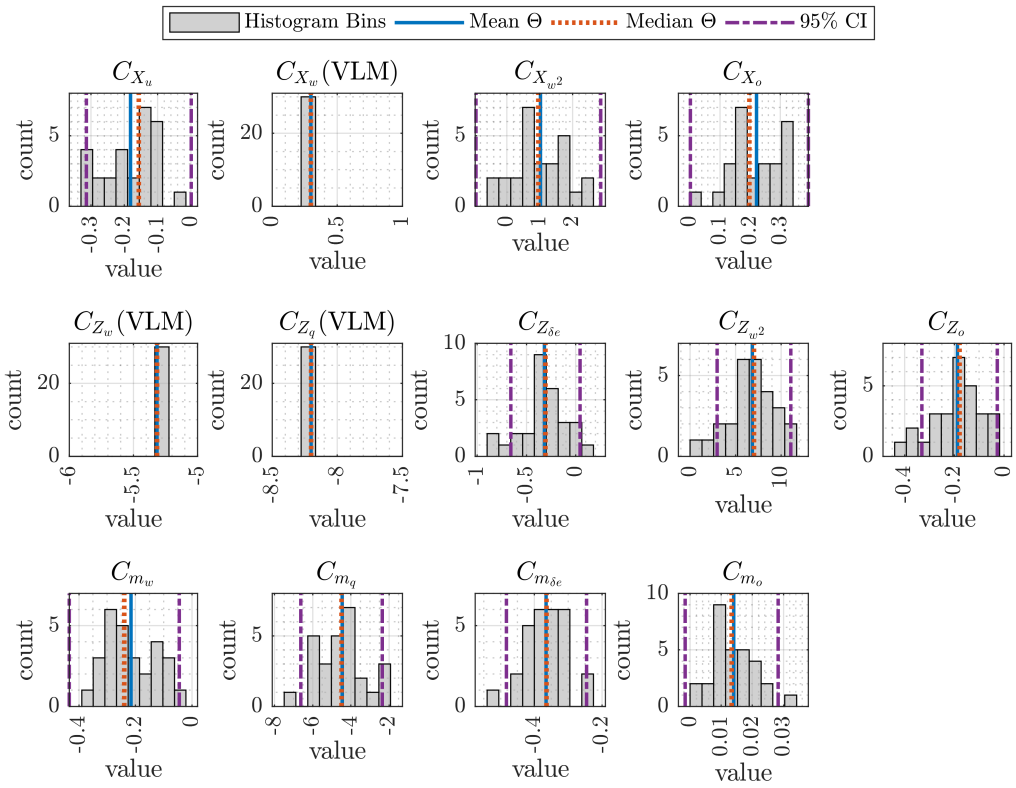

Figure A.4: Histograms of individual longitudinal parameter estimates (Θ) from individual maneuvers fixing VLM values of C_{X_w}, C_{Z_w} and C_{Z_q}, and then estimating the remaining terms from flight test data

A.2 Histograms of Lateral-Directional Parameter Estimates

This section contains additional figures to accompany the lateral-directional parameter estimation results presented in Section 4.4.

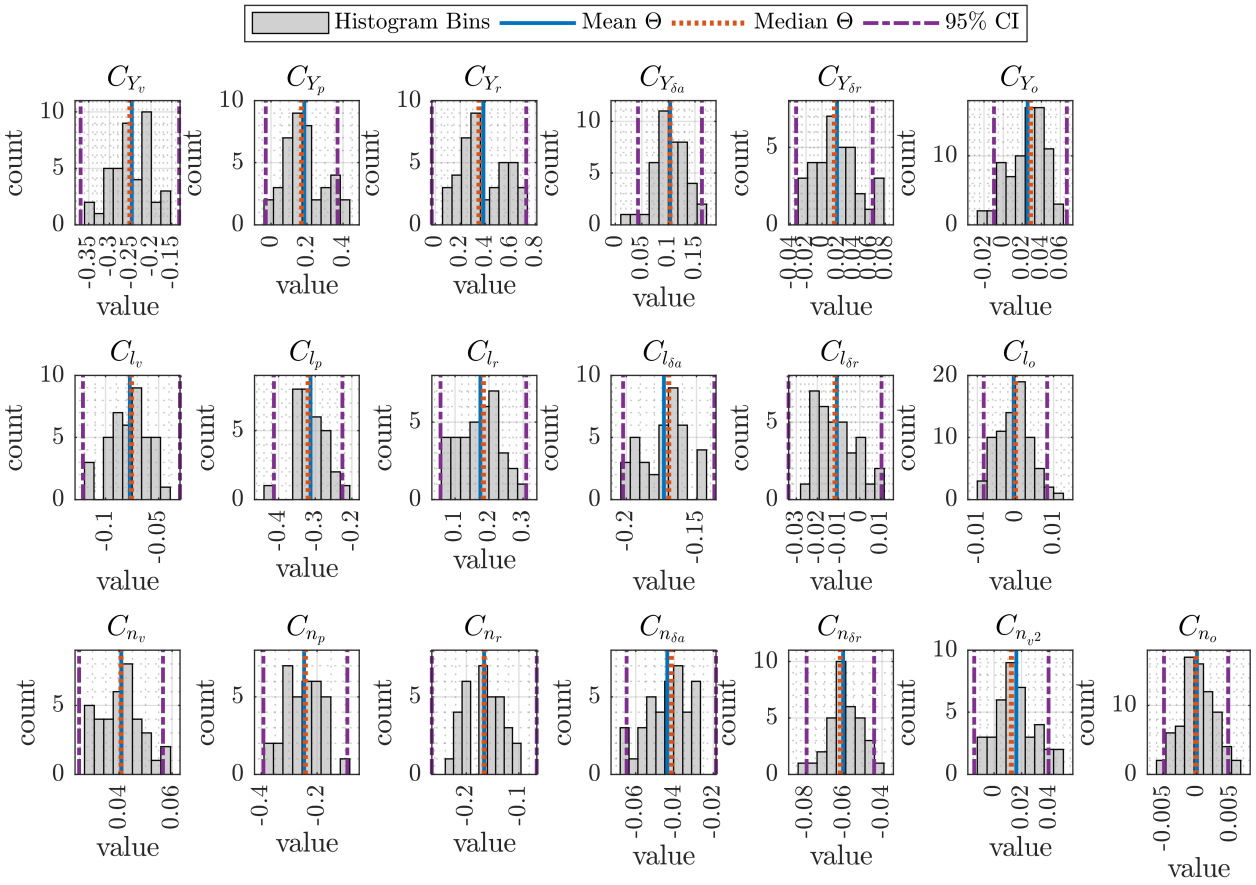

Figure A.5: Histograms of the distribution of individual lateral-directional parameter estimates (Θ) from flight test data only using the steps in Table 4.6

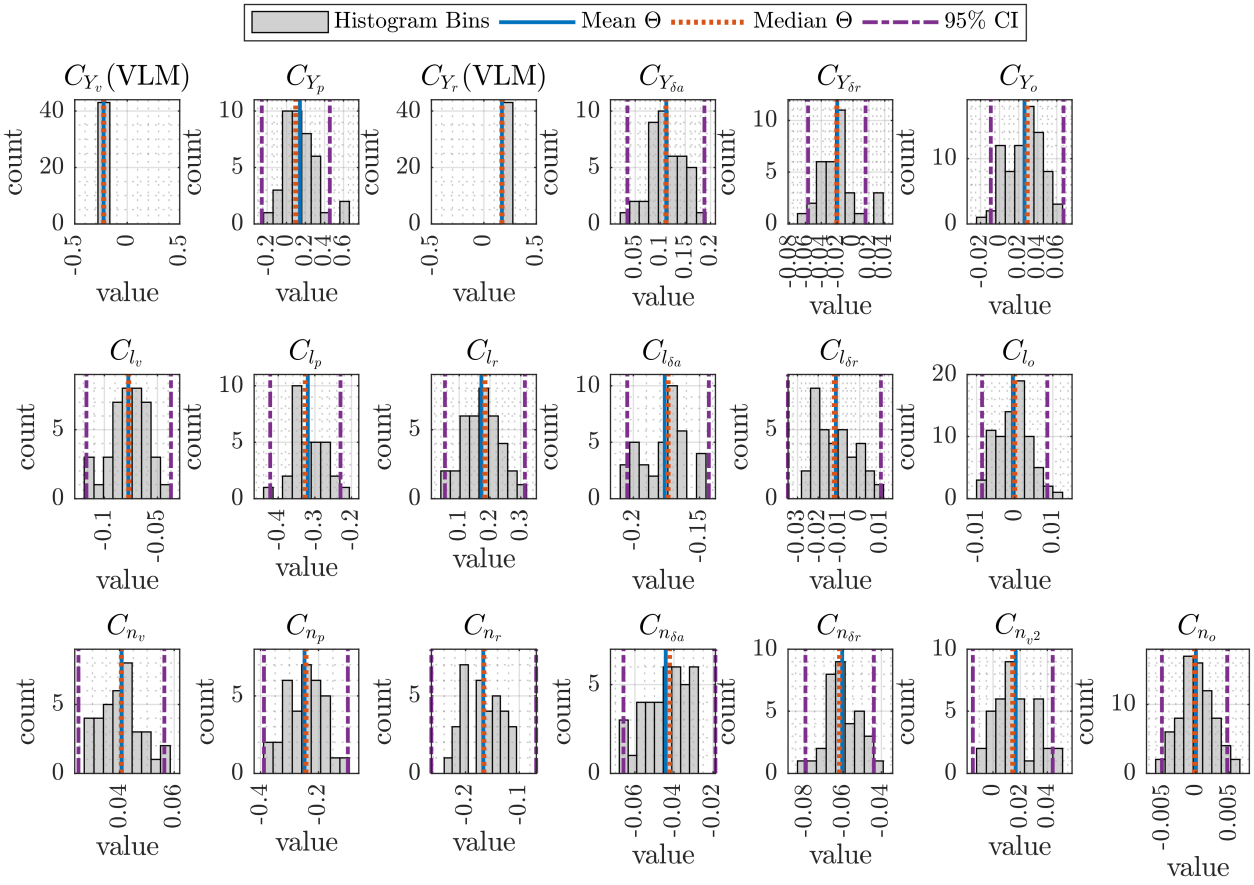

Figure A.6: Histograms of lateral-directional parameter estimates (Θ) from individual maneuvers fixing VLM values of C_{Y_v} and C_{Y_r} then using the steps in Table 4.6 to estimate the remaining parameters from flight test data

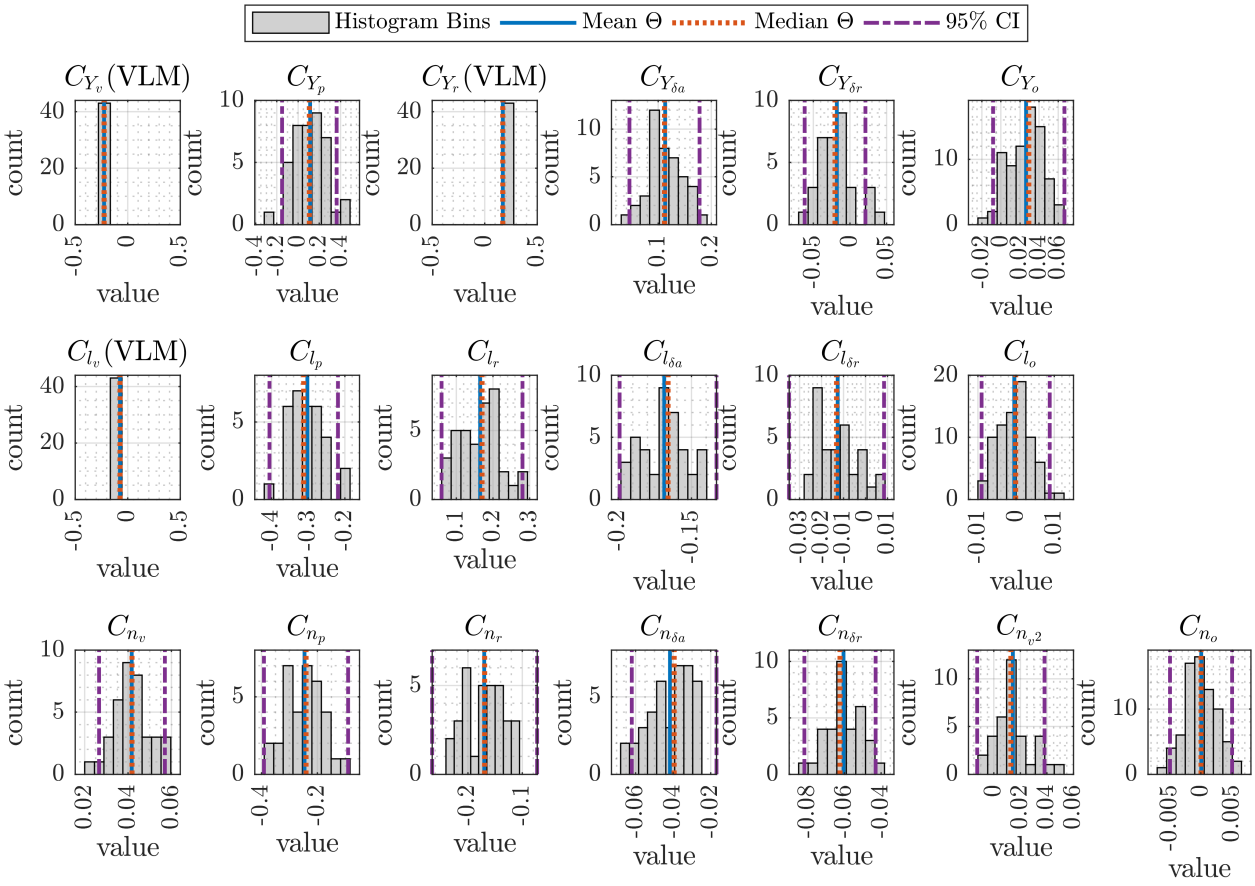

Figure A.7: Histograms of individual longitudinal parameter estimates (Θ) from individual maneuvers fixing VLM values of C_{Y_v}, C_{Y_r} and C_{l_v} then using the steps in Table 4.6 to estimate the remaining parameters from flight test data

A.3 Simulation Results for the Final Model

This section contains figures to accompany the discussion of results for the validation of the final model presented in Section 4.5. Note that the longitudinal signals correspond to the dominant signals for Short Period maneuver and the lateral-directional signals correspond to the dominant signals for the Dutch Roll and Bank-to-Bank Roll maneuvers.

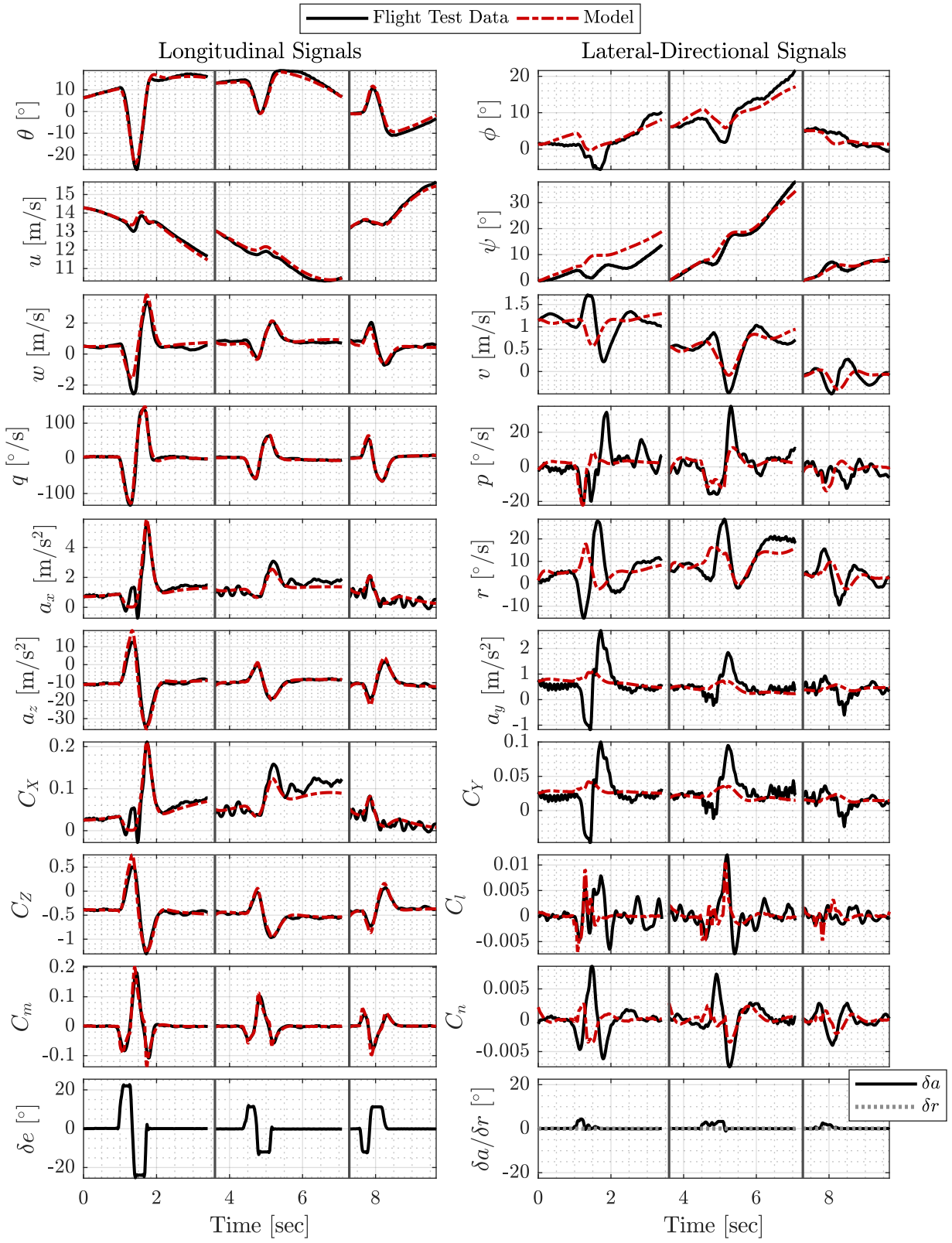

Figure A.8: Predicted model response of the final model compared to measured flight test data for the validation Short Period maneuvers including time histories of on- and off-axis signals

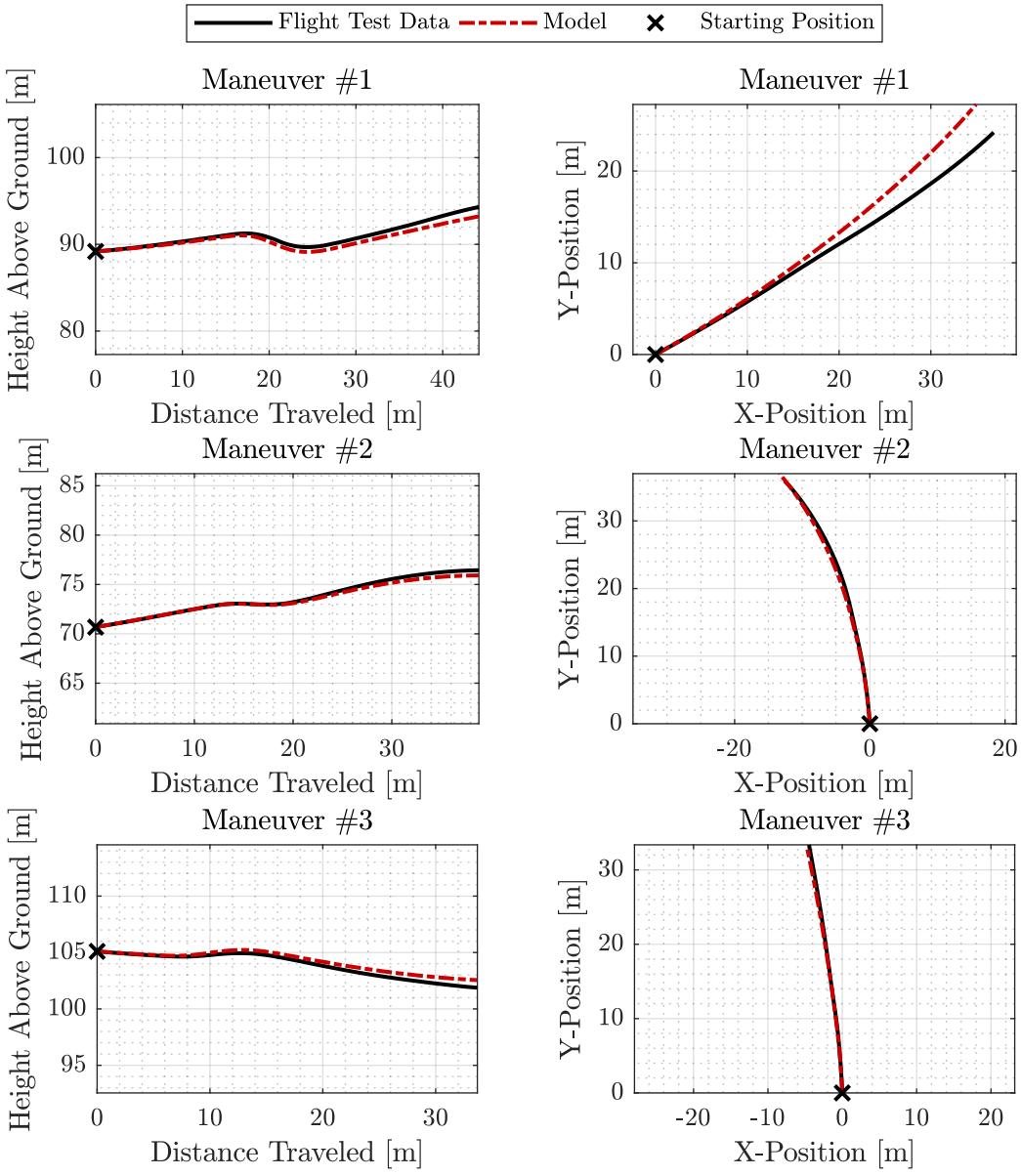

Figure A.9: Predicted flight path of the final model compared to measured flight test data for the validation Short Period maneuvers

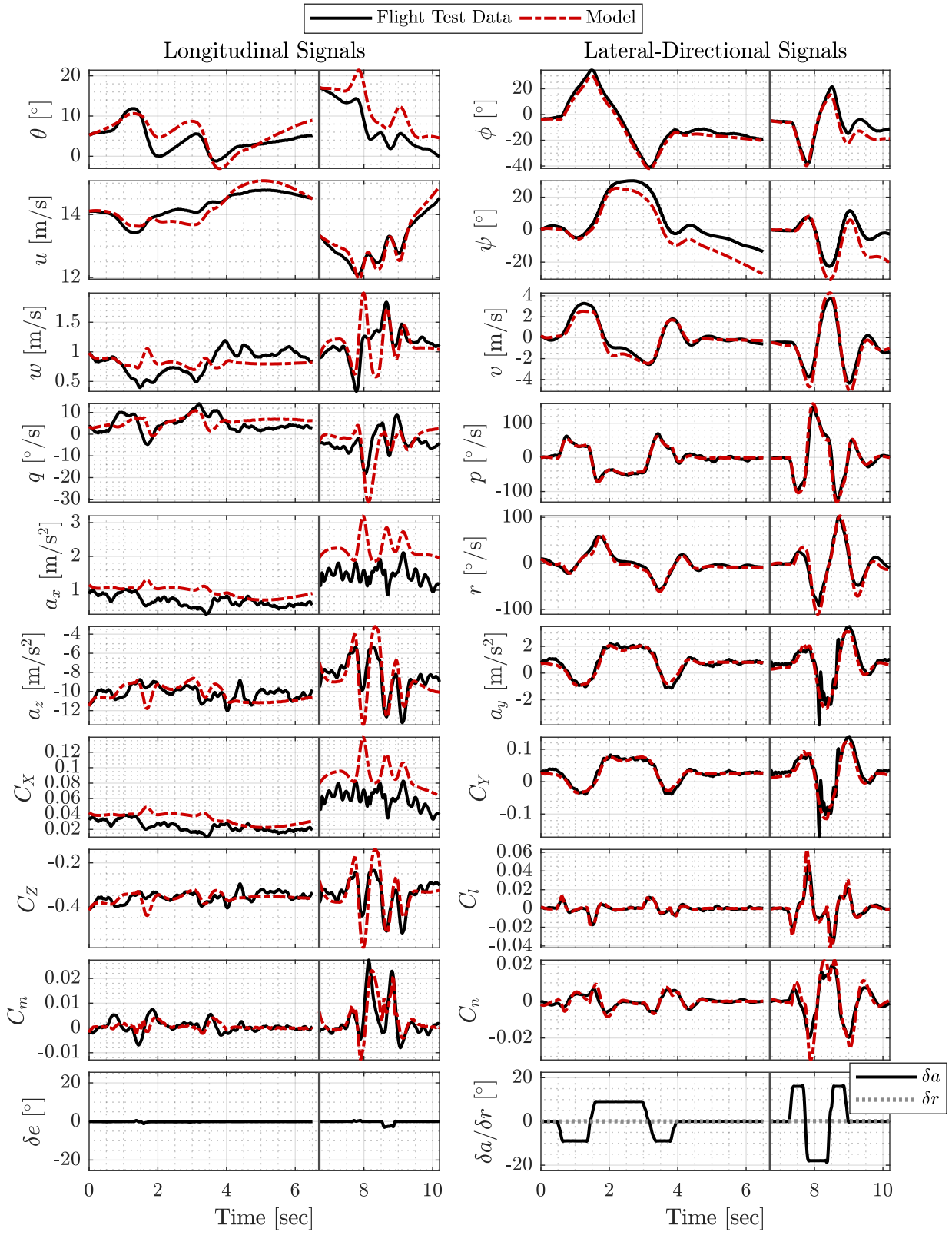

Figure A.10: Predicted model response of the final model compared to measured flight test data for the validation Bank-to-Bank Roll maneuvers including time histories of on- and off-axis signals

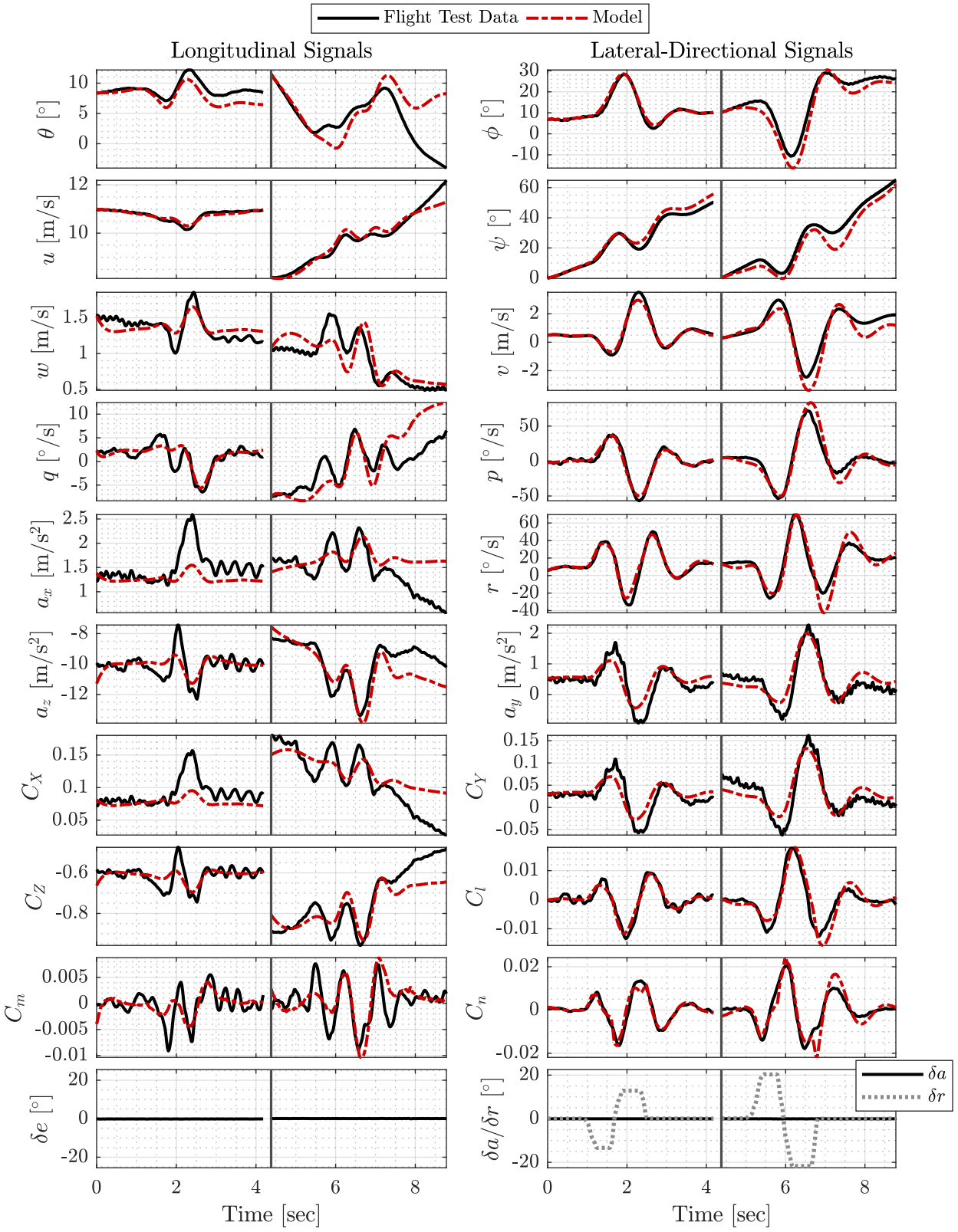

Figure A.11: Predicted model response of the final model compared to measured flight test data for the validation Dutch Roll maneuvers including time histories of on- and off-axis signals

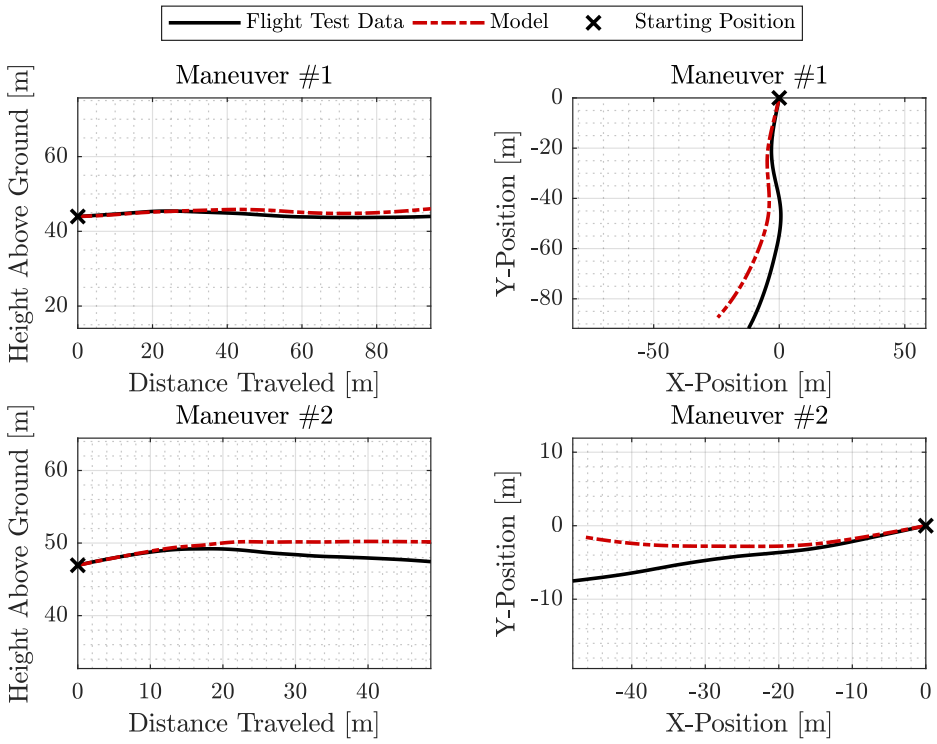

(a) Bank-to-Bank Roll flight path

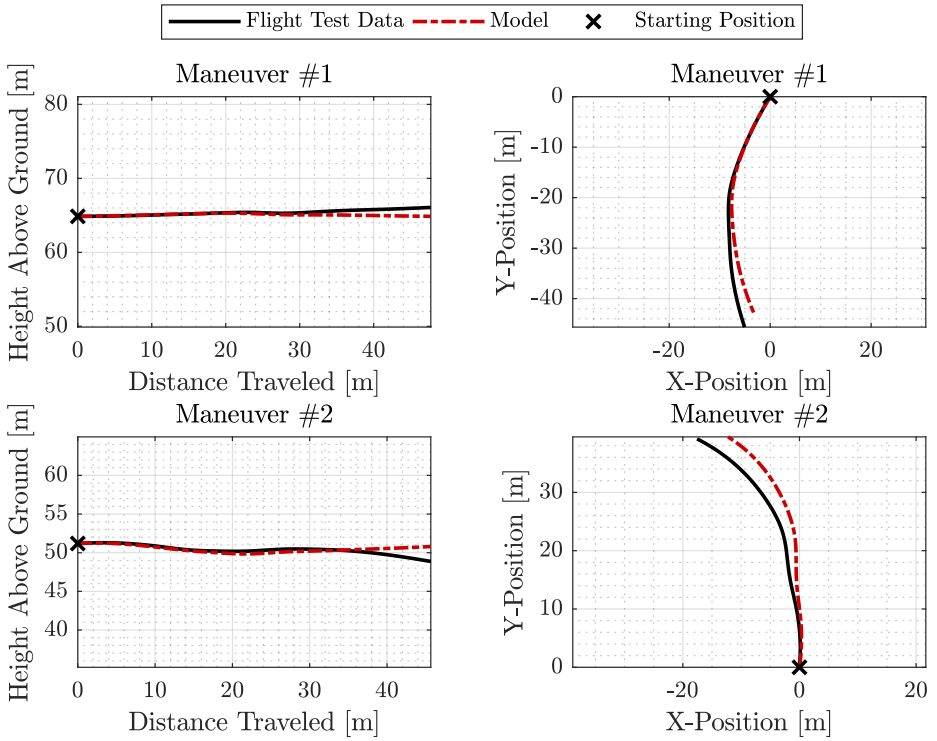

(b) Dutch Roll flight path

Figure A.12: Predicted flight path of the final model compared to measured flight test data for the validation (a) Bank-to-Bank Roll maneuvers, and (b) Dutch Roll maneuvers